The Use and Performance of Graphite and Metal ISSECs in Tokamak Fusion Reactors

H.I. Avci, Y. Gohar, T.Y. Sung, and G.L. Kulcinski

April 1977

UWFDM-202

Nucl. Engr. and Design 45, 285 (1978).

FUSION TECHNOLOGY INSTITUTE

UNIVERSITY OF WISCONSIN

MADISON WISCONSIN

The Use and Performance of Graphite and Metal ISSECs in Tokamak Fusion Reactors

H.I. Avci, Y. Gohar, T.Y. Sung, and G.L. Kulcinski

Fusion Technology Institute
University of Wisconsin
1500 Engineering Drive
Madison, WI 53706

http://fti.neep.wisc.edu

April 1977

UWFDM-202

Nucl. Engr. and Design 45, 285 (1978).

The Use and Performance of Graphite and Metal ISSECs in Tokamak Fusion Reactors

by

H. I. Avci
Y. Gohar
T. Y. Sung
G. L. Kulcinski
C. W. Maynard

April 1977

UWFDM-202

Fusion Technology Program
Nuclear Engineering Department
University of Wisconsin
Madison, Wisconsin 53706

Table of Contents

		Page
I.	Introduction	1
II.	Calculational Procedures	5
III.	Effects of ISSEC on 316 SS Structural First Wall	9
	III-A. Reduction of Displacement Damage	9
	III-B. Reductions in He and H Production Rates	11
	III-C. Radioactivity and Afterheat	14
IV.	Effects of ISSEC on the Total Blanket	19
	IV-A. Tritium Breeding Ratio	19
	IV-B. Energy Multiplication in the Blanket	21
	IV-C. Radioactivity, BHP and Afterheat of the Blanket	23
V.	Radiation Damage in ISSEC	27
	V-A. Displacement Damage and Gas Production	27
	V-B. Radioactivity, BHP and Afterheat	33
VI.	Mechanical Design and Heat Transfer of ISSECs	39
VII.	Other Considerations Affecting ISSECs	60
	VII-A. Cost and Availability	60
	VII-B. Vacuum Properties and Vapor Pressure	65
	VII-C. Surface Effects	68
	VII-C-1. Sputtering	68
	VII-C-2. Blistering	80
	VII-D. Thermal Shock Resistance	81
VIII.	Conclusions	83
	References	89
	Appendix A Neutron and Gamma Multi-group Structures Used in This Study	95
	Appendix B A Note on Displacement Cross Sections	98

I. Introduction

One of the major obstacles to the successful operation of a nuclear fusion power reactor will be the ability of its structural components to withstand the extremely harsh radiation damage environment and to maintain structural integrity over an extended period of time. A flux of 14.1 MeV neutrons and charged particles from a D-T plasma incident on the first structural wall around the plasma will cause such mechanical property degradation and erosion of the first wall that it will have to be replaced after a certain amount of time. Several studies have concluded that the periodic replacement of a 316 SS first structural wall might take place at intervals anywhere between 2 to 5 years under typical 1-5 MW/m^2 neutron wall loadings.[1-3] One economic assessment study of fusion reactors concludes that for the UWMAK-I[4] and UWMAK-II[5] reactors cost of electricity is significantly increased with decreasing first wall lifetime.[6] In fact, it was shown that in these reactors the cost of electricity increased over the 10-year first wall lifetime value by 17-28% if the wall life is only 2 years and 35 to 65% for a wall life of one year. Therefore, it is apparent that a great incentive exists for seeking ways to increase the first wall lifetimes. It has been shown that one way of obtaining higher wall lives is by placing passive shields between the plasma and the first wall.[7-9] It has been demonstrated that a graphite shield reduces both the displacement damage and the gas production rates in the first structural wall. For example, some slab geometry calculations for the non-breeding blanket structure of references 8 and 9 showed that a 12.5 cm thick carbon shield reduces the displacement rate in various metallic first walls by a factor of 3 to 5 in a DT or DD fusion neutron environment.

When the graphite thickness was increased to 25 cm, the factors of reduction in the displacement damage varied between 8 and 20 in the various first wall materials and the two plasma cycle systems. The passive shield employed was given the name ISSEC, for Internal Spectral Shifter and Energy Converter.[7]

It was shown in references 8 and 9 that the helium and hydrogen production rates in the various first wall materials were also reduced when protected by an ISSEC. In fact, gas production rates were lowered by factors of 7 to 14 when a 12.5 cm thick carbon ISSEC was used. With a 25 cm shield the gas production rates in various first wall materials dropped by factors of 17 to 80 over the unprotected wall case.

Depending on whether the isotopes responsible for the first wall radioactivity are produced as a result of fast or thermal neutron activation, the first wall radioactivity either went up or down with increasing carbon shield thickness. It was found that at shutdown, the radioactivity in 316 SS, Al and Nb first walls was reduced with increasing carbon thickness while the activities in V and Ta were increased. Long term radioactivity displayed the same trends in Al, 316 SS and Ta as did short term radioactivity. However, the long term activity in Nb increased and that in V decreased with increasing shield thickness.

In previous studies two concepts of an ISSEC have been investigated;[8,10] the full ISSEC and the partial ISSEC. In the full ISSEC concept, the shield extends all the way around the plasma and the plasma is never exposed directly to the first wall. In the partial ISSEC concept, the spectral shifter is used to protect only the inner blanket, nearest to the axis of a Tokamak where access and maintenance is most difficult. From a neutronics point of view, it does not make much difference whether the protected wall is behind a full ISSEC or partial ISSEC; it is the thickness of the ISSEC that is important. One added advantage of a partial ISSEC, however, is that it allows larger thicknesses of shield to be used because now the ISSEC is cooled from both sides by radiation and the temperature level is not as high as in the full ISSEC case for the same thickness of material. It was shown that a partial ISSEC can employ up to 30 cm of carbon without exceeding a 2000°C temperature limit compared to 7 cm for a full ISSEC.[10] A 2000°C temperature limit was imposed on carbon because at that temperature the vapor pressure of carbon becomes comparable to the pressure in the vacuum chamber of a Tokamak, i.e. $\sim 10^{-5}$ torr.

In this paper we expand the ISSEC concept to the area of high temperature refractory metals. We also study the effects in a more realistic cylindrical geometry blanket model and include the effects of breeding tritium. Furthermore, we deal with the more realistic mechanical and heat transfer design characteristics of ISSECs. The layout of the paper is as follows. In Chapter II, a description of the way the calculations were carried out is given and the model blanket design used in this study is presented. Chapter III shows how various ISSECs affect the 316 SS first structural wall radiation damage parameters. Chapter IV outlines the effects of ISSECs on the parameters characterizing the whole blanket, e.g., tritium breeding ratio, energy multiplication, radioactivity.

In Chapter V we elaborate on the radiation damage inside the ISSECs themselves. Chapter VI investigates how an ISSEC might mechanically be constructed as well as the associated heat transfer and stress problems. Chapter VII details some other considerations that might affect the choice of an ISSEC material. For example, it deals with the cost and availability, vacuum properties, chemical activity,sputtering, and thermal shock properties. Conclusions from the study are given in Chapter VIII.

Finally, we have limited our discussion to a full ISSEC only and we did not consider such aspects as internal breeding, as it is treated elsewhere.[7]

II. Calculational Procedures

The one-dimensional, homogeneous, cylindrical geometry, model blanket design used in this study is shown in Figure II-1. A variable thickness ISSEC zone was placed between the plasma and the 316 SS first structural wall. A density factor (D.F.) of 1.0 was used for neutronic calculations although in practice a density factor of somewhat less than 1.0 would be reasonable, especially for carbon. This would result in a thicker ISSEC region. However, the neutron "optical" thickness would be the same in both cases. The materials studied for an ISSEC were carbon, molybdenum, niobium, vanadium and tungsten.

The first wall material used in all cases was 316 SS with 1 cm thickness at a D. F. of 0.5. The first wall is followed by a 60 cm thick breeding zone composed of 95% natural lithium and 5% 316 SS for structural material. Behind the breeding zone is a 30 cm thick reflector zone with a composition of 95% C and 5% 316 SS. Both the breeding zone and the reflector zone have a D.F. of 1.0 although in reality in the reflector zone a D.F. of less than 1.0 would be more appropriate to take into account the coolant passages. To simulate the final shield albedos of 0.05, 0.10, 0.20, 0.25 were used for neutron groups 1 through 5 (9 to 14.9 MeV) of the 46 group energy structure shown in Appendix A, respectively. An albedo of 0.3 was used for neutrons of lower energy.

The nuclear performance of this type of reactor design was studied by solving the discrete ordinates form of the neutron transport equation for a cylinder using the ANISN[11] program with a S_4-P_3 approximation. It has been shown elsewhere[12] that this approximation is adequate to predict integral parameters such as tritium breeding and gas production rates to within approximately 2% of a higher order calculation like the S_{16}-P_5.

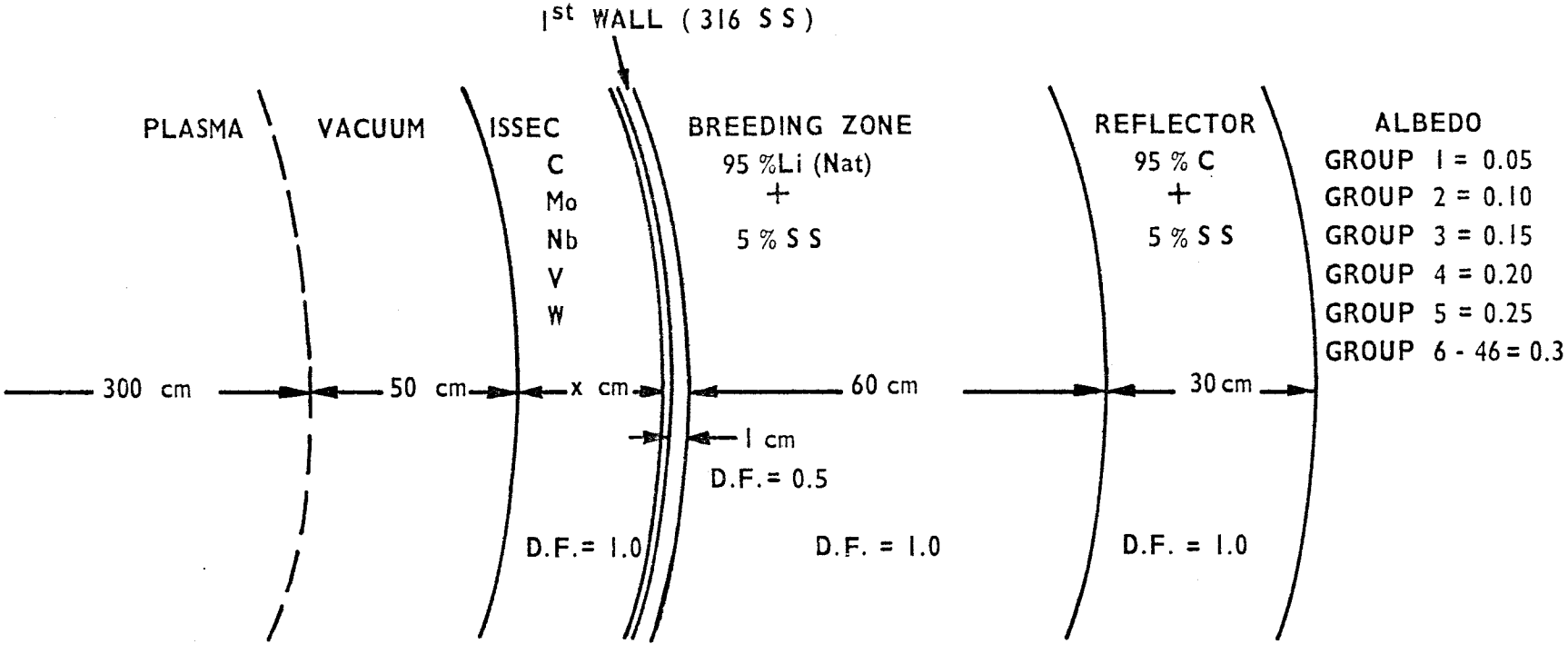

1 - DIMENSIONAL CYLINDRICAL BLANKET MODEL USED IN THIS STUDY

Figure II-1

The neutron and gamma production cross sections were obtained as a coupled set of 100 neutron groups and 21 gamma groups produced for EPR calculations.[13] This data set was generated with the AMPX modular code system[14] from nuclear data in ENDF/B-IV. The only exception is Nb where evaluation of the cross sections is based on ENDF/B-III data. (Previous calculations in references 7 to 10 were all based on ENDF/B-III data).

Due to the costs and computer memory limitations, the 100 neutron group cross sections were collapsed to 46 groups keeping the same fine group structure above 2 MeV as in the original set. The 46 group neutron and 21 group gamma interaction cross sections' group structures used in these calculations, are given in Appendix A.

Neutron kerma factors were generated using the MACK program[15] based on data in ENDF/B-III. The gamma kerma factors were calculated using the MUG[16] code and ENDF/B-III data.

The displacement cross sections were calculated from a computer code developed by Doran[17,18] except the displacement cross sections for carbon were from W. C. Morgan.[19] The values used in these calculations are given in references 8 and 9.

Radioactivity calculations have been performed with the DKR[20] code. DKR is a special program developed at the University of Wisconsin for radioactivity calculations in fusion reactors. It constructs linear decay chains and solves them to compute radioactivity, biological hazard potential (BHP), and afterheat using the fluxes calculated by ANISN and nuclear data from Decay Chain Data Library (DCDLIB).[21]

The heat transfer problems involving thermal radiation were solved using the program HEAT.[22] A simpler finite element code FEM2D[23] was used for problems involving conduction only. For radiation problems,

all radiative surfaces were assigned emissivities of 0.9 keeping in mind that metal surfaces would have to be painted black or carbon coated to achieve an emissivity that high. Other thermal properties data used in the calculations are given in Table VI-2 in Chapter VI. In all cases, a first structural wall temperature of 500°C was assumed. However, the ISSEC temperatures are not very sensitive to this choice.

All results are normalized to 1 MW/m^2 neutronic wall loading, i.e., 1 MW of neutron energy passing through the first wall (or inner ISSEC surface) per m^2 of area. A surface heat load of 4 W/cm^2 was taken assuming there would be a divertor to reduce the charged particle flux incident on the first wall or inner ISSEC surface. The heat flux number is consistent with calculations reported for UWMAK-II[5] and UWMAK-III.[24]

III. Effects of ISSEC on the 316 SS Structural First Wall

III-A. Reduction of Displacement Damage in the First Wall

The first wall neutron spectra obtained using the ANISN[11] program in the cylindrical geometry of the model blanket shown in Figure II-1 of Section II is combined with the 316 SS displacement cross sections, to yield the displacement rates shown in Figure III-1. The absolute values of the displacement rates, in units of dpa per 1 MW/m^2 neutronic wall loading per year, are plotted as a function of increasing ISSEC thickness for five different ISSEC materials. As can be seen in Figure III-1, tungsten is most effective in reducing the displacement damage in the first wall while carbon is least effective. In fact, we can see from the figure that the higher the atomic number of the ISSEC material, the more effective it is. This is mainly due to the higher neutron inelastic cross sections of higher Z metals at high neutron energies .

Factors of reduction in the displacement rates in the 316 SS first wall vary between 2 for C and approximately 5 for W for a 10 cm thick spectral shifter. These reductions are much higher for a 25 cm ISSEC varying between approximately 5 for C and approximately 50 for W. The significance of this observation is that <u>if</u> the wall life is predominantly determined by the level of the total displacement damage, then one might extend the wall lifetime due to radiation damage alone by factors of 2-50.

The displacement cross sections for various elements have recently been recalculated with proper inclusion of charged particle-out reactions [(n,p), (n,α), etc.] and using the ENDF-IV data[25,26] rather than ENDF-III as in previous calculations.[17] The newer calculations show the displacement cross

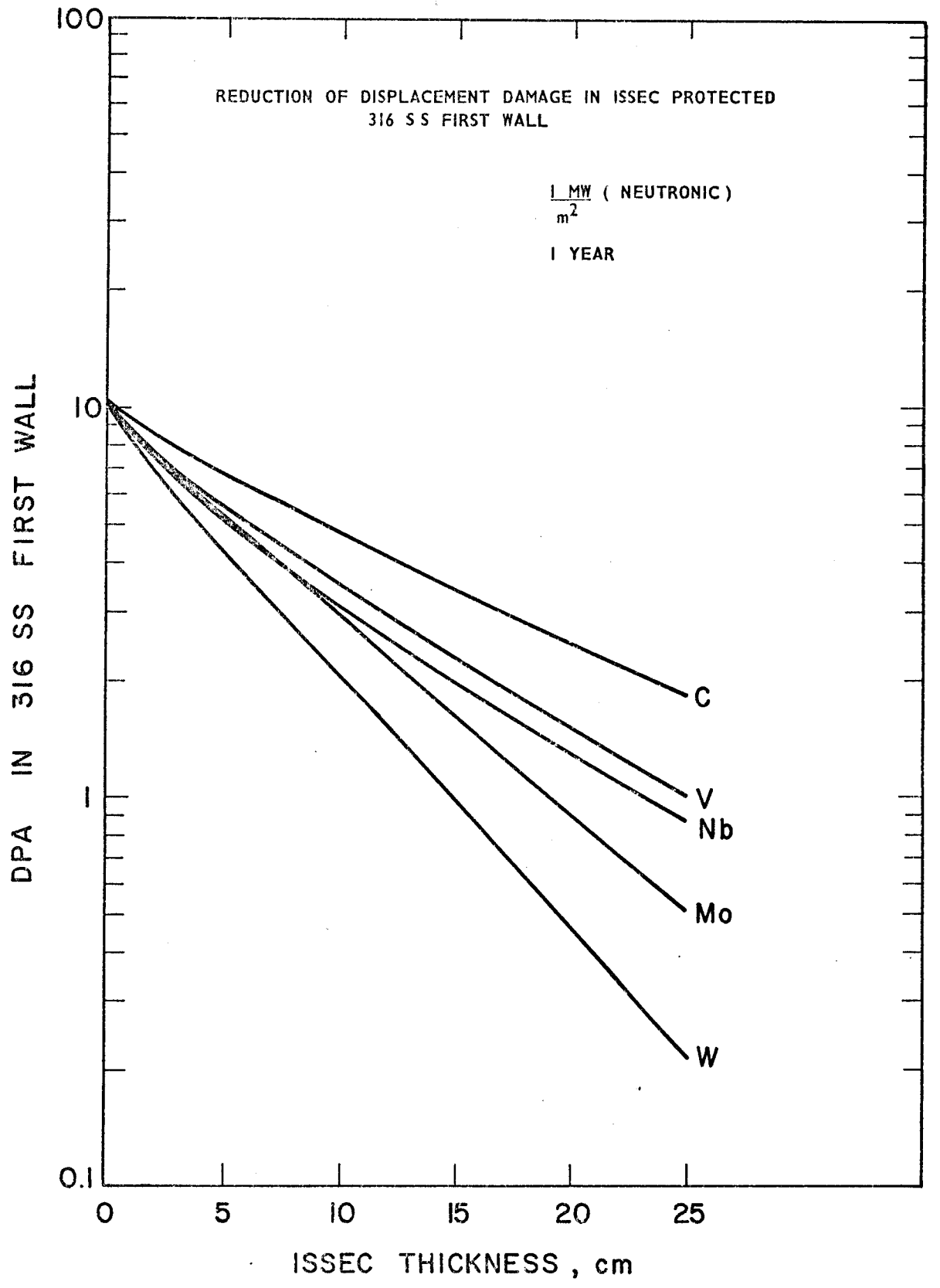
REDUCTION OF DISPLACEMENT DAMAGE IN ISSEC PROTECTED
316 S S FIRST WALL
1 MW / m² (NEUTRONIC)
1 YEAR
DPA IN 316 SS FIRST WALL
100
10
1
0.1
0
5
10
15
20
25
ISSEC THICKNESS , cm
C
V
Nb
Mo
W

FIGURE III-1

sections to be higher than the old ones at high neutron energies. These newer cross sections were available to us after the bulk of calculations for this paper were finished. How the displacement rates in the 316 SS first wall are affected by them is briefly explained in Appendix B.

III-B. Reductions in He and H Production Rates

The effects of 5 different ISSEC materials on the helium and hydrogen production rates in the 316 SS first wall are shown in Figures III-2 and III-3 respectively. The gas production rates are given in terms of appm per 1 MW/m^2 neutronic wall loading per year. The absolute effect here is more pronounced than in the case of displacement damage. This is due to the fact that gas production cross sections have the threshold reactions which occur above 2 MeV whereas the displacement cross sections are continuous from thermal energies.

The factors of reduction in helium production rates in the first wall vary between 3.2 for C and 12 for W for 10 cm thickness and between 12 and 275 for a 25 cm ISSEC of the respective materials. Similar reductions are seen in the hydrogen production

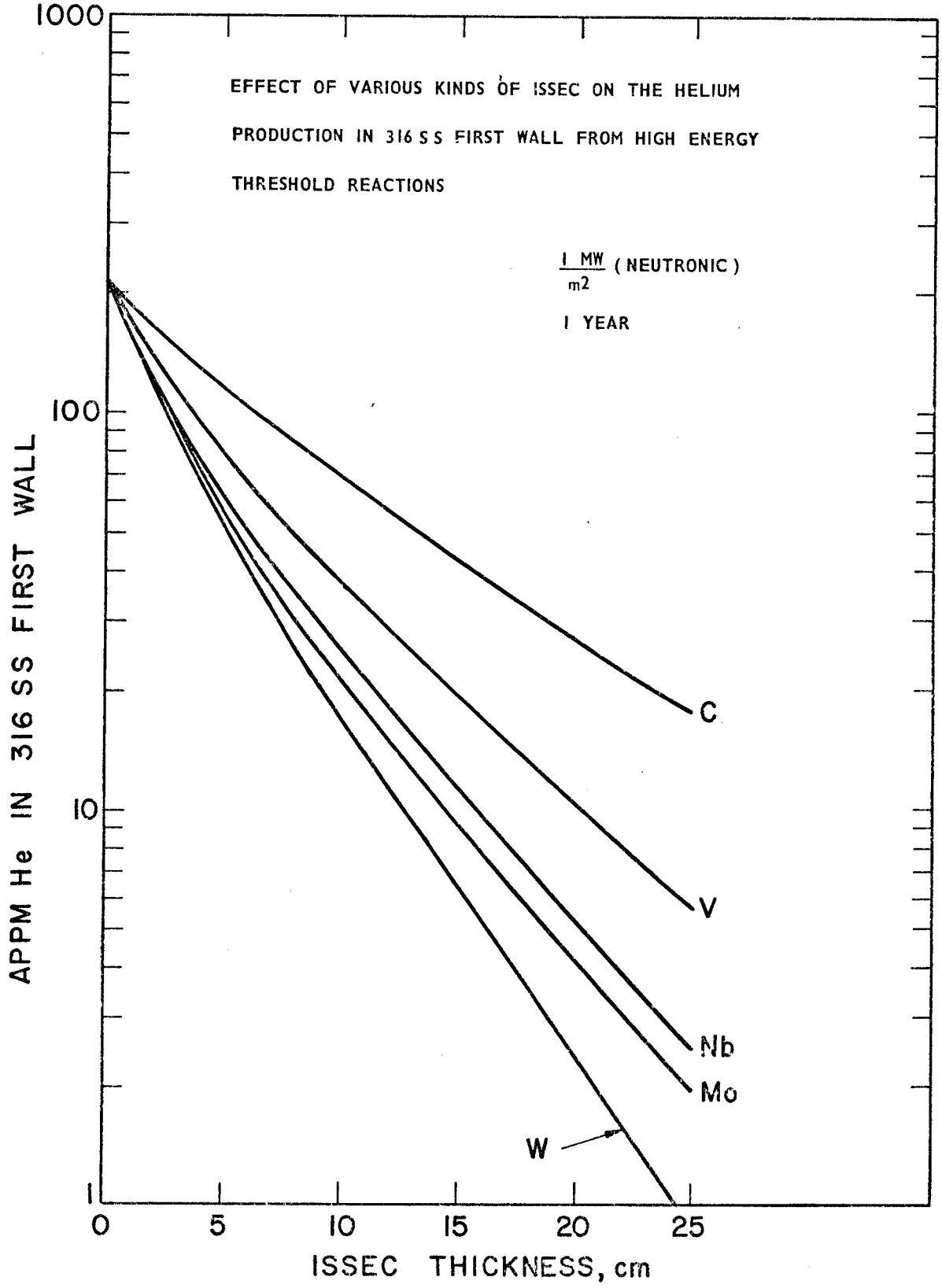
EFFECT OF VARIOUS KINDS OF ISSEC ON THE HELIUM PRODUCTION IN 316 S S FIRST WALL FROM HIGH ENERGY THRESHOLD REACTIONS
1 MW/m2 (NEUTRONIC)
1 YEAR
APPM He IN 316 SS FIRST WALL
ISSEC THICKNESS, cm
1000
100
10
1
0
5
10
15
20
25
C
V
Nb
Mo
W

FIGURE III-2

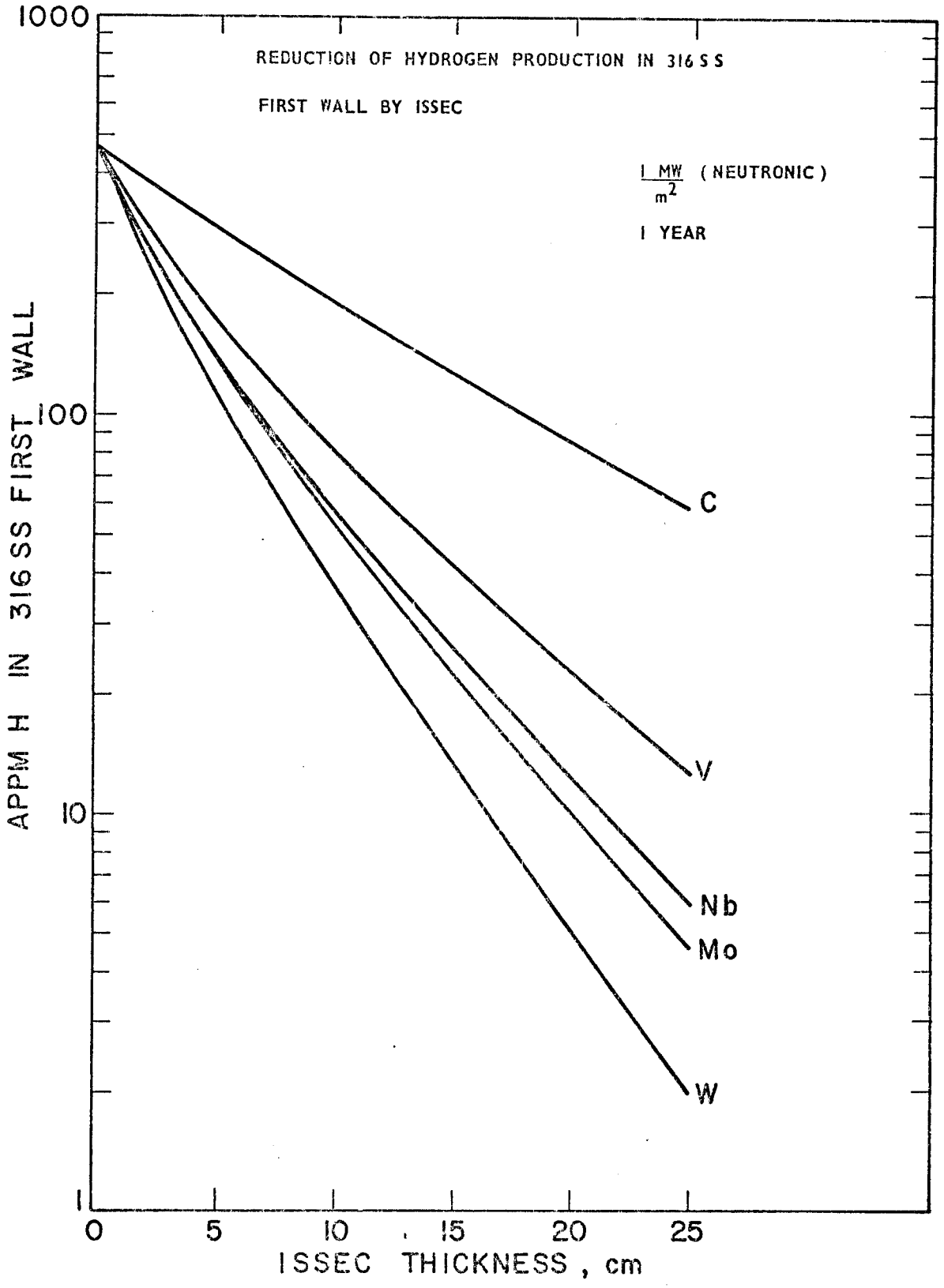
REDUCTION OF HYDROGEN PRODUCTION IN 316 S S
FIRST WALL BY ISSEC
1 MW / m² (NEUTRONIC)
1 YEAR
APPM H IN 316 SS FIRST WALL
1000
100
10
1
0
5
10
15
20
25
ISSEC THICKNESS, cm
C
V
Nb
Mo
W

FIGURE III-3

rates. The helium production rates shown in 316 SS do not include thermally produced α's from the $Ni^{58}(n,\gamma)$ $Ni^{59}(n,\alpha)$ reaction sequence, but as was shown earlier in the case of a D-T plasma[9] thermally produced helium constituted less than 18% of total helium production in a 316 SS first wall protected by a 12.5 cm carbon ISSEC up to 5 years of operation time. After 1 year, it was 4% and after 20 years of continuous operation that number was 46%. Considering the differences due to 1.) geometrical effects between the slab geometry calculation of reference 9 and cylindrical geometry calculations of this study, 2.) differences in blanket structures and 3.) the effectiveness of metals versus carbon in softening the neutron spectrum, the absolute values given in Figure III-2 for helium production might be too low by 5-10% for a 10 cm ISSEC thickness and somewhat lower for greater thicknesses.

III-C. Radioactivity and Afterheat

The ISSECs can change the neutron induced radioactivity in the first structural wall. Since most of the activity of 316 SS is the result of transmutations due to high energy neutrons, the presence of an ISSEC reduces, to varying degrees, the activity of the first wall. However, at long times after shutdown when only a few nuclides dominate the radioactivity, the activation due to thermal neutrons may cause a deviation from this trend.

At shutdown, the major contributors to the radioactivity of the 316 SS first wall are $^{55}Fe(t_{1/2}$ = 2.6 yr), $^{56}Mn(t_{1/2}$ = 2.6 hr), $^{51}Cr(t_{1/2}$ = 27.8 days), $^{58}Co(t_{1/2}$ = 71.3 days), $^{54}Mn(t_{1/2}$ = 303 days); these contribute more than 85% of the total activity in the case of an unprotected wall. After one year of decay, ^{55}Fe alone contributes greater than 80% of the radioactivity. Other radioisotopes such

as ^{54}Mn, $^{57}Co(t_{1/2}$ = 270 days), $^{60}Co(t_{1/2}$ = 5.26 yrs) and ^{58}Co contribute 18% of the radioactivity. The major contributors to 316 SS at 100 years after shutdown are long half-life radioisotopes; $^{93}Mo(t_{1/2}$ = 1000 yrs.), $^{93m}Nb(t_{1/2}$ = 13.6 yrs, from β^+ decay of ^{93}Mo) and $^{63}Ni(t_{1/2}$ = 92 yrs).

Tables III-1, III-2 and III-3 show the changes in the first wall radioactivity, biological hazard potential (BHP) in air, and afterheat respectively, at various times after shutdown for different ISSEC materials and thicknesses.

At shutdown and until 1 year after shutdown, tungsten is the most effective ISSEC material to reduce the first wall radioactivity, mainly because of its absorption and inelastic scattering properties. A factor of 10 reduction of the activity in the first wall can be achieved by tungsten of 10 cm thickness.

Tungsten is followed by molybdenum and niobium which are nearly the same in reducing the radioactivity. They reduce the activity by a factor of 3 for an ISSEC of 5 cm thickness and by a factor of 7 for 10 cm of material. The vanadium ISSECs of 5 cm and 10 cm thickness reduce the activity by factors of 2 and 4 respectively. Carbon is the least effective one in reducing the activity among these materials. The activity reduction of carbon is a factor of 1.8 for 5 cm thick case and a factor of 2.5 for 10 cm thickness. At 100 years after shutdown, the activity reduction due to ISSECs is not as great as at shutdown and the differences among these materials become smaller. One interesting fact at this time is that the activity of the first wall actually increases as the carbon thickness increases because of ^{63}Ni produced from ^{62}Ni by an (n,γ) reaction.

By the same token, the BHP and the afterheat of the first wall decreases in the same proportion as the radioactivity decreases.

Table III-1 Specific Radioactivity of First Wall* (Ci/cm^3)

ISSEC Material	ISSEC Thickness	Time After Shutdown: 0	1 h	1 d	1 Mo	1 y	100 y
No ISSEC		75.89	66.12	52.59	42.25	22.47	3.37×10^{-3}
C	5 cm	43.41	37.44	28.29	22.61	11.54	2.72×10^{-3}
	10 cm	29.99	25.77	18.28	14.08	6.79	6.64×10^{-3}
Mo	5 cm	23.14	19.85	15.57	12.16	6.40	2.27×10^{-3}
	10 cm	9.71	8.30	6.31	4.63	2.40	1.55×10^{-3}
W	5 cm	19.91	17.10	13.47	10.56	5.60	1.95×10^{-3}
	10 cm	7.20	6.17	4.74	3.53	1.85	1.08×10^{-3}
Nb	5 cm	24.02	20.65	16.39	12.96	6.87	2.21×10^{-3}
	10 cm	10.14	8.70	6.78	5.14	2.70	1.72×10^{-3}
V	5 cm	31.83	27.52	20.85	16.40	8.68	2.34×10^{-3}
	10 cm	18.00	15.27	10.20	7.59	3.97	1.89×10^{-3}

* 2 years operation, 1 MW/m^2 neutron wall loading

Table III-2 Specific BHP of First Wall* (km^3 of air/W-cm^3)

ISSEC Material	ISSEC Thickness	Time After Shutdown 0	1 h	1 d	1 Mo	1 y	100 y
No ISSEC		67.80	66.53	58.45	42.33	18.36	3.66×10^{-3}
C	5 cm	38.39	37.61	33.14	24.44	10.19	3.18×10^{-3}
	10 cm	23.43	22.92	20.05	14.95	6.06	1.02×10^{-2}
Mo	5 cm	17.87	17.49	15.29	10.96	4.76	1.42×10^{-3}
	10 cm	6.45	6.30	5.47	3.88	1.67	7.27×10^{-4}
W	5 cm	16.14	15.79	13.79	9.87	4.32	1.28×10^{-3}
	10 cm	5.29	5.16	4.49	3.18	1.39	5.68×10^{-4}
Nb	5 cm	20.31	19.89	17.41	12.48	5.45	1.54×10^{-3}
	10 cm	7.92	7.75	6.75	4.81	2.09	9.02×10^{-4}
V	5 cm	26.99	28.59	24.84	17.83	7.78	2.11×10^{-3}
	10 cm	14.44	14.01	11.86	8.44	3.67	1.57×10^{-3}

* 2 years operation, 1 MW/m^2 neutron wall loading

Table III-3 First Wall Afterheat Density* (Watt/cm^3)

ISSEC Material	ISSEC Thickness	Time After Shutdown: 0	1 h	1 d	1 Mo	1 y	100 y
No ISSEC		0.419	0.299	0.107	0.85×10^{-1}	0.30×10^{-1}	0.42×10^{-6}
C	5 cm	0.269	0.193	0.62×10^{-1}	0.49×10^{-1}	0.16×10^{-1}	0.33×10^{-6}
	10 cm	0.206	0.147	0.39×10^{-1}	0.31×10^{-1}	0.95×10^{-2}	0.80×10^{-6}
Mo	5 cm	0.133	0.906×10^{-1}	0.31×10^{-1}	0.24×10^{-1}	0.84×10^{-2}	0.26×10^{-6}
	10 cm	0.574×10^{-1}	0.395×10^{-1}	0.13×10^{-1}	0.92×10^{-2}	0.32×10^{-2}	0.17×10^{-6}
W	5 cm	0.113	0.770×10^{-1}	0.26×10^{-1}	0.21×10^{-1}	0.73×10^{-2}	0.22×10^{-6}
	10 cm	0.417×10^{-1}	0.266×10^{-1}	0.92×10^{-2}	0.68×10^{-2}	0.24×10^{-3}	0.19×10^{-6}
Nb	5 cm	0.135	0.921×10^{-1}	0.32×10^{-1}	0.25×10^{-1}	0.90×10^{-2}	0.25×10^{-6}
	10 cm	0.580×10^{-1}	0.398×10^{-1}	0.13×10^{-1}	0.10×10^{-1}	0.35×10^{-2}	0.19×10^{-6}
V	5 cm	0.189	0.136	0.42×10^{-1}	0.32×10^{-1}	0.11×10^{-1}	0.27×10^{-6}
	10 cm	0.127	0.917×10^{-1}	0.20×10^{-1}	0.15×10^{-1}	0.52×10^{-2}	0.21×10^{-6}

*2 years operation, 1 MW/m^2 neutron wall loading

IV. Effects of ISSEC on the Total Blanket

We will be concerned here with only three parameters out of the many that characterize a certain type of blanket. These parameters are the tritium breeding ratio, energy multiplication (total energy available per fusion event) and radioactivity.

IV - A) Tritium Breeding Ratio

In figure IV-1 the total breeding ratio in the model blanket of figure II-1 is plotted as a function of increasing ISSEC thickness for five different ISSEC materials. Other dimensions and compositions of each region in figure II-1 were kept constant. We see from figure IV-1 that the breeding ratio is less in an ISSEC protected system than in systems with no ISSEC. The reason for this is that when an ISSEC is placed between the plasma and the first structural wall, the lower energy spectrum reduces the Li-7 (n,n'T) reaction rate and there are generally fewer neutrons available in the breeding zone to breed tritium by Li-6 (n,T). Some neutrons interact in the ISSEC either through high energy or low energy reactions and convert their kinetic energy to heat energy or gamma energy which later gets transported by photons to be absorbed in the blanket. Also the amount of thermal neutron capture increases in the first wall and the structure as the ISSEC thickness increases. If an ISSEC material has a high (n,2n) reaction cross section, that helps the neutron inventory in the breeding zone a bit and the breeding ratio does not drop as fast as it would just due to the neutron energy degradation. Such is the case with vanadium, and molybdenum ISSECs. On the other hand, carbon, the material with the least parasitic absorption cross section, does not produce as much T as does a vanadium ISSEC (up to about 20 cm thickness) because of the high (n,2n) cross section of vanadium. Beyond a 20 cm thickness it appears that the thermal neutron captures in vanadium outweight the (n,2n) reactions and the breeding ratio in the vanadium ISSEC case drops below that in the carbon ISSEC case.

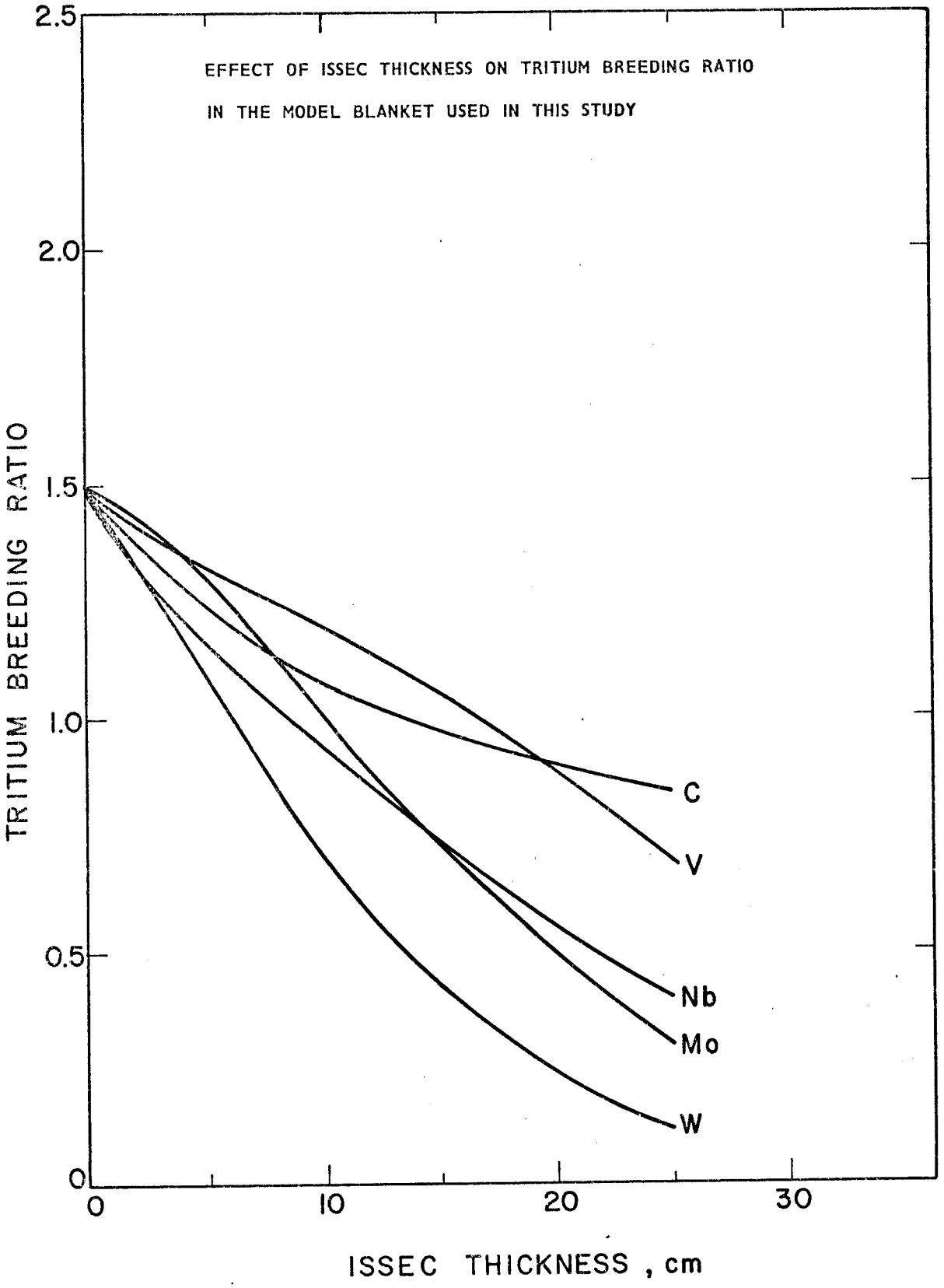
EFFECT OF ISSEC THICKNESS ON TRITIUM BREEDING RATIO
IN THE MODEL BLANKET USED IN THIS STUDY
TRITIUM BREEDING RATIO
2.5
2.0
1.5
1.0
0.5
0
0
10
20
30
ISSEC THICKNESS , cm
C
V
Nb
Mo
W

FIGURE IV-1

Similarly a molybdenum ISSEC system has a higher breeding ratio than a carbon ISSEC system up to about 8 cm of ISSEC thickness.

The maximum useful thickness of an ISSEC in a certain blanket might be limited by the amount of breeding required. For example, in our model blanket of figure II-1, if we require a minimum breeding ratio of 1.0, the maximum thickness of a carbon ISSEC is limited to ~13 cm, vanadium ISSEC to ~18.5 cm, molybdenum ISSEC to 10 cm, niobium to 8.5 cm and tungsten ISSEC to about 6 cm.

IV-B. Energy Multiplication in the Blanket

Table IV-1 lists the nuclear heating by neutrons and gammas and gives the total energy deposited in the blanket (including the 3.52 MeV α energy) per fusion event in the various designs studied.

It is seen from this table that a carbon ISSEC reduces the total energy deposited in the blanket per fusion event by 3-4%. Neutron heating is somewhat reduced (fewer exothermic Li-6 (n,T) reactions and more endothermic reactions in carbon) and the gamma heating is increased compared to the no ISSEC case. This reduction in neutron heating and increase in gamma heating is more apparent in metal ISSEC cases. Vanadium ISSECs also reduce the total energy output of the blanket per fusion as do the carbon ISSECs. The reason for that is the endoergic neutron reactions in vanadium.

For the case of metal ISSECs most gammas are born in the ISSEC itself. W. F. Vogelsang and E. Ramer [27] point out that the importance of a unit gamma source at the inner part of a blanket for a dose at the outer edge of shield is negligible compared to the importance of the same source in the outer part of the blanket. Therefore, the increase in the gamma heating of the blanket should not pose problems from a shielding point of view. It is apparent from the results in Table IV-1 that for the same neutronic wall loading, a reactor with a molybdenum ISSEC will have a higher thermal power output than reactors either with no ISSEC or C, Nb, V or W ISSECs. A

Table IV-1

Nuclear Heating in the Model Blanket and ISSEC Used in this Study

ISSEC Material	ISSEC Thickness (cm)	Neutron Heating (MeV)[a]	Gamma Heating (MeV)[a]	Total Energy (a,b Per Fusion (MeV)
No ISSEC		12.9	3.2	19.6
C	5	12.4	3.2	19.1
	10	12.1	3.3	18.9
	25	11.8	3.6	18.9
Mo	5	9.4	8.5	21.4
	10	6.9	12.6	23.0
	25	2.6	20.3	26.4
Nb	5	8.8	7.6	19.9
	10	6.7	10.3	20.5
	25	3.2	15.3	22.0
V	5	10.2	3.9	17.6
	10	8.8	4.8	17.1
	25	6.2	8.8	18.5
W	5	7.7	9.2	20.4
	10	4.6	13.0	21.1
	25			

(a) Per neutron born in plasma

(b) Includes 3.52 MeV α energy

vanadium ISSEC system will have the least output power. The significance of this is that if all the results in this paper were to be normalized per megawatt of thermal power (MW_{th}) output, a molybdenum ISSEC system would have the additional advantage of running at a lower neutronic wall loading, and consequently a higher ISSEC thickness would be allowed.

IV-C. Radioactivity, Biological Hazard Potential, and Afterheat of Blanket

Total radioactivity of the blanket (including the ISSEC) strongly depends on the choice of ISSEC material, because the ISSEC, which protects the first wall from high energy neutrons, is itself subject to the neutron activation and may show high or low activity.

Total blanket activities are shown in Figs. IV-2, IV-3 and IV-4. Compared to the no ISSEC case, the amount of total radioactivity at shutdown is slightly decreased in a carbon and vanadium ISSEC protected blanket while in the tungsten, molybdenum and niobium ISSEC cases it increases.

After 10 years of decay, the radioactivity for all cases falls in the same order of magnitude. The activity of molybdenum is the highest, followed by niobium, and the other three cases in decreasing order, after 1000 years of decay. The BHP of the blanket at shutdown is highest for the tungsten ISSEC case and less for molybdenum, no ISSEC, carbon, vanadium and niobium ISSEC cases in decreasing order. At 1000 years after shutdown, the BHP and radioactivity curves look similar in trend. As can be seen from Figure IV-4, the afterheat of the blanket is about the same in all cases except at long times after shutdown it falls in line with radioactivity. The activity of the various ISSECs themselves will be discussed in the next chapter.

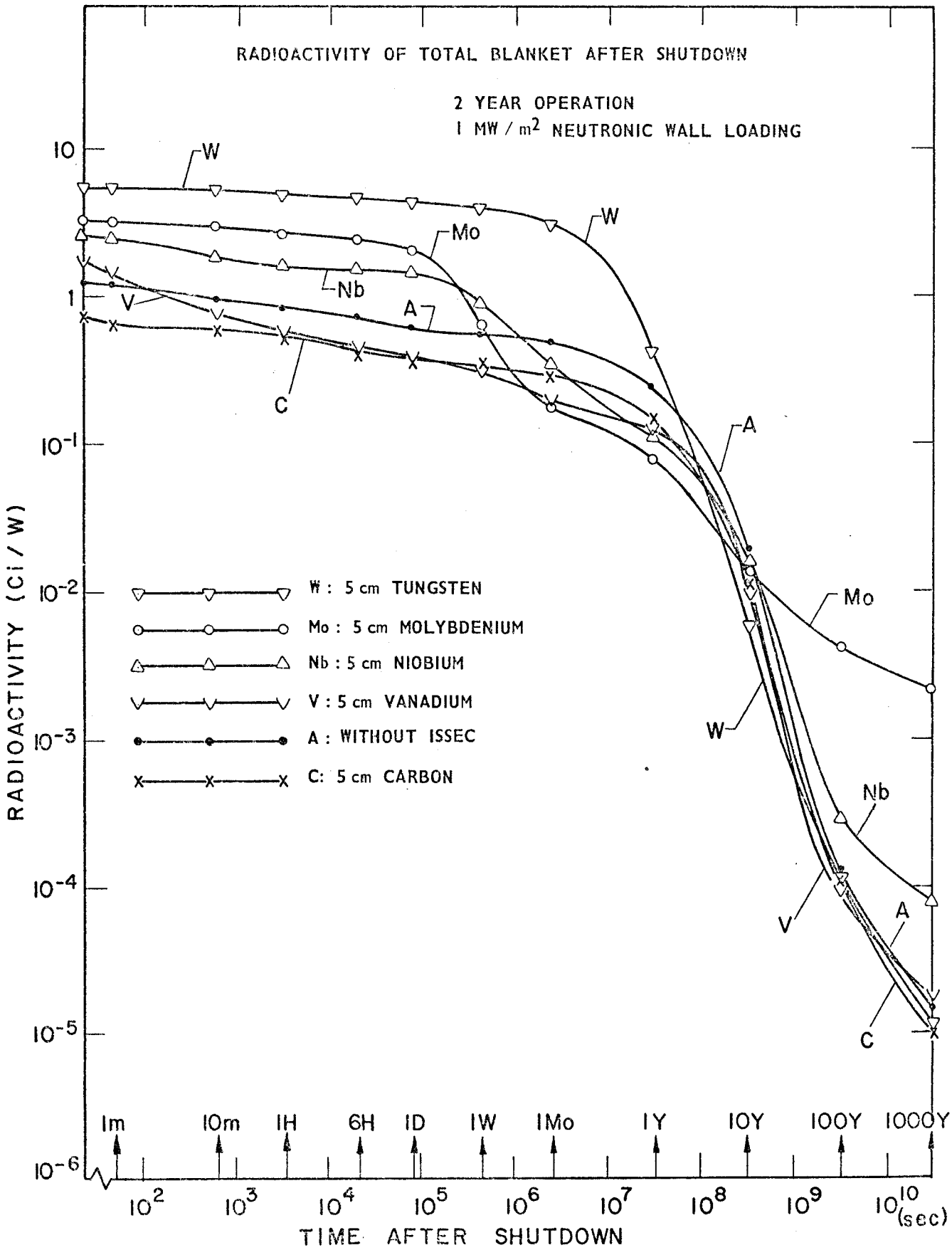
RADIOACTIVITY OF TOTAL BLANKET AFTER SHUTDOWN
2 YEAR OPERATION
1 MW / m2 NEUTRONIC WALL LOADING
RADIOACTIVITY (Ci / W)
TIME AFTER SHUTDOWN
W : 5 cm TUNGSTEN
Mo : 5 cm MOLYBDENIUM
Nb : 5 cm NIOBIUM
V : 5 cm VANADIUM
A : WITHOUT ISSEC
C: 5 cm CARBON
Im
10m
1H
6H
1D
1W
1Mo
1Y
10Y
100Y
1000Y
(sec)

Figure IV-2

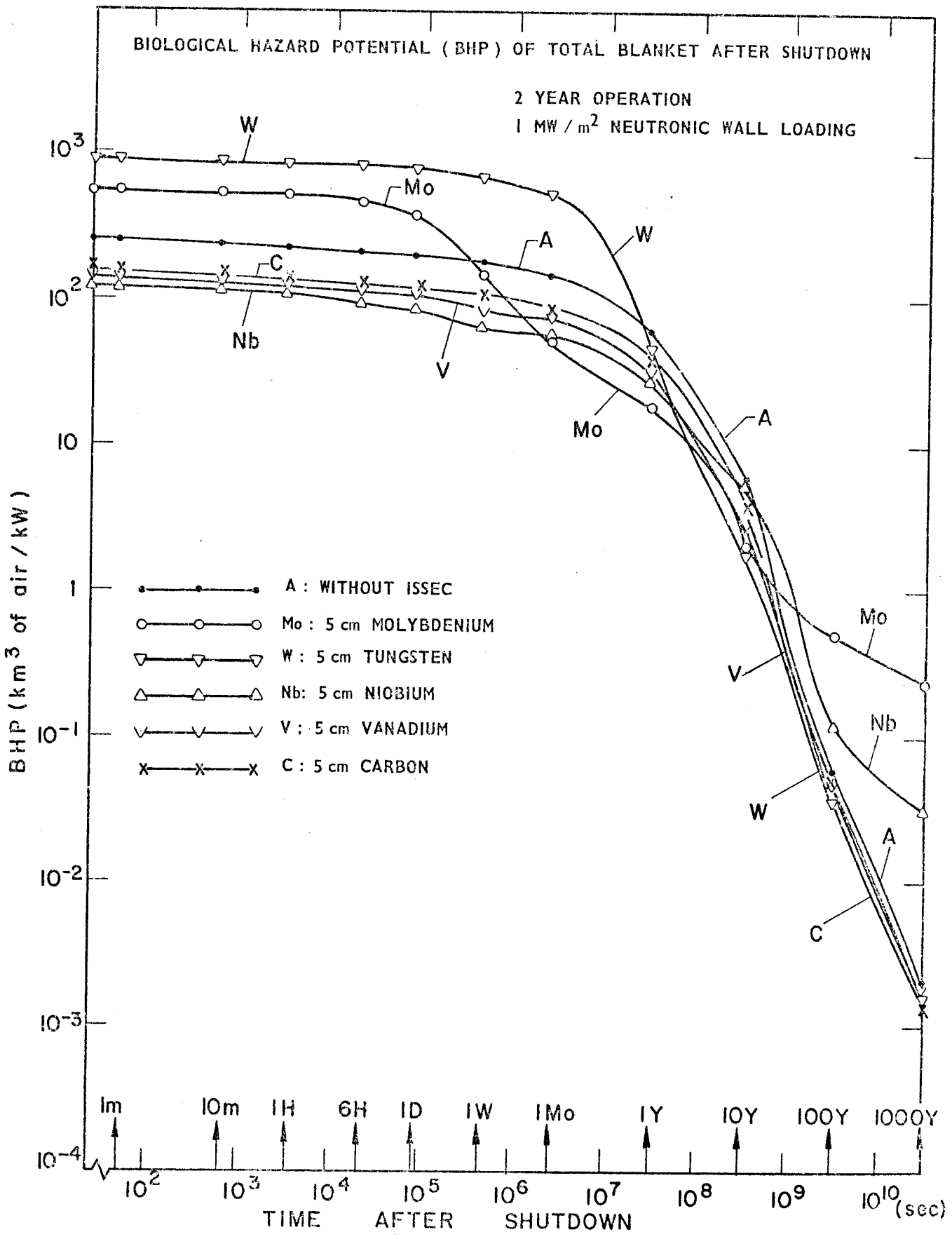
BIOLOGICAL HAZARD POTENTIAL (BHP) OF TOTAL BLANKET AFTER SHUTDOWN
2 YEAR OPERATION
1 MW / m2 NEUTRONIC WALL LOADING
BHP (km3 of air / kW)
A : WITHOUT ISSEC
Mo : 5 cm MOLYBDENIUM
W : 5 cm TUNGSTEN
Nb: 5 cm NIOBIUM
V : 5 cm VANADIUM
C : 5 cm CARBON
Im
10m
1H
6H
1D
1W
1Mo
1Y
10Y
100Y
1000Y
TIME AFTER SHUTDOWN
(sec)

Figure IV-3

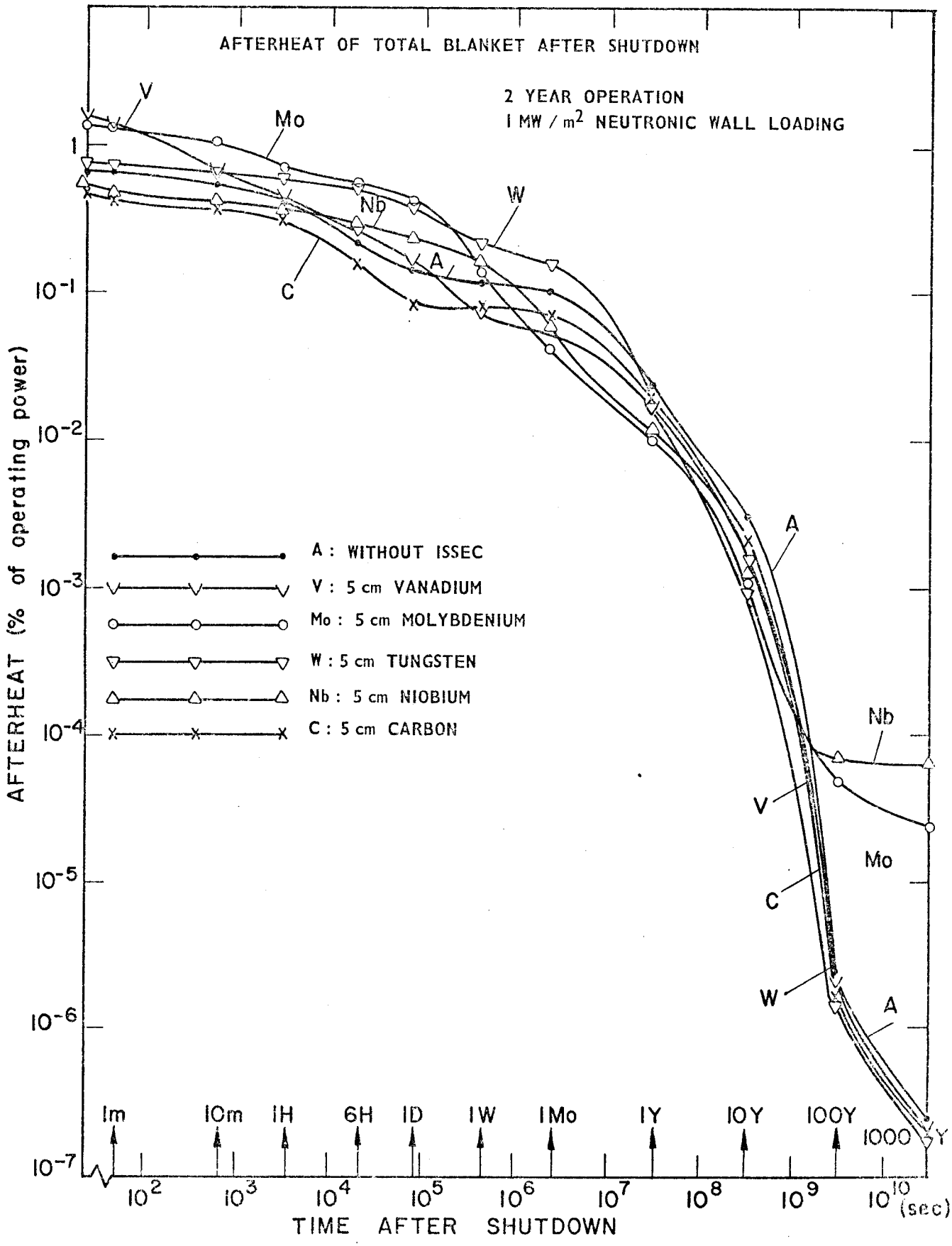
AFTERHEAT OF TOTAL BLANKET AFTER SHUTDOWN
2 YEAR OPERATION
1 MW / m2 NEUTRONIC WALL LOADING
AFTERHEAT (% of operating power)
A : WITHOUT ISSEC
V : 5 cm VANADIUM
Mo : 5 cm MOLYBDENIUM
W : 5 cm TUNGSTEN
Nb : 5 cm NIOBIUM
C : 5 cm CARBON
1m
10m
1H
6H
1D
1W
1Mo
1Y
10Y
100Y
1000Y
TIME AFTER SHUTDOWN
(sec)

Figure IV-4

V. Radiation Damage in ISSEC

V-A. Displacement Damage and Gas Production

While the radiation damage in the first structural wall is being reduced to levels discussed in Section III, the ISSEC itself encounters the same sort of high energy neutron fluxes that the first wall would without an ISSEC. That gives rise to the dpa rates on the order of 8-13 dpa/yr and helium production rates on the order of 20-2400 Appm He/yr (the high number being for carbon) per 1 MW/m^2 neutronic wall loading in the front few layers of an ISSEC.

Dpa rates, helium and hydrogen production rates in the five ISSEC materials as a function of distance into the ISSEC are tabulated in Tables V-1 and V-2, V-3, and shown in Figures V-1 and V-2, respectively.

The amount of helium generated in carbon may be somewhat overstated here, because the (n,n') 3α reaction cross sections used for carbon (as listed in ENDF) are actually the sum of (n,n') continuum and (n,n')3α. Nevertheless, the helium generation rate in carbon is expected to be much higher than in metals. It was originally thought that this much helium could coalesce to form large bubbles and cause considerable dimensional changes and tearing. But some recent experiments tend to show that helium generated in carbon may in fact diffuse out at T>800°C with almost 100% efficiency without any build-up inside.[28-30]

The bulk radiation effects in carbon and graphite have been reviewed elsewhere[31-40] and will not be covered in detail here. Basically, carbon or graphite goes through two stages during bombardment with neutrons. The first stage is shrinkage by different amounts in volume and the second stage is expansion. In most data reported to date on the dimensional changes in carbon and graphite with neutron irradiation, the reversal from shrinkage to expansion takes place at fluences of about 1-2 x 10^{22} n/cm^2 (5-10 dpa) at temperatures of 800-1400°C. Above 1400°C, the fluence required for runaway swelling is not certain at this time.[41,42] However, the bulk of the data predicts a lower damage rate at the higher temperatures.[42] The surface effects regarding carbon and graphite will be examined in Chapter VII.

Table V-1

Displacement Damage in Various ISSEC Materials

Distance From Front Surface (cm)	dpa/MW-yr per m^2				
	C	Mo	Nb	V	W
0	8.60	9.73	8.37	12.5	NA**
5	6.50	5.41	4.71	7.94	
10	4.91	3.16	2.91	5.28	
15	3.71	1.18	1.81	3.52	
20	2.80	0.95	1.07	2.25	
25	2.26	0.47	0.62	1.50	

** not available

Table V-2

Helium Production in Various ISSEC Materials

Distance From Front Surface (cm)	C	Appm He/1 MW-Yr/m² neutronic Mo	Nb	V	W
0	2340	43.0	21.8	54.5	3.71
5	1245	12.7	6.9	21.4	0.91
10	715	4.84	2.75	9.83	0.30
15	435	2.06	1.23	4.98	0.11
20	275	0.91	0.58	2.65	0.04
25	190	0.49	0.33	1.63	0.02

Table V-3

Hydrogen Production in Various ISSEC Materials

Distance From Front Surface (cm)	C	Appm H/1 $\frac{\text{MW-Yr}}{\text{m}^2}$ neutronic			
		Mo	Nb	V	W
0	None	70.5	71.3	91.3	7.98
5		20.9	22.7	36.4	1.95
10		7.96	9.05	16.9	0.65
15		3.39	4.06	8.66	0.23
20		1.50	1.93	4.69	0.084
25		0.80	1.12	3.02	0.036

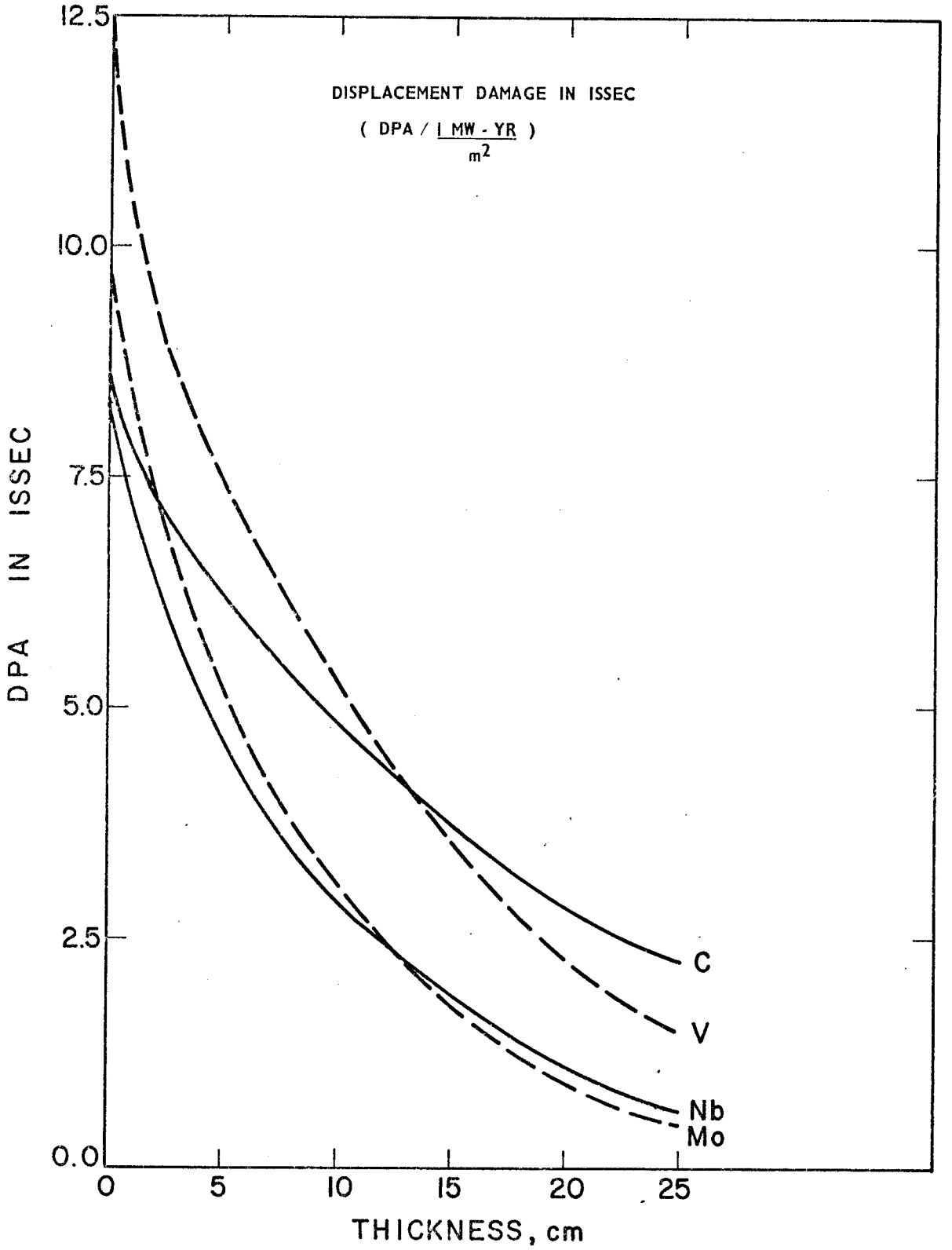
DISPLACEMENT DAMAGE IN ISSEC
(DPA / I MW - YR / m2)
DPA IN ISSEC
12.5
10.0
7.5
5.0
2.5
0.0
0
5
10
15
20
25
THICKNESS, cm
C
V
Nb
Mo

FIGURE V-1

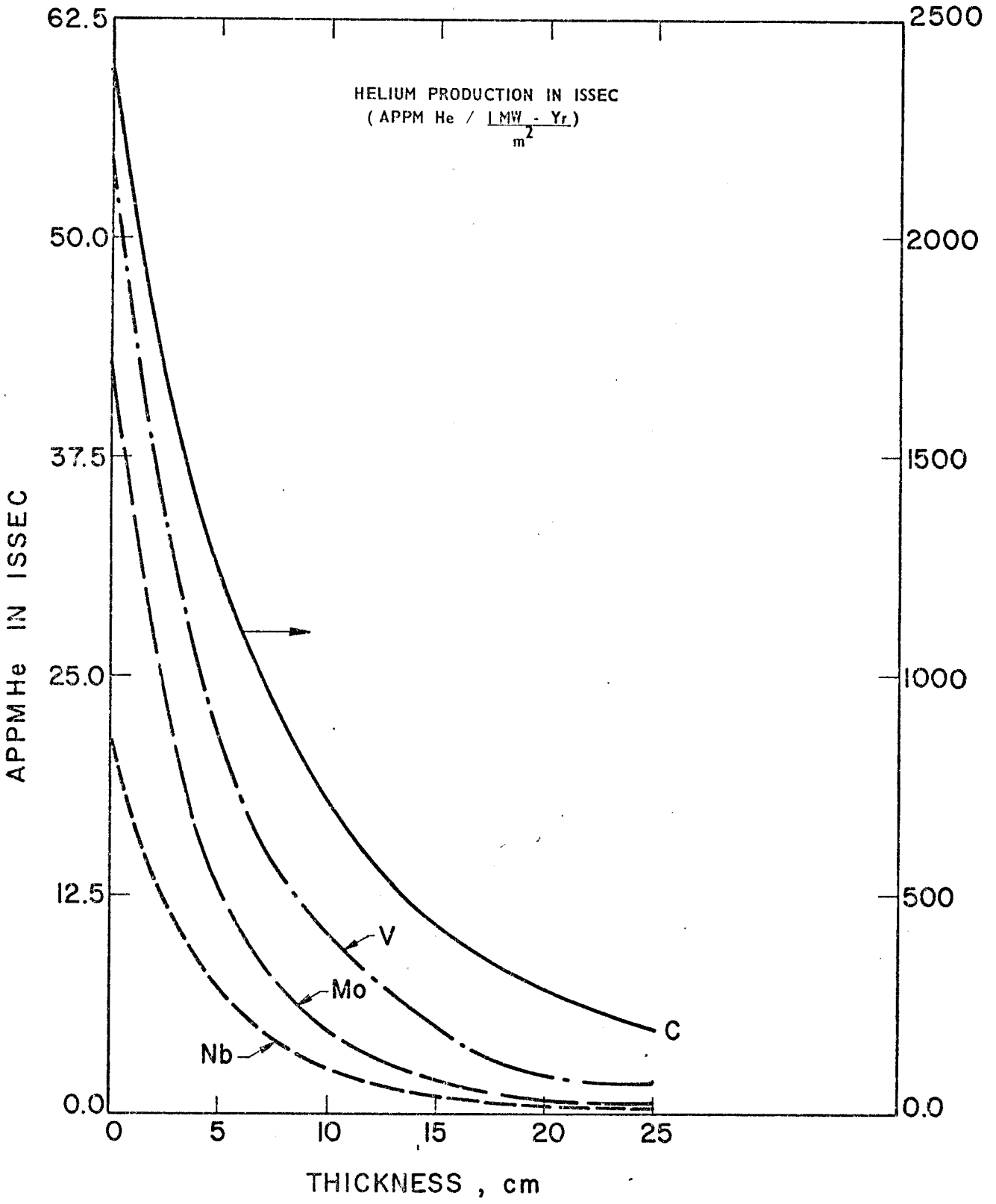
HELIUM PRODUCTION IN ISSEC
(APPM He / LMW - Yr)
m²
APPM He IN ISSEC
62.5
50.0
37.5
25.0
12.5
0.0
2500
2000
1500
1000
500
0.0
0
5
10
15
20
25
THICKNESS , cm
V
Mo
Nb
C

FIGURE V-2

The effect of the displacement rates and gas production rates as listed in Tables V-1, V-2 and V-3 on the metal ISSECs are not known, especially at temperatures of 1500-2000^{o}C. It is expected that at such high temperatures point defects such as vacancies and interstitials may anneal out or recombine quickly, and insoluble gas atoms will form bubbles. The lack of void swelling will be countered by the swelling due to gas bubbles and the net effect is also unknown at this time. However, an ISSEC, being a non-structural non-load bearing member, could operate with some deformations and cracks. As will be discussed in Chapter VI, if the ISSEC could be constructed in such a fashion that it is free to expand in all directions, tolerance limits might be quite liberal.

V-B. Radioactivity, Biological Hazard Potential and Afterheat of ISSEC

As discussed earlier, the ISSECs generally reduce the first wall activity while they themselves become active. The amount of activity induced in the ISSEC varies greatly depending on the ISSEC material. The activities of different materials for 5 cm ISSECs areshown in Figs. V-3, V-4, and V-5 with those for the first wall without an ISSEC.

One observation is that the activity of carbon, mainly from ^{6}He ($t_{1/2}$ = 0.8 sec), is three orders of magnitude lower than that of the others at shutdown. After one minute, the activity is dominated by ^{14}C ($t_{1/2}$ = 5730 yr) whose magnitude is six orders lower than the shutdown value of carbon.

The intensity of radioactivity at shutdown is highest for tungsten with molybdenum, niobium, and vanadium following in decreasing order. This order changes to tungsten, niobium, vanadium, and molybdenum after 1 year of decay. After 100 years, both molybdenum and niobium show the long-term

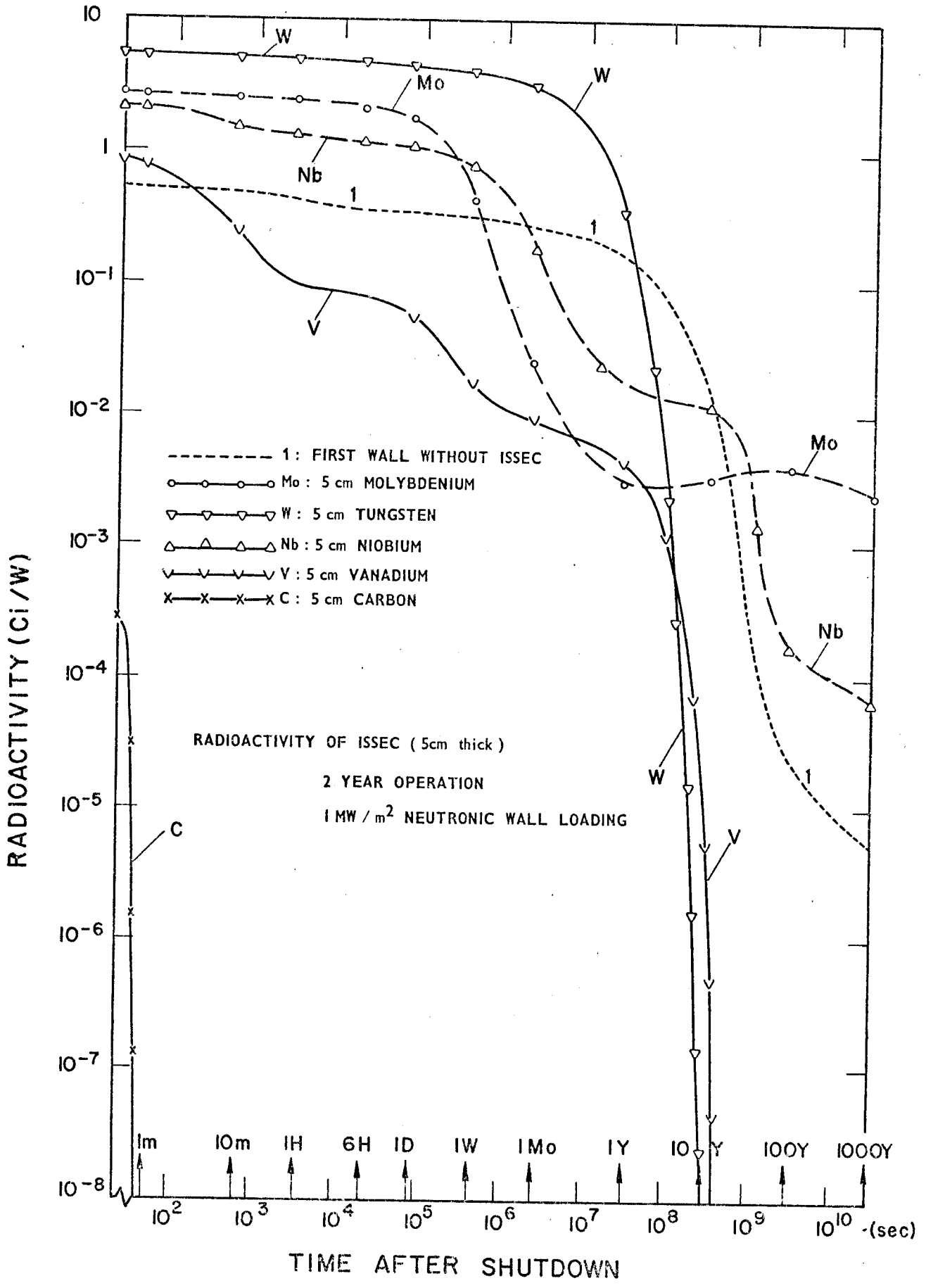
RADIOACTIVITY (Ci/W)
TIME AFTER SHUTDOWN
1 : FIRST WALL WITHOUT ISSEC
Mo : 5 cm MOLYBDENIUM
W : 5 cm TUNGSTEN
Nb : 5 cm NIOBIUM
V : 5 cm VANADIUM
C : 5 cm CARBON
RADIOACTIVITY OF ISSEC (5cm thick)
2 YEAR OPERATION
1 MW / m2 NEUTRONIC WALL LOADING
W
Mo
Nb
V
C
1
1m
10m
1H
6H
1D
1W
1Mo
1Y
10Y
100Y
1000Y
-(sec)

FIGURE V-3

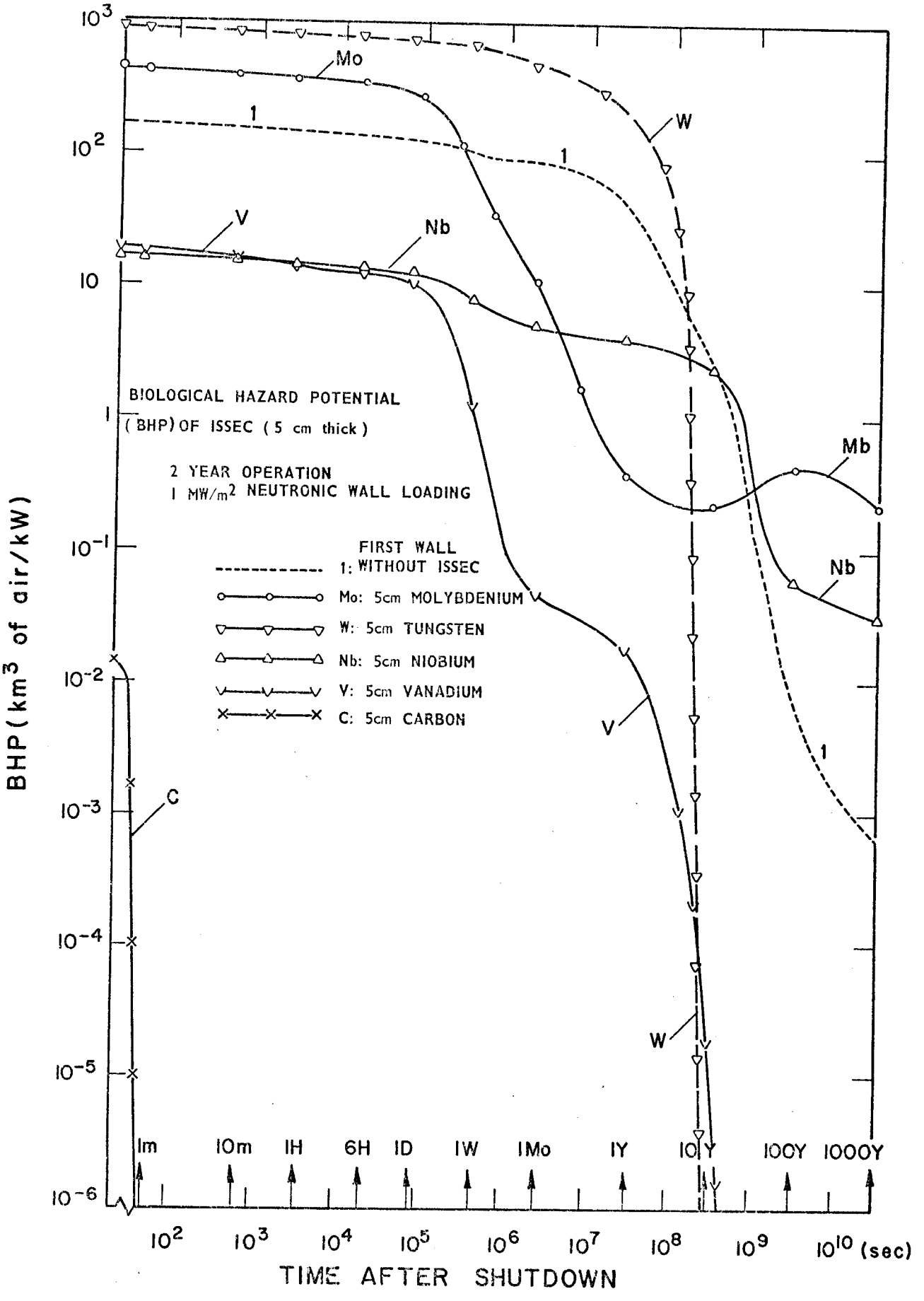
BIOLOGICAL HAZARD POTENTIAL
(BHP) OF ISSEC (5 cm thick)
2 YEAR OPERATION
1 MW/m2 NEUTRONIC WALL LOADING
FIRST WALL
1: WITHOUT ISSEC
Mo: 5cm MOLYBDENIUM
W: 5cm TUNGSTEN
Nb: 5cm NIOBIUM
V: 5cm VANADIUM
C: 5cm CARBON
Mo
W
V
Nb
Mb
C
1
BHP (km3 of air/kW)
10^3
10^2
10
1
10^-1
10^-2
10^-3
10^-4
10^-5
10^-6
1m
10m
1H
6H
1D
1W
1Mo
1Y
10Y
100Y
1000Y
10^2
10^3
10^4
10^5
10^6
10^7
10^8
10^9
10^10 (sec)
TIME AFTER SHUTDOWN

FIGURE V-4

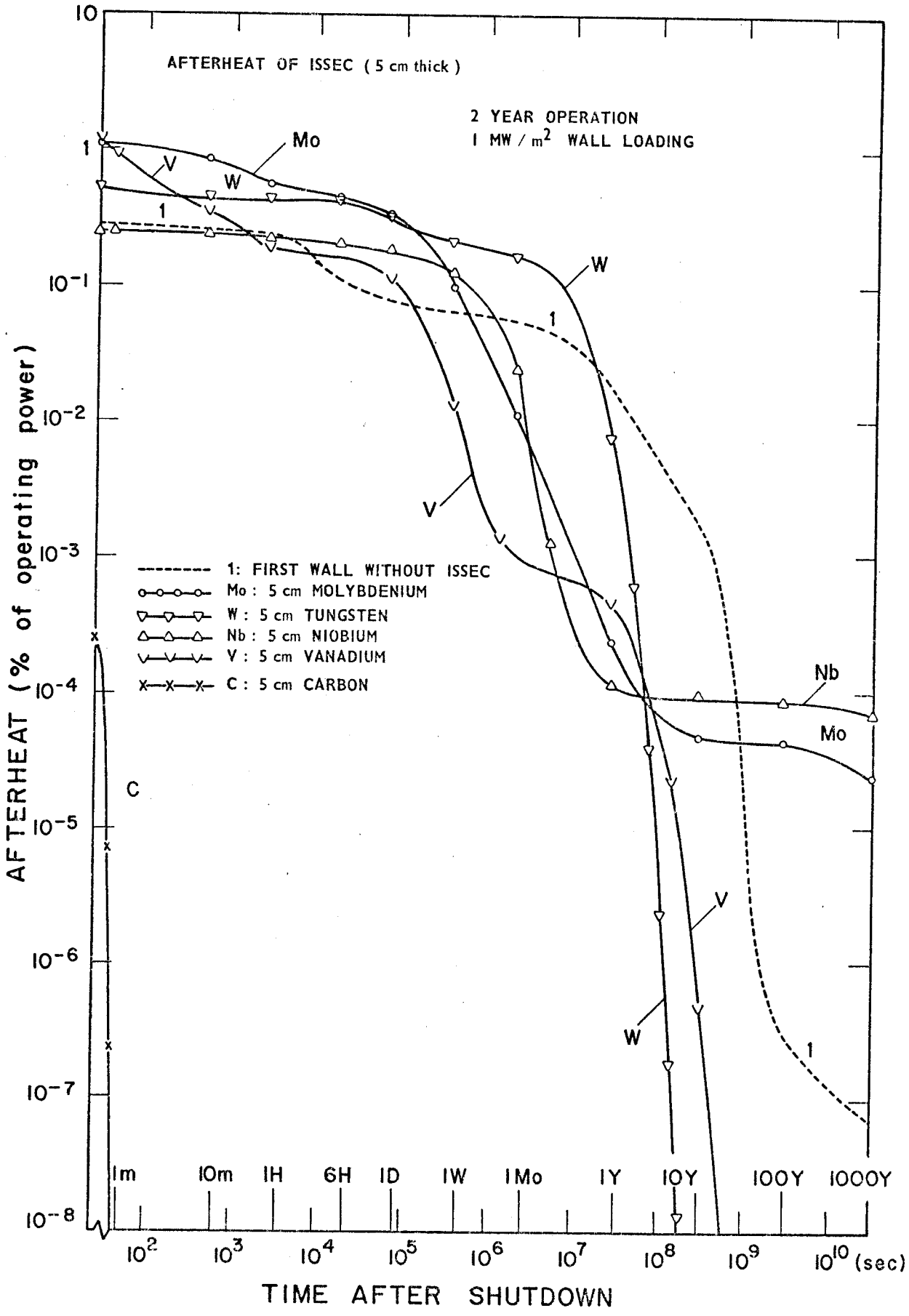
AFTERHEAT OF ISSEC (5 cm thick)
2 YEAR OPERATION
1 MW / m2 WALL LOADING
1: FIRST WALL WITHOUT ISSEC
Mo : 5 cm MOLYBDENIUM
W : 5 cm TUNGSTEN
Nb : 5 cm NIOBIUM
V : 5 cm VANADIUM
C : 5 cm CARBON
AFTERHEAT (% of operating power)
TIME AFTER SHUTDOWN
1m
10m
1H
6H
1D
1W
1Mo
1Y
10Y
100Y
1000Y
(sec)

FIGURE V-5

activities, and with the molybdenum level only three orders of magnitude lower than that at shutdown.

Table V-4 lists the radioisotopes (and their half lives) that are major contributors of radioactivity in ISSEC materials at various times after shutdown.

The biological hazard potential (BHP) of the ISSEC generally follows the behavior of radioactivity. BHP is another measure of radiological hazard by weighting the amount of radioactivity with the maximum permissible concentration of each radioisotope. The long-term BHP is governed by ^{93}Mo in the molybdenum ISSEC, and ^{93m}Nb in the niobium ISSEC.

The afterheat of the various ISSECs at shutdown varies among vanadium, molybdenum, tungsten, and niobium in decreasing order, and after 1 year of decay the order changes to tungsten, vanadium, molybdenum, and niobium. Beyond 100 years, only niobium and molybdenum show any afterheat, but at relatively minor levels.

Table V-4

Major Contributing Isotopes of Radioactivity in ISSEC Materials Considered in This Study

Time After Shutdown	C	Mo	Nb	V	W
Shutdown	^{6}He(0.8s)*	^{99}Mo(66.7 hr)	^{92m}Nb(10.2 d)	^{52}V(3.8 min)	^{185}W(75 d)
		^{99m}Tc(6.05 hr)	^{94m}Nb(6.3 min)	^{51}Ti(5.8 min)	^{181}W(140 d)
		^{91}Mo(15.5 min)			^{187}W(23.9 hr)
1 year	^{14}C(5730 yr)	^{93}Mo(1000 yr)	^{93m}Nb(13.6 yr)	^{49}V(330 d)	^{185}W(75 d)
			^{94}Nb(20,000 yr)		^{181}W(140 d)
>100 years	^{14}C(5730 yr)	^{93}Mo(1000 yr)	^{94}Nb(20,000 yr)		

* numbers given in parentheses are half lives

VI. Mechanical Design and Heat Transfer of ISSEC's

An ISSEC (Internal Spectrum Shifter and Energy Converter) is envisioned as some passive non-structural member placed between the plasma and the first structural vacuum wall. In the process of softening the neutron spectrum, a considerable amount of heat will be generated inside an ISSEC. This heat, plus the heat incident on the front surface of an ISSEC due to ions and electromagnetic radiation originating in the plasma, will have to be transferred to the blanket behind. We considered two processes by which heat could be transferred from an ISSEC to the first wall. They are thermal radiation and simple conduction mechanisms. For the present we have excluded any active cooling schemes for ISSECs.

For reasons of simplicity in design radiation cooled ISSECs made of a high temperature material like graphite or a refractory metal have received the most attention. Figure VI-1 shows the temperature profiles in 5, 10 and 25 cm thick carbon and molybdenum ISSEC's cooled by radiation only. All radiating metal surfaces were assumed to be painted black and were assigned thermal emissivities of 0.9. The neutron wall loading was 1 MW/m^2 and the surface heat load was taken to be 4 W/cm^2. The heating rates used were calculated by the ANISN[11] program. The structural first wall temperature was assumed to be 500^oC. Figure VI-2 shows the front and back surface temperatures of carbon, niobium, and vanadium ISSECs as a function of increasing ISSEC thickness. Table VI-1 lists the front and back surface temperatures of the five ISSEC materials considered at 5, 10 and 25 cm thickness and Table VI-2 gives some selected thermal properties of importance for the ISSEC materials and stainless steel.

We see from Figures VI-1, VI-2 and Tables VI-1 and VI-2 that beyond some certain thickness the front surface temperature of the spectral shifter

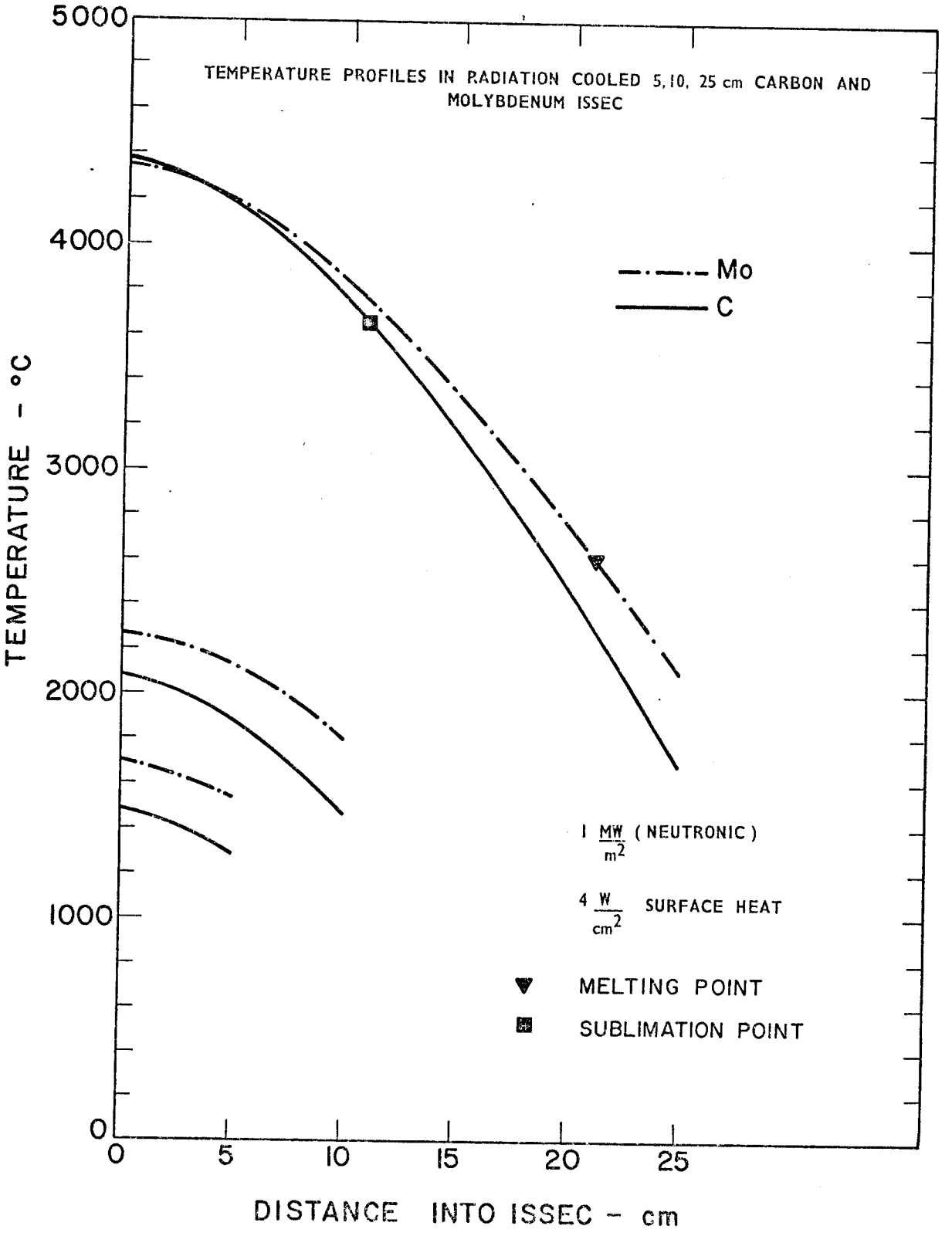
TEMPERATURE PROFILES IN RADIATION COOLED 5, 10, 25 cm CARBON AND MOLYBDENUM ISSEC
Mo
C
1 MW/m² (NEUTRONIC)
4 W/cm² SURFACE HEAT
MELTING POINT
SUBLIMATION POINT
TEMPERATURE - °C
DISTANCE INTO ISSEC - cm
5000
4000
3000
2000
1000
0
0
5
10
15
20
25

Figure VI-1

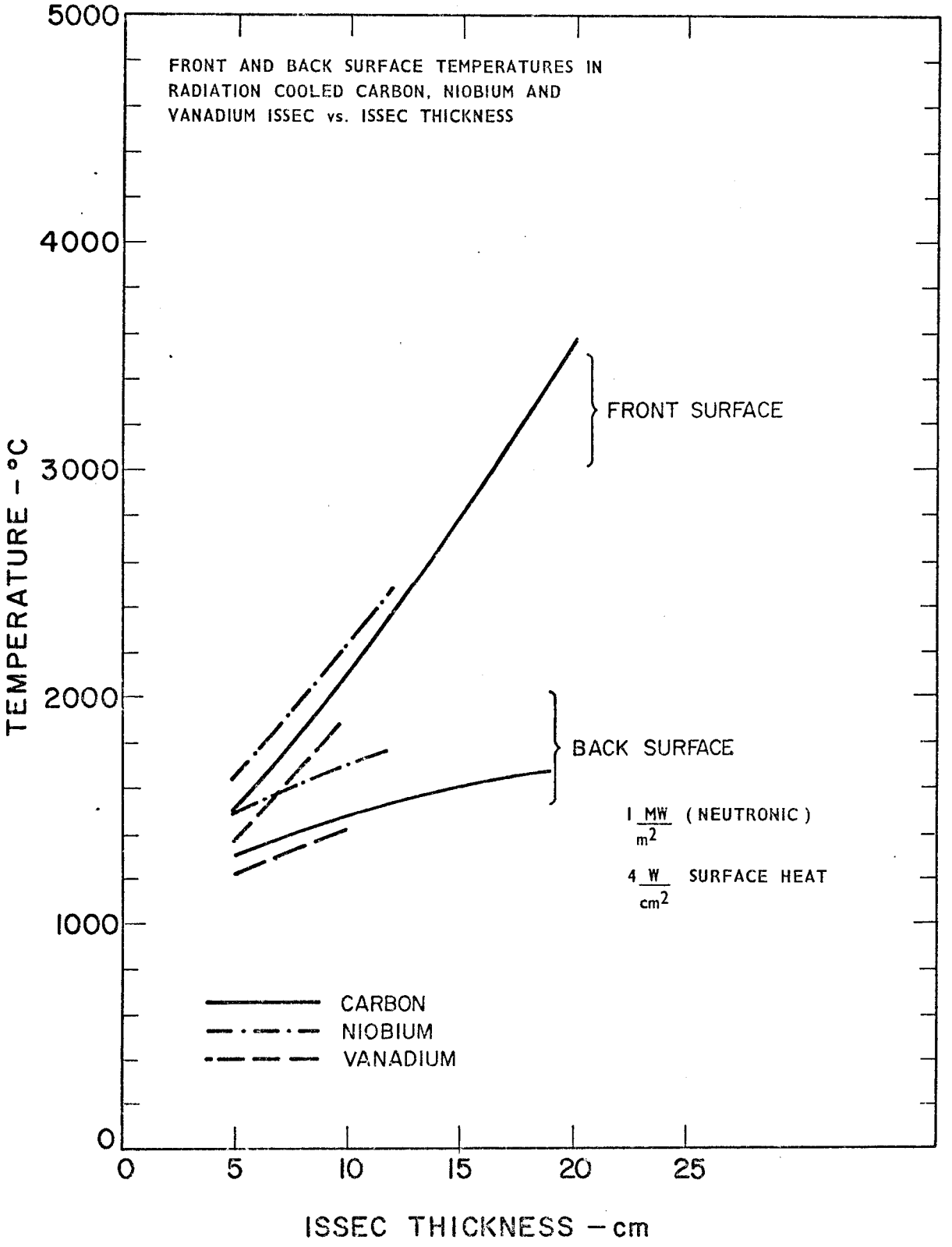
FRONT AND BACK SURFACE TEMPERATURES IN
RADIATION COOLED CARBON, NIOBIUM AND
VANADIUM ISSEC vs. ISSEC THICKNESS
5000
4000
3000
2000
1000
0
TEMPERATURE - °C
0
5
10
15
20
25
ISSEC THICKNESS — cm
FRONT SURFACE
BACK SURFACE
1 MW/m² (NEUTRONIC)
4 W/cm² SURFACE HEAT
CARBON
NIOBIUM
VANADIUM

Figure VI-2

Table VI-1

Front and Back Surface Temperatures in the

Radiation Cooled 5, 10 and 25 cm ISSEC's*

(°C)

	5 cm ISSEC		10 cm ISSEC		25 cm ISSEC	
Material	T_{Front}	T_{Back}	T_{Front}	T_{Back}	T_{Front}	T_{Back}
C	1480	1290	2085	1465	(**)	1680
Mo	1670	1545	2265	1810	(**)	2110
Nb	1630	1485	2210	1710	(**)	1960
V	1370	1215	(**)	1400	(**)	1755
W	1790	1630	2350	1850	(**)	2060

*For 1 MW/m^2 neutronic and 4 W/cm^2 surface heat loading

**Exceeds melting point

Table VI-2

Selected Thermal Properties of Importance

For ISSEC Materials and 316 S.S.

Property	C	Mo	Nb	V	W	Steel
Melting point (°C)	~3600° (sublime)	2620	2468	1900	3400	~1430
Thermal Conductivity (W/cm°C)						
100°C	1.46	1.34	0.48	0.32	1.63	0.17
400°C	1.00	1.21	0.50	0.35	1.36	0.21
800°C	0.68	1.11	0.53	0.39	1.17	0.27
1200°C	0.52	0.98	0.61	0.45	1.09	---
1600°C	0.44	0.92	0.65	0.47	1.03	---
Coefficient of Thermal Expansion ($°C^{-1} \times 10^{-6}$)						
100°C	2	5	7	9	5	16.5
400°C	8	5	7	10	5	17.5
800°C	13	6	9	11	5	19.0
1200°C	17	6	10	13	6	---
1600°C	19	7	11	15	6	---
Heat Capacity ($\frac{W\text{-}sec}{gr\ °C}$)						
100°C	0.96	0.26	0.27	0.46	0.13	0.46
400°C	1.51	0.28	0.29	0.55	0.14	0.54
800°C	1.80	0.31	0.31	0.64	0.15	0.63
1200°C	1.95	0.33	0.33	0.72	0.16	---
1600°C	2.05	0.36	0.36	0.80	0.16	---
Vapor Pressure (torr)						
1500°C	2.5×10^{-10}	1.2×10^{-9}	5.4×10^{-11}	5×10^{-4}	3.7×10^{-15}	1×10^{-1}
2000°C	1.0×10^{-5}	1.9×10^{-5}	2.5×10^{-6}	---	1.2×10^{-9}	---
2500°C	2.4×10^{-2}	8.6×10^{-3}	---	---	4.1×10^{-6}	---
3000°C	5.0	---	---	---	1.2×10^{-3}	---

exceeds the melting point of the material. Obviously one can not allow the ISSEC to melt during operation. If the absolute maximum temperature the front wall of the ISSEC can attain is taken to be the melting point of the respective material, it is found that with radiation cooling only, ISSEC's can not have a thickness any greater than 20.5 cm for carbon and 13 cm, 11.5 cm, 10 cm and 18.5 cm for Mo, Nb, V and W respectively. In actual practice the limits would be set much lower than these given here.

In a tokamak reactor the pressure inside the plasma chamber is $\sim 10^{-5}$ torr. Another important thickness criteria then is that the vapor pressure of any material enclosed in the vacuum chamber be kept below that value. Figure VI-3 plots the vapor pressure of the five ISSEC materials considered in this study versus temperature. If we draw a line at 10^{-5} torr, that sets an upper limit on the maximum temperature a carbon ISSEC can have at about 2000°C, Mo at ~1950°C, Nb 2100°C, V ~1300°C, and W 2600°C. These temperatures under the conditions stated previously, translate into maximum allowable thicknesses of 9.5 cm for C, 7.5 cm for Mo, 9 cm for Nb, and 4.5 cm for V and 12.5 cm for W as shown in table VI-3.

It is important that a radiation cooled ISSEC be an unrestricted, free to move body. Otherwise the kind of thermal stresses set up inside an ISSEC of any appreciable thickness will far exceed the yield strength of the material at such elevated temperatures. One such scheme where the ISSEC could expand freely in all directions could be an ISSEC made up of a series of square plates. Each square plate could be attached to the first wall through its center by a non-conducting ceramic stud. Because of the type of temperature profile shown in fig VI-1, the front wall of the ISSEC will expand more than the back surface and the square plate would tend to bow outwards (towards the first wall).

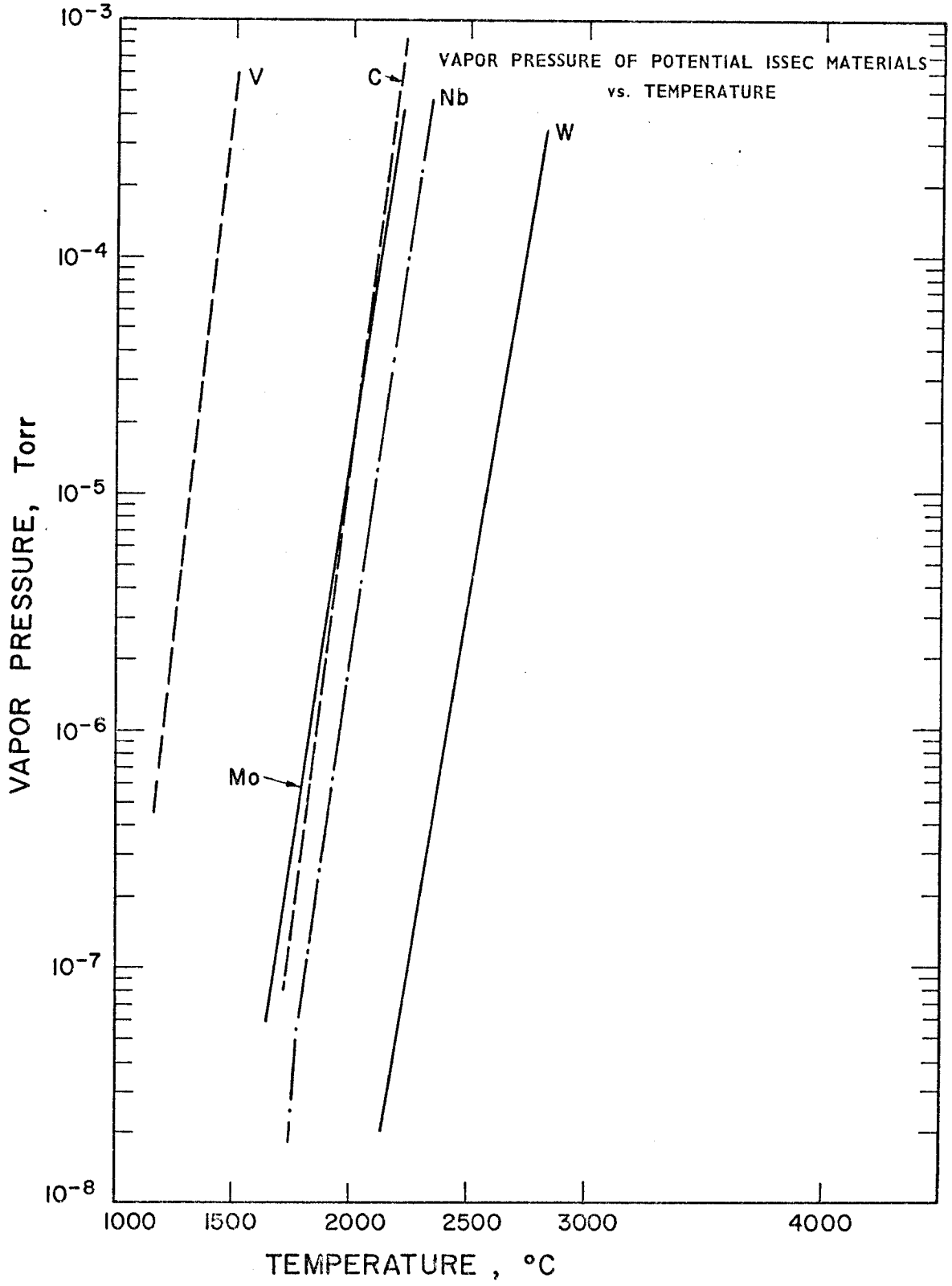
VAPOR PRESSURE OF POTENTIAL ISSEC MATERIALS
vs. TEMPERATURE
V
C
Nb
W
Mo
VAPOR PRESSURE, Torr
10-3
10-4
10-5
10-6
10-7
10-8
1000
1500
2000
2500
3000
4000
TEMPERATURE , °C

Figure VI-3

Table VI-3

Maximum Allowable ISSEC Thicknesses[a] in Three Limiting Cases With Radiation Cooling Only

ISSEC Material	Maximum Temperature Limit[b] (cm)	Maximum Vapor Pressure Limit (cm)	Breeding Ratio[c] Limit (cm)
C	20.5	9.5	13
Mo	13	7.5	10
Nb	11.5	9	8.5
V	10	4.5	18.5
W	18.5	12.5	6

(a) 1 MW/m^2 neutronic and 4 W/cm^2 surface heat load.
(b) For melting.
(c) For the model blanket used in this study and a breeding ratio of 1.0.

The absolute maximum temperature would be reached when the inside corners of the plate touch the 316 SS first structural wall to cause partial melt-down of the first wall.

If an ISSEC is taken as a square plate of length ℓ and thickness t, and the temperature profile inside it is considered as linear, the deflection x at the corners of the plate due to differential expansion between the front and the back surfaces is

$$x = \frac{\ell^2}{2t} \alpha\Delta T$$

where α is the thermal expansion coefficient and ΔT is the temperature difference between the front and the back. As an example, if the plates are 20 cm x 20 cm by 5 cm thickness, and are attached to the first wall by 1.0 cm long studs and if we set the maximum deflection x at 0.25 cm,the maximum temperature difference between surfaces, ΔT is found to be 350°C for carbon, 1035°C for Mo, 620°C for Nb, 475°C for V and 1550°C for W. If the plate thickness is 10 cm, ΔT_{max} is 700°C for carbon, 2070°C for Mo, 1240°C for Nb, 950°C for V and 3100°C for W. As we see from table VI-1, these numbers are well above the actual temperature differences calculated. So it appears that with proper choice of the size of the plates and the length of the connecting studs both carbon and metal ISSECs can run safely without ever touching the first wall.

In the hot state during the time of normal operation most stresses will be relieved by creep so that the plate will be stress free. Several questions then arise such as, how fast will the ISSEC cool down if the plasma is suddenly turned off? Will there be any residual stresses to cause an ISSEC to rupture?

We have calculated the temperature profiles in carbon and molybdenum ISSECs as a function of time after shutoff. The results are plotted in

figures VI-4 and VI-5 and Figure VI-6 shows the front and back surface temperatures of carbon and molybdenum ISSEC's as a function of time.

It is apparent from figures VI-4 - VI-6 that it takes a short time for the temperature profile in a 5 cm ISSEC to flatten out by conduction and then a relatively long time to cool down to first wall temperatures by radiation. Since flattening out of the temperature profiles takes place still at high temperatures and in times on the order of 5-10 minutes the material might have enough time to respond to any internal stresses that may be generated. After the first flattening out of the temperature profile it is like uniform cooling of an unsupported free plate with no stresses produced. Of course, one needs to do a detailed calculation to show how much those stresses actually are, but it is expected that in a radiation cooled ISSEC (free to expand in all directions and attached to the first wall through its center by a non-conducting ceramic stud), the limiting factor on the maximum allowable thickness that can be used will be the vapor pressure criteria rather than the thermal stresses.

If an ISSEC could be designed in such a way that it can still expand freely in all directions to minimize thermal stresses, but cooled by conduction plus radiation so that the front surface temperature is lower than the pure radiation cooled ISSEC case, thicker ISSECs could be used in actual designs. One such design will be described below but it should be emphasized that this is <u>not</u> the only way an ISSEC can be supported from and conduct its heat to the first wall. The following is an example only.

Assume the ISSEC is made up of an array of rectangular plates with each plate having its longer dimension along the toroidal axis of a tokamak reactor plasma chamber. Behind each plate there is the structure shown in Figure VI-7 and the attachment of the plates to the first wall is

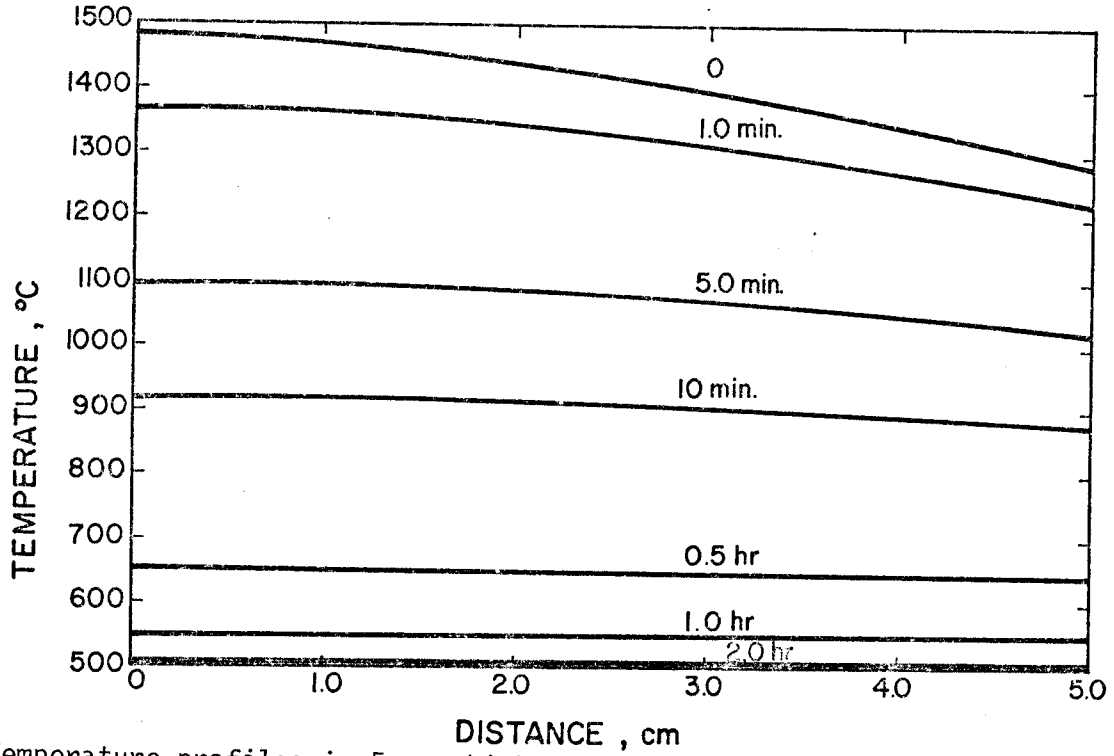

Fig. VI-4 Temperature profiles in 5 cm thick radiation cooled carbon ISSEC at times after shutdown

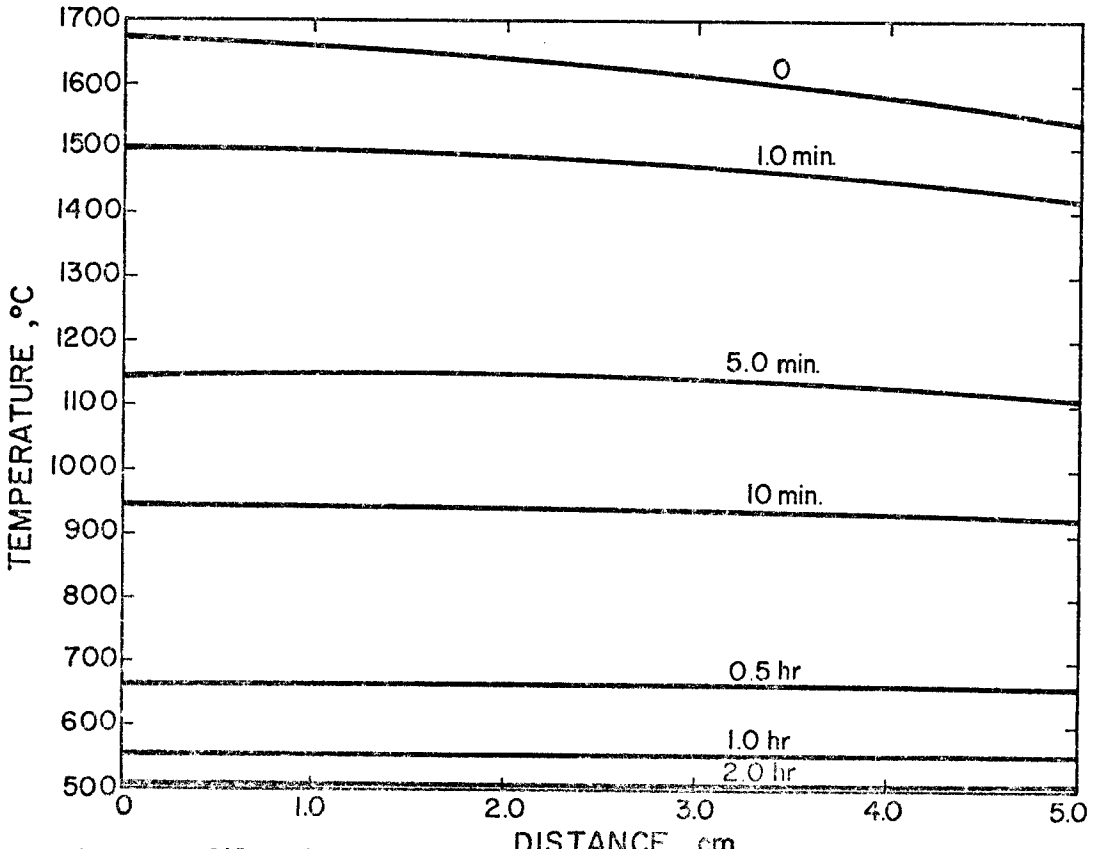

Fig. VI-5 Temperature profiles in 5 cm thick radiation cooled molybdenum ISSEC at times after shutdown

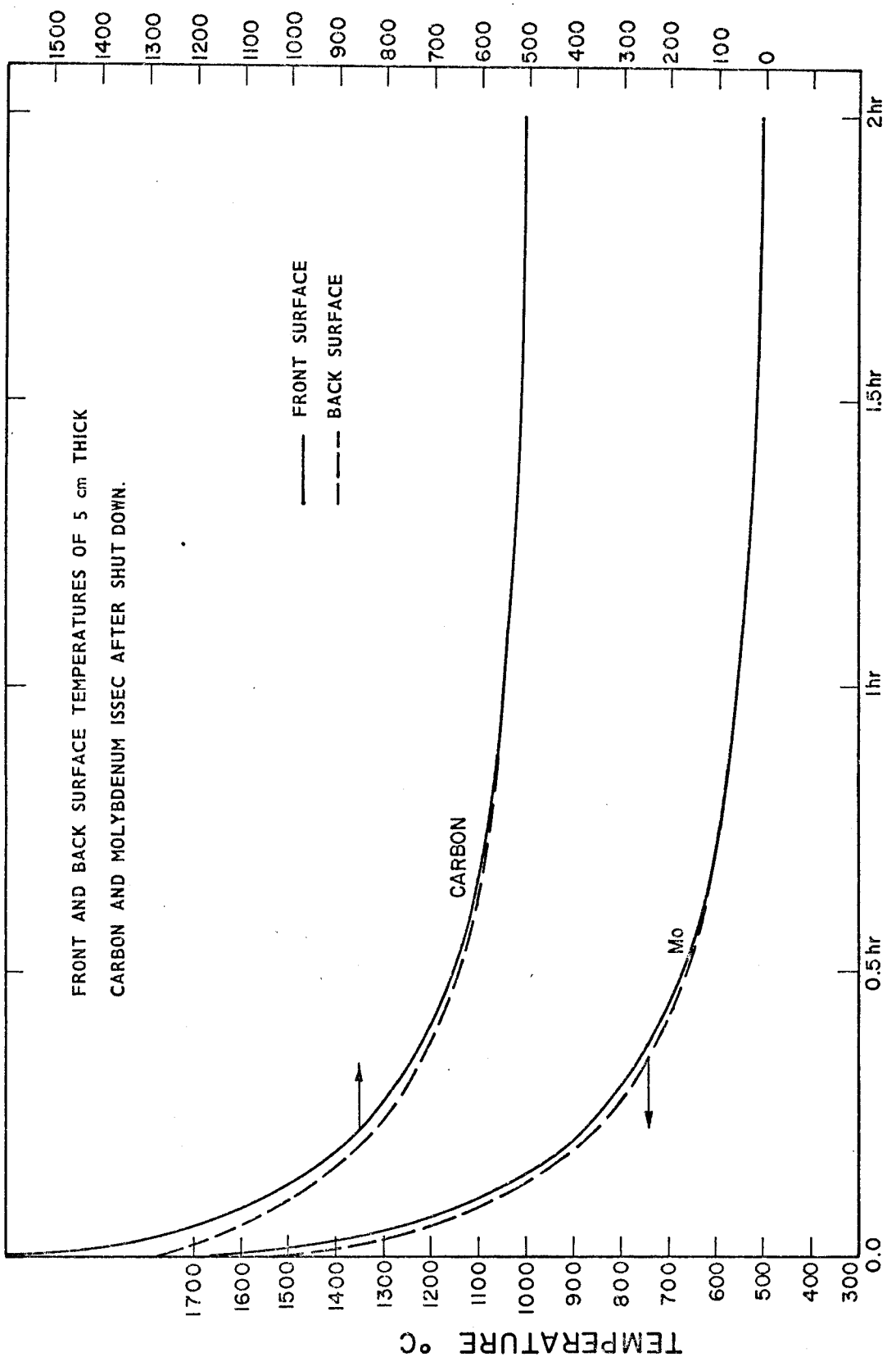
FRONT AND BACK SURFACE TEMPERATURES OF 5 cm THICK
CARBON AND MOLYBDENUM ISSEC AFTER SHUT DOWN.
FRONT SURFACE
BACK SURFACE
CARBON
Mo
TEMPERATURE °C
TIME AFTER SHUT DOWN
0.0
0.5hr
1hr
1.5hr
2hr
300
400
500
600
700
800
900
1000
1100
1200
1300
1400
1500
1600
1700
0
100
200
300
400
500
600
700
800
900
1000
1100
1200
1300
1400
1500

Fig. VI-6

Side and Front View of ISSEC Plates Cooled by
Conduction Plus Radiation

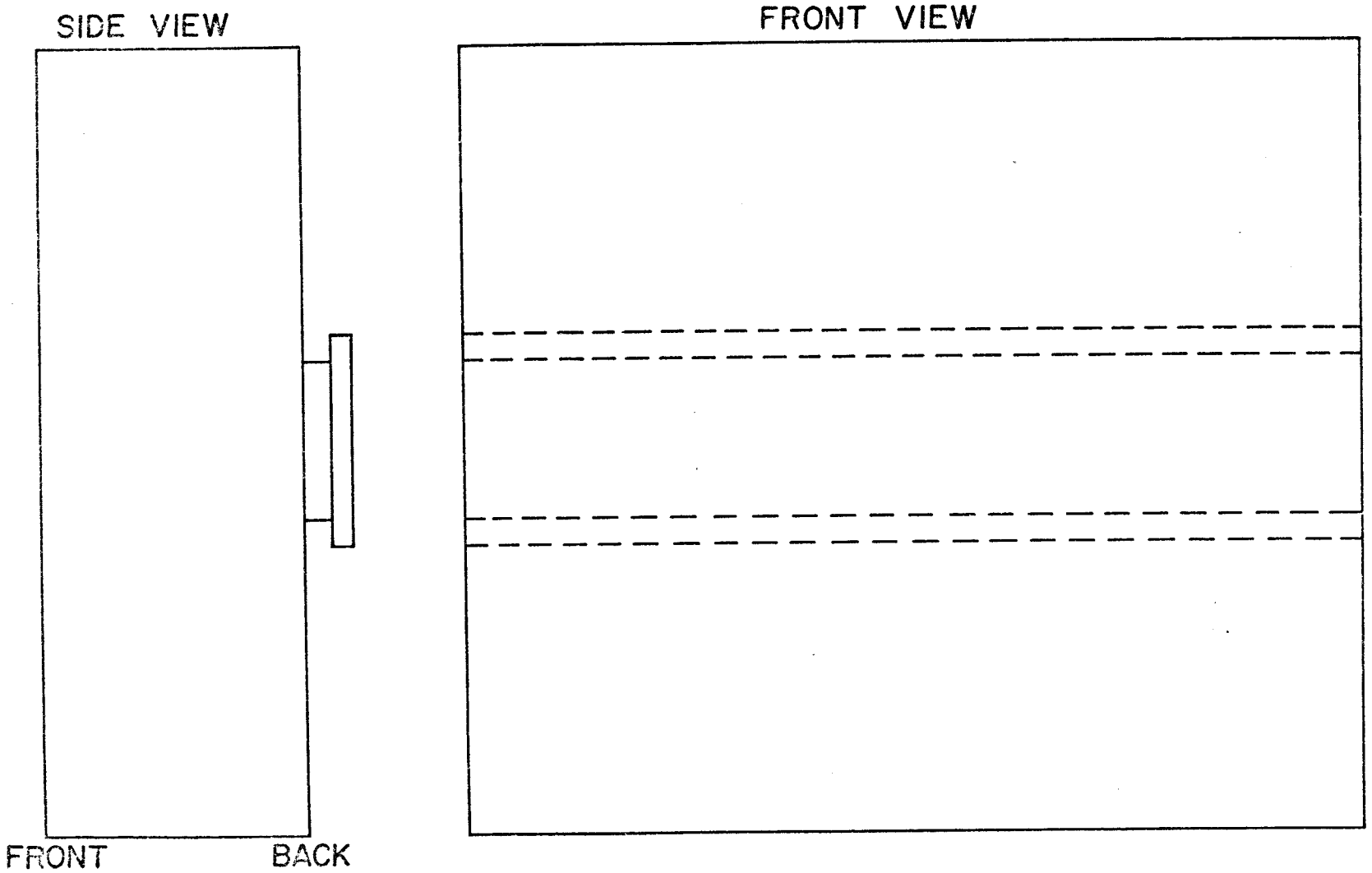

Figure VI-7

illustrated in Figure VI-8. The stem connecting the ISSEC to the first wall may or may not be of the same material as the ISSEC. If it would be necessary to change the ISSEC during the lifetime of the plant, plates could be moved in and out of each module along those tracks. If the ISSEC is stuck to the first wall, it could be cutoff from the stem, and the other two spare slots in the first wall under each plate, shown in figure VI-8, can be used. If the diamond shaped blanket concept of I. Sviatoslavsky[43] or rectangular shaped blanket model of R. Benenati et al.[44] or the cassette blanket concept of D. Steiner et al.[45] with sliding first walls is adopted, changing the ISSEC should be fast and easy. Figure VI-9 shows schematically the blanket arrangement of I. Sviatoslavsky with a diamond shaped first wall arrangement. The arrows show the directions in which each blanket segment moves.

Because of symmetry, the heating rates and temperature do not vary along the toroidal length of the plates. The variation in temperature is only along the width (poloidal direction) and thickness of each plate. Along the poloidal direction the temperature can be taken as symmetrical with respect to the centerline. Fig. VI-10 shows half the side view of 5 cm thick 15 cm wide molybdenum ISSEC. The nodal points 14 and 15 were assumed at 500°C constant temperature. The connecting stem, 0.5 cm long, was also taken to be molybdenum and good contact was assumed between the ISSEC and the 316SS first wall. The temperatures shown at the nodal points are for three different contact areas between the ISSEC and the first wall; 15%, 20% and 22.5% of the ISSEC back surface. The heat was assumed to be transferred through the throat by conduction only. It was found that in this case more than 90% of heat transfer was by conduction and inclusion of radiative heat transfer did not change nodal point temperatures by more than 5%. Figure VI-11 shows the nodal temperatures in 5 cm thick, 15 cm wide ISSEC plates of molybdenum, niobium, vanadium, tungsten and carbon. Figure VI-12 shows the temperatures for 10 cm thick ISSEC cases. For

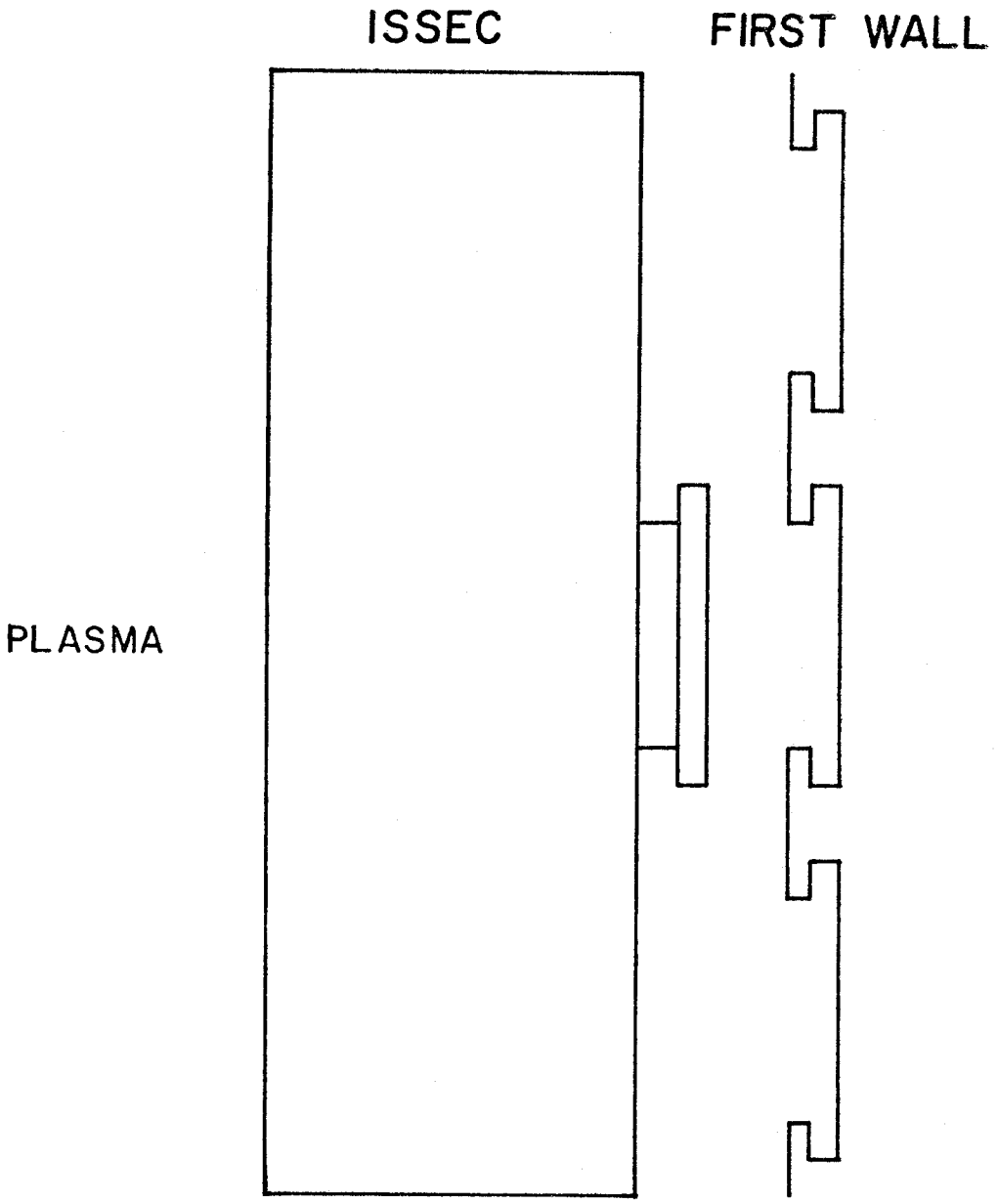

Figure VI-8

Attachment of Conduction Plus Radiation Cooled ISSEC to the First Wall

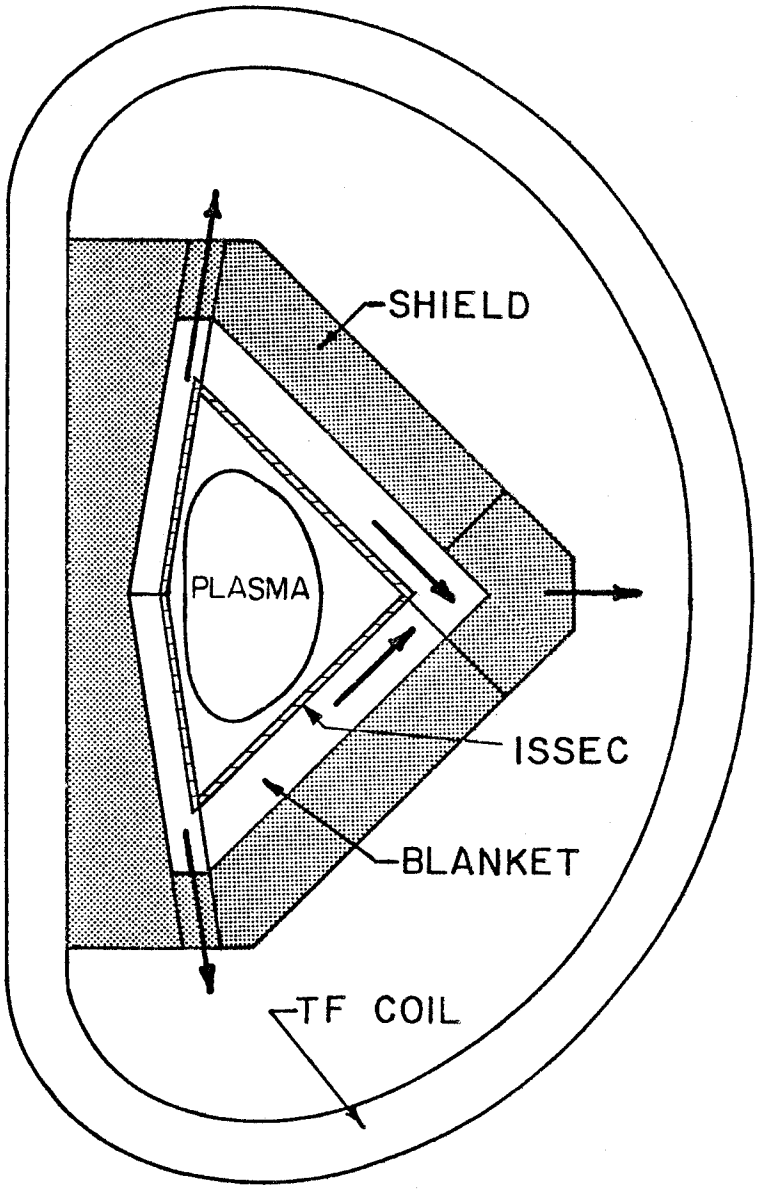

Figure VI-9 Incorporation of ISSEC into Moveable Blanket Concept[43]

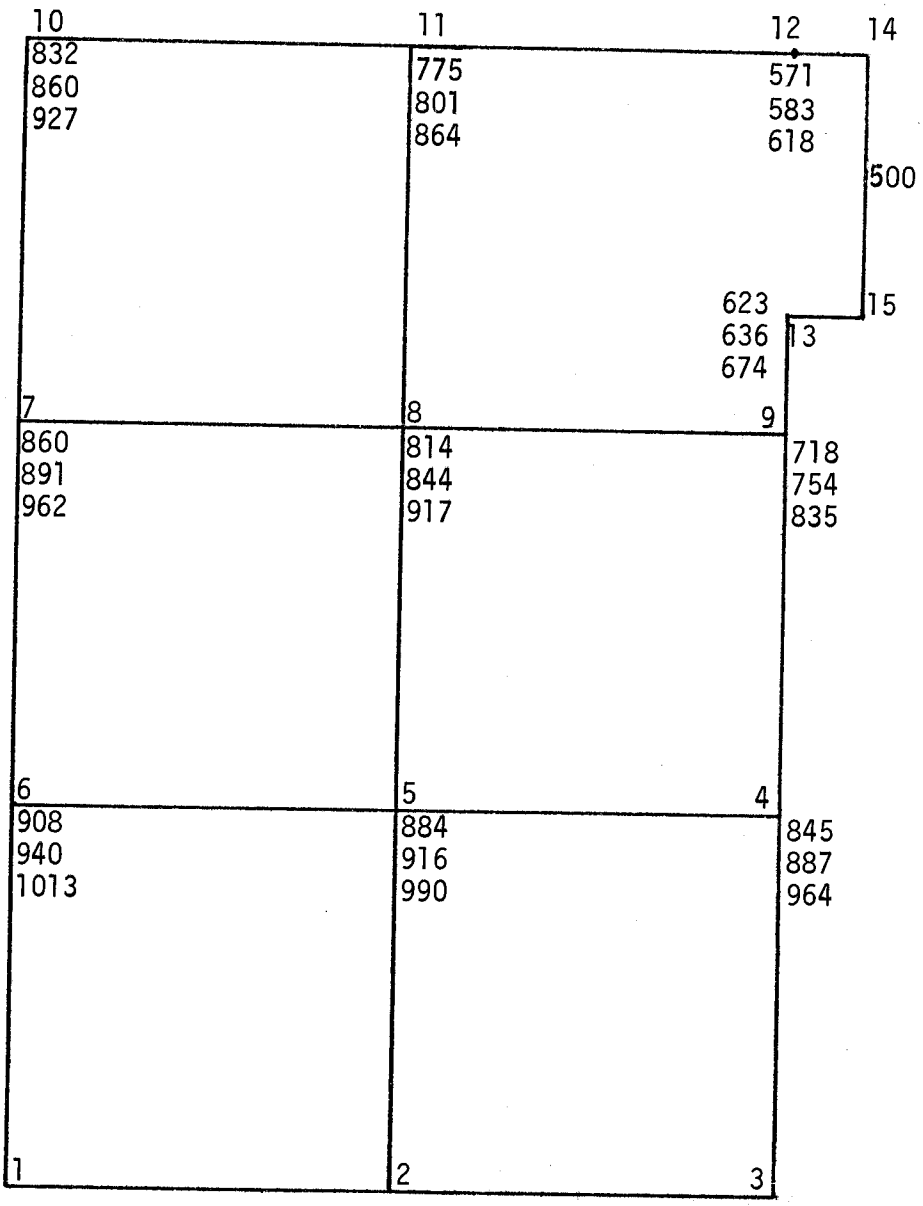

Contact Area 22.5%:	932	909	889
20%:	964	941	921
15%:	1037	1015	997

Temperatures (^{o}C) in 5 cm thick, 15 cm wide molybdenum ISSEC, cooled by conduction only, for three different conduction areas.

Figure VI-10

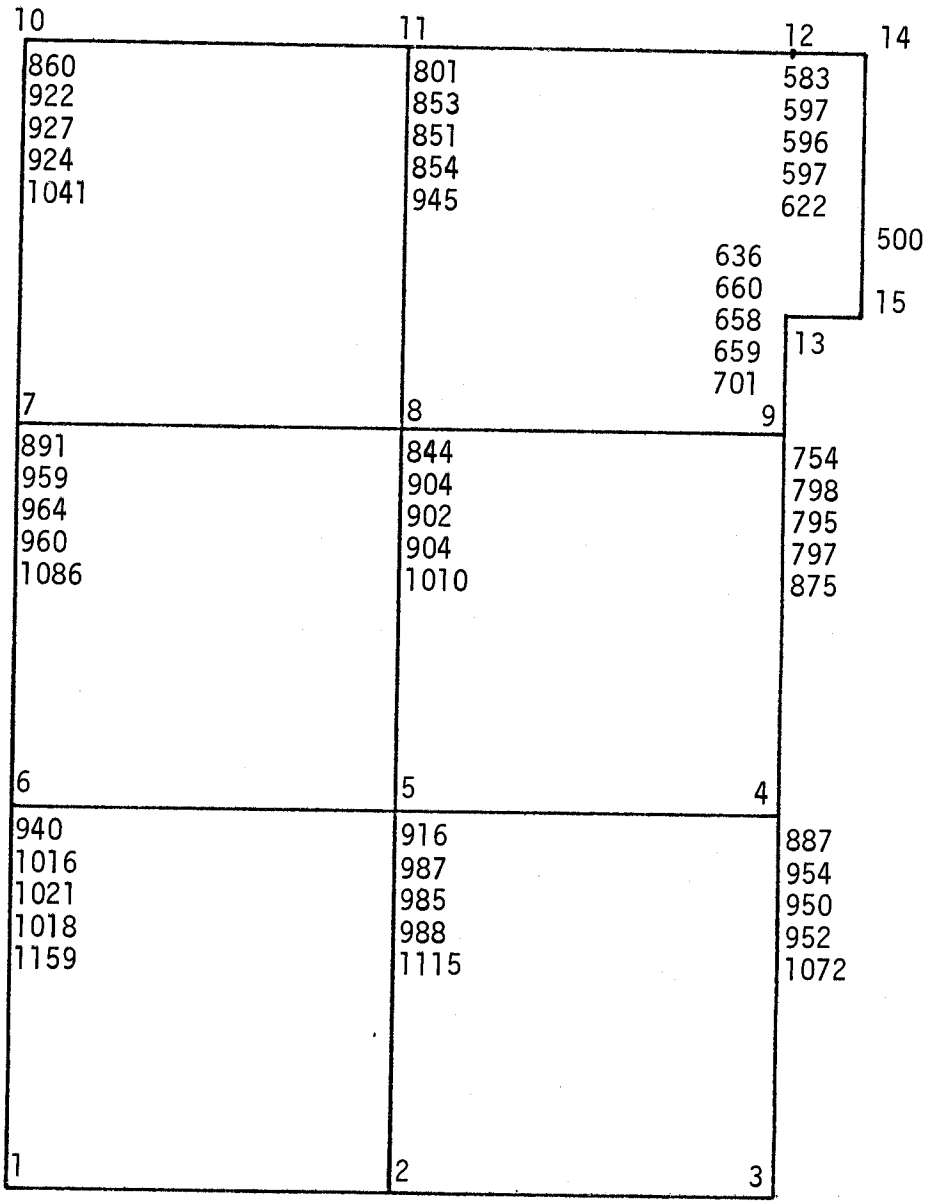

Molybdenum:	964	941	921
Niobium :	1044	1017	994
Vanadium :	1048	1014	990
Tungsten :	1045	1017	992
Carbon :	1193	1152	1122

Nodal point temperatures (^{o}C) in 5 cm thick, 15 cm wide ISSECs cooled by conduction only. Contact area is 20% of ISSEC back surface area.

Figure VI-11

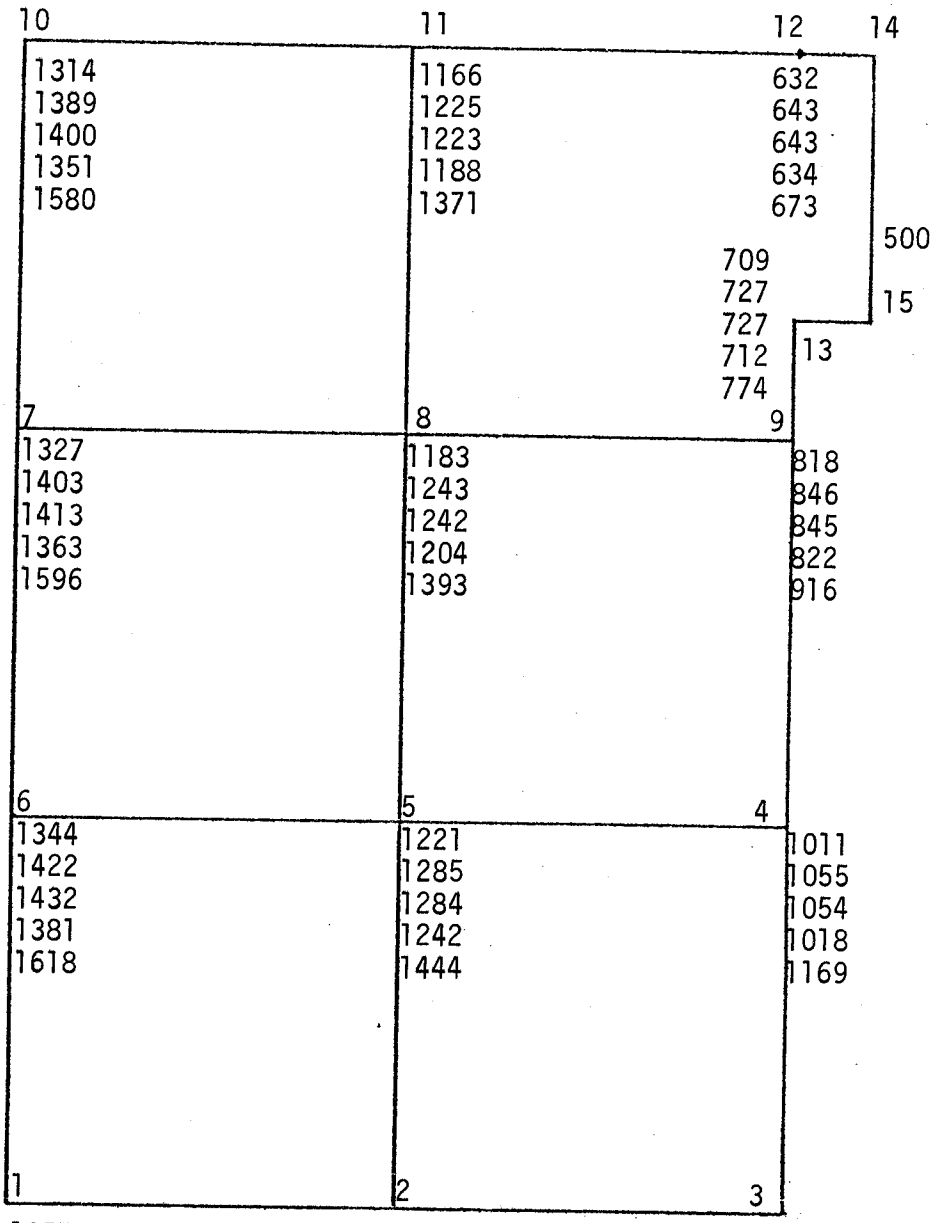

Molybdenum:	1357	1236	1064
Niobium :	1435	1300	1113
Vanadium :	1445	1300	1112
Tungsten :	1393	1255	1073
Carbon :	1634	1463	1239

Nodal point temperatures (^{o}C) in 10 cm thick, 15 cm wide ISSECs cooled by conduction only. Contact area is 22.5% of ISSEC back surface area.

Figure VI-12

both figures VI-11 and VI-12 the connecting stem was taken as 0.5 cm long and the same material as the ISSEC.

For the 5 cm thick ISSEC cases, a contact area equivalent to 20% of ISSEC back surface (3.0 cm^2 per cm of length of rectangular slab of 15 cm width) was assumed. Contact area was 22.5% for 10 cm cases. Actually the above assumptions are for the cross sectional area of the throat between the ISSEC and the first wall. As can be seen from Figures VI-7 and VI-8, the actual heat transfer area between the ISSEC and the first wall will be higher than just the area of the throat, especially if the material making up the ISSEC and the connecting stem has a much higher thermal conductivity than the first wall material, which is the case with 316 SS and materials considered for an ISSEC in thisstudy. The significance of this increase in contact area is not only that the temperatures shown in figures IV-10 - IV-12 will be lower than shown but also the flux of heat conducted to the first wall will be less. Table VI-4 lists the total heat generated in 5 and 10 cm thick ISSECs per cm of length and 15 cm of width. It also gives the amount of heat conducted to the first wall, conduction heat flux, temperature drop across 316 SS first wall and the thermal stresses generated in it for the given heat fluxes. The yield strength of 316 SS is 475 Mpa at 500°C and higher at lower temperatures. The thermal stresses listed in Table VI-4 are lower than 475 Mpa by 12-75%. If another material with a higher thermal conductivity were to be used for the first wall, the temperature gradients and thermal stresses listed in table IV-4 would be lower by as much as the increase in thermal conductivity.

Even though the ultimate ISSEC design has not been presented it can be seen from calculations that a 1 MW/m^2 neutronic and 4 W/cm^2 surface heat loading would allow either a graphite or a metal ISSEC with thicknesses of at least 15 cm to be employed in a tokamak reactor of dimensions similar to the UWMAK class.[4,5,24]

Table VI-4

Generation and Conduction of Heat From ISSECs to 316 SS First Wall and the Thermal Stress Generated in the First Wall

ISSEC Thickness (cm)	ISSEC Material	Total Heat[1,2] Generated (W)	Total Heat Conducted (W)	Conduction[5] Heat Flux to First Wall (W/cm^2)	Temp.[6] Drop Across First Wall (°C)	Thermal[6] Stresses in First Wall (Mpa)
5	C	330	352[3]	65.2	74.1	144
	Mo	688	674	125	142	275
	Nb	592	586	109	124	240
	V	262	290	53.7	61.0	119
	W	844	814	151	172	332
10	C	550	488[4]	84.1	95.6	185
	Mo	1254	1052	181	206	397
	Nb	1002	850	147	167	323
	V	470	414	73.1	83.1	161
	W	1320	1104	190	216	417

(1) For 15 cm width and unit length plates.

(2) Nuclear heating per 1 MW/m^2 neutronic wall load. Does not include 4 W/cm^2 surface heat.

(3) For 5 cm cases 90% of heat transfer was assumed by conduction and 10% by thermal radiation.

(4) For 10 cm cases, 80% of heat transfer was assumed by conduction and the rest by radiation.

(5) Conduction areas of 5.4 and 5.9 cm^2 per unit length of slab was assumed for 5 and 10 cm thick cases, respectively.

(6) A thickness of 0.25 cm was assumed between coolant and the front surface of the first wall.

VII. Other Considerations Affecting ISSECs

VII-A. Cost and Availability

Table VII-1 lists the raw and the fabricated material costs of the various ISSEC materials considered in this study. The high cost of vanadium is due to the fact that there is not as well established a mining and milling industry for that metal. Among the five materials listed in Table VII-1, the most available and the least expensive one is carbon (which is also the easiest to fabricate). Molybdenum, niobium and tungsten cost about the same but tungsten is the hardest to fabricate followed by molybdenum and niobium. The thickest tungsten plate that could be fabricated by forging at the present time is about 2-3 cm x 10 cm x 30 cm dimensions at 92% theoretical density.[46] The dimensions of molybdenum, niobium and vanadium plates that can be fabricated by forging at present are about 5 cm x 15 cm x length, 5 cm x 30 cm x length, and 5 cm x 30 cm x length respectively with desired length up to 150 cm.[46]

Table VII-2 shows the availability of metals considered for an ISSEC. Listed in Table VII-2 are the U.S. and the world reserves at present day prices and reserves in the U.S. at three times the present prices, and U.S. and free world production and consumption of these metals in 1974.

For illustration purposes assume a tokamak fusion reactor like UWMAK-I[4] or UWMAK-II[5] with a 13 m major radius and a 5 m plasma radius. Also assume the presence of an ISSEC in such a reactor with a 5 m inner radius and a 10 cm thickness. The volume the ISSEC would occupy would be $\sim$ 259 m^3. This would correspond to 2640 tonnes of material for Mo, 2220 tonnes for Nb, 1540 tonnes for V and 5000 tonnes for W. At 1974 rates the excess

Table VII-1

Current Materials Costs for ISSECs[46]

Material	$/kg Raw	Fabricated
Carbon	3	10
Molybdenum	55	110
Niobium	65	100
Vanadium	100	200
Tungsten	35	70

Table VII-2

Data Relating Availability of Metals for ISSECs in Fusion Reactors (all quantities are in millions of metric tonnes)

	U.S.A.				Free World: Ex-U.S.A.	
Material	Reserves 1x[1]	Reserves 3x[2]	Production 1974	Consumption 1974	Reserves 1x[1]	Production 1974
Mo[3]	5.41	>2	0.06	0.04	13.0	0.21
Nb[3]	0.006	0.07	0.00	0.001	7.0	0.006
V[5]	0.1	1.3	0.033[4]	-	26	-
W	1.08					

(1) Reserves at present metal prices.

(2) Additional reserves at 3 times present prices.

(3) From reference 5.

(4) Estimated production capacity in 1980. From ref. 47.

(5) From ref. 4, volume 2.

production of molybdenum in the U.S. could supply about 8 UWMAK size reactors per year with enough material for a 10 cm ISSEC. At the 1974 rate of production molybdenum reserves in the U.S. would last at least 100 years. Niobium, even though it had a zero production rate in the U.S. in 1974, is not expected to present any resource problems, either.[46,48] Vanadium seems to have plenty of reserves and given the need, technology could be developed enough for its production for use in fusion reactors. Tungsten seems to have a serious resource problem. 1970 estimates of tungsten reserves were 1.36 million metric tonnes. In 1974 the estimates were reduced to 1.08 million metric tonnes and its production capacity is not certain.

To compare the various ISSEC materials on the basis of how much they will cost we must allow for the difference in their effectiveness in reducing the radiation damage to the first structural wall. For the purposes of comparison, if we calculate the amount of material needed for an x cm thick ISSEC in a UWMAK type reactor, where x is the required thickness of ISSEC to reduce the displacement damage to the first wall by a certain amount, say a factor of 2, we can find the cost of each ISSEC to produce the same effect. From Figure III-1 of Chapter III, we see that to get a factor of 2 reduction in the first wall displacement damage, we need 9.5 cm carbon ISSEC, 5.5 cm Mo, 5.2 cm Nb, 6 cm V, and 4 cm W ISSEC. Table VII-3 lists the amount of ISSEC material required for an ISSEC with 5 m minor and 13 m major radius and the thickness given above for each material. It also gives raw and fabricated costs of each ISSEC. We can see from this table that for the same effect a carbon ISSEC costs the least and a vanadium ISSEC costs the most, followed by molybdenum, tungsten and niobium ISSECs.

Table VII-3

Comparison Costs of Various ISSECs for the Same Effect in Reducing the Displacements Damage to the First Sturctural Wall

ISSEC Material	Effective * Thickness (cm)	Amount ** Required (kg)	Raw Cost, $x10^6	Fabricated Cost, $x10^6
C	9.5	$.394x10^6$	1.18	3.94
Mo	5.5	$1.45x10^6$	79.8	160.
Nb	5.2	$1.15x10^6$	74.8	115.
V	6	$.923x10^6$	92.3	185.
W	4	$1.99x10^6$	69.5	139.

* Thickness required to reduce the displacement damage to the first wall by a factor of 2.

** For a tokamak reactor with 13 m major and 5 m minor radius

VII-B. Vacuum Properties and Vapor Pressure

Vapor pressures of the five ISSEC materials considered in this study were given in Figure VI-3 and Table VI-2 of Chapter VI. The free vaporization rates of these materials as a function of temperature are presented in Table VII-4. Values for carbon are taken from reference 49 and the free vaporization rates of the other four materials are calculated using the formula[54]

$$\dot{n}(T) \cong \frac{3.5 \times 10^{22}}{\sqrt{M}} \frac{P(T)}{\sqrt{T}}$$

where $\dot{n}(T)$ is the free vaporization rate in units of atoms/cm^2 sec at temperature T

P(T) is the vapor pressure in torrs

M is the atomic weight of material

and T is the temperature in ^{o}K.

We see from Tables VII-4, VI-2, and Figure VI-3 that tungsten is the best of the five materials from a vacuum properties standpoint. It is followed by niobium. Molybdenum and carbon have similar vapor pressures. Vanadium is the least suitable of these five materials for vacuum applications.

Other criteria that affect the use of materials in vacuum environments are the gas content, and absorption of gases on the material. The gas content of metals is not expected to present a problem. Carbon which may have a high gas content before baking was originally thought by many to be unsuitable for hard vacuum applications. However, several experiments have shown that with proper outgassing and baking at high temperatures, the residual

Table VII-4

Free Vaporization Rate of Various ISSEC Materials
(atoms/cm^2 sec)

Temperature (^oC)	C	Mo	Nb	V	W
1000	5.5×10^{2}	3.0×10^{4}	2.4×10^{1}	2.4×10^{11}	4.0×10^{-5}
1500	9.8×10^{10}	1.0×10^{11}	4.7×10^{9}	5.8×10^{16}	2.3×10^{5}
2000	4.0×10^{15}	3.0×10^{13}	1.9×10^{14}	-	6.5×10^{10}
2500	4.4×10^{18}	5.8×10^{17}	-	-	2.0×10^{14}
3000	1.0×10^{21}	-	-	-	5.4×10^{16}

gas content in carbon could be lowered drastically.[50-52] G. A. Beitel[51] measured the quantity and composition of gases retained in several graphites and tungsten. After 300°C and 24 hour bake out, he found that the results were quite similar for graphite and tungsten.

More recently G. P. Lang and V. L. Holmes[52] measured the gas content of WCA and Thornel 50 S graphite fibers. They found that relatively large amounts of gas (0.04-0.1 torr liters/gram for WCA and 0.2-0.5 torr liters/gram for Thornel 50 S at 1500-2000°C) are removed from the fibers during an initial desorption. But after the first desorption the amount of gas removed from the samples was very small (0.001-0.01 torr liters/gram for WCA and 0.01-0.03 torr liters/gram for Thornel 50 S at 1500-2000°C).

Long and Holmes[52] also measured the sticking probability of hydrogen and air on WCA and Thornel 50 S fibers at simulated tokamak fusion reactor operating conditions. They showed that the sticking probability of both hydrogen and air on these fibers was very low on the order of 10^{-8} - 10^{-10}, which should present no problem during refueling operations between burns.

VII-C. Surface Effects

The side of the ISSEC facing the plasma in a tokamak fusion reactor will be subjected to high fluxes of high energy atomic D^+, T^+ AND He^+ ions, 14.1 MeV neutrons as well as lower energy back scattered neutrons and impurity ions present in the plasma. All of these particles to some degree will cause sputtering of atoms off the surface of an ISSEC. D^+, T^+ ions could react chemically with carbon and add to removal rate of surface atoms through formation of some volatile hydrocarbons. He^+ and D^+ ions could also cause blisters in metals. The surface effects problem cannot be covered in any detail here and we will only mention some of the more important experiments in this area and comment on their results.

VII-C-1. Sputtering

R. Behrish has recently summarized the light ion sputtering values for molybdenum[53] and niobium[54] and these are given in Figures VII-1 and VII-2, respectively. Behrish has drawn the most likely curve through the data and estimated the sputtering curve for tritium with both metals. From Figures VII-1 and VII-2 one might draw the following conclusions.

(1) Sputtering yields of Mo and Nb are very similar.

(2) There will be very little sputtering of Mo and Nb by D and T below 200 eV and by He below 100 eV.

(3) The maximum in the sputtering curves occurs at 3-4 keV for D and T and at approximately 5 keV for He.

(4) The maximum sputtering coefficients are:

for Mo: 0.008 for D^+, 0.02 for T^+ and 0.05 for He,

and for Nb: 0.012 for D^+, 0.018 for T^+ and 0.1 for He.

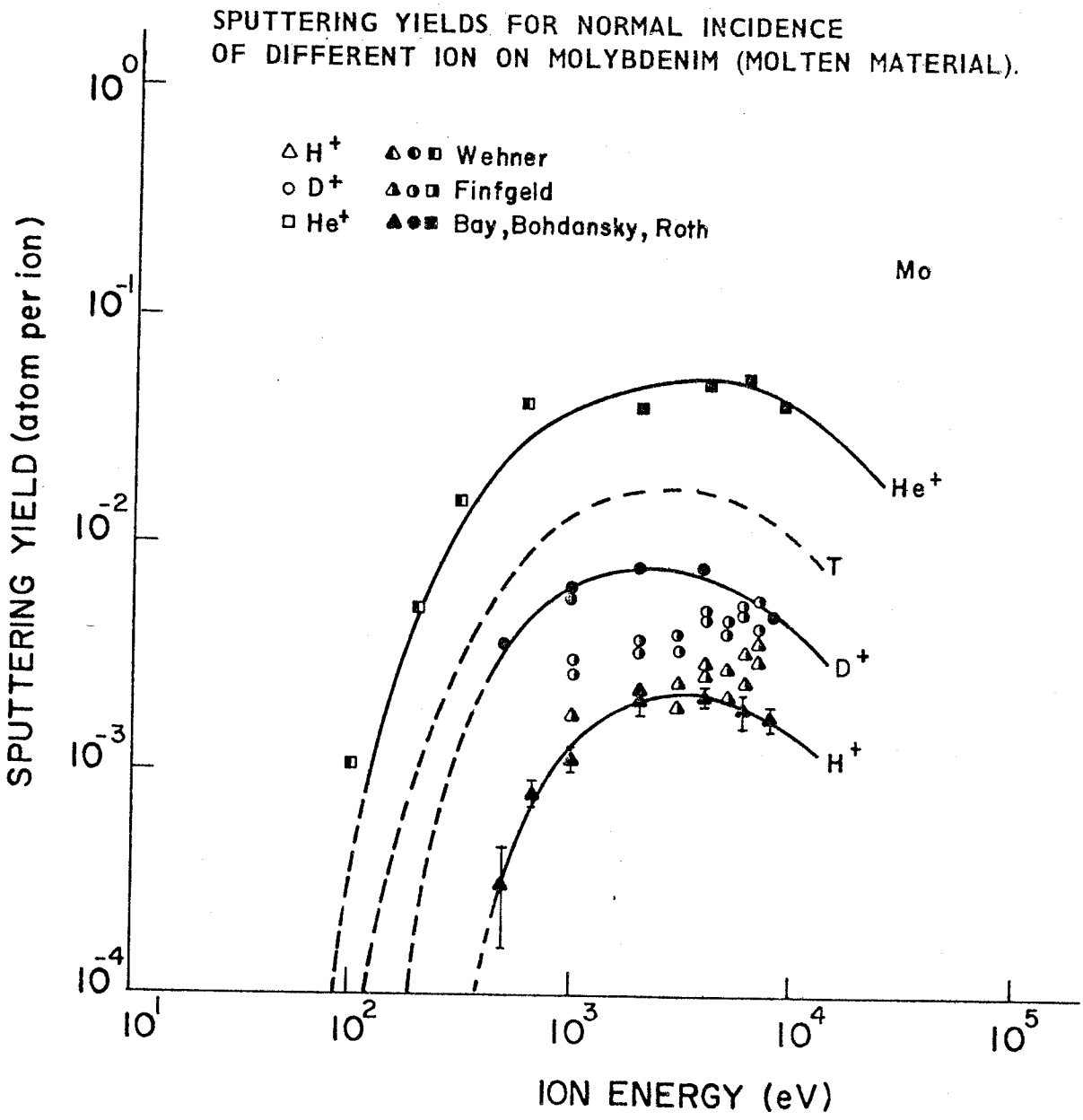
SPUTTERING YIELDS FOR NORMAL INCIDENCE
OF DIFFERENT ION ON MOLYBDENIM (MOLTEN MATERIAL).
△ H+ ▲●■ Wehner
○ D+ ▲●■ Finfgeld
□ He+ ▲●■ Bay, Bohdansky, Roth
Mo
SPUTTERING YIELD (atom per ion)
ION ENERGY (eV)
He+
T
D+
H+
10^0
10^-1
10^-2
10^-3
10^-4
10^1
10^2
10^3
10^4
10^5

Figure VII-1

Sputtering Yields for Normal Incidence of Different Ions
on Polycrystalline Niobium

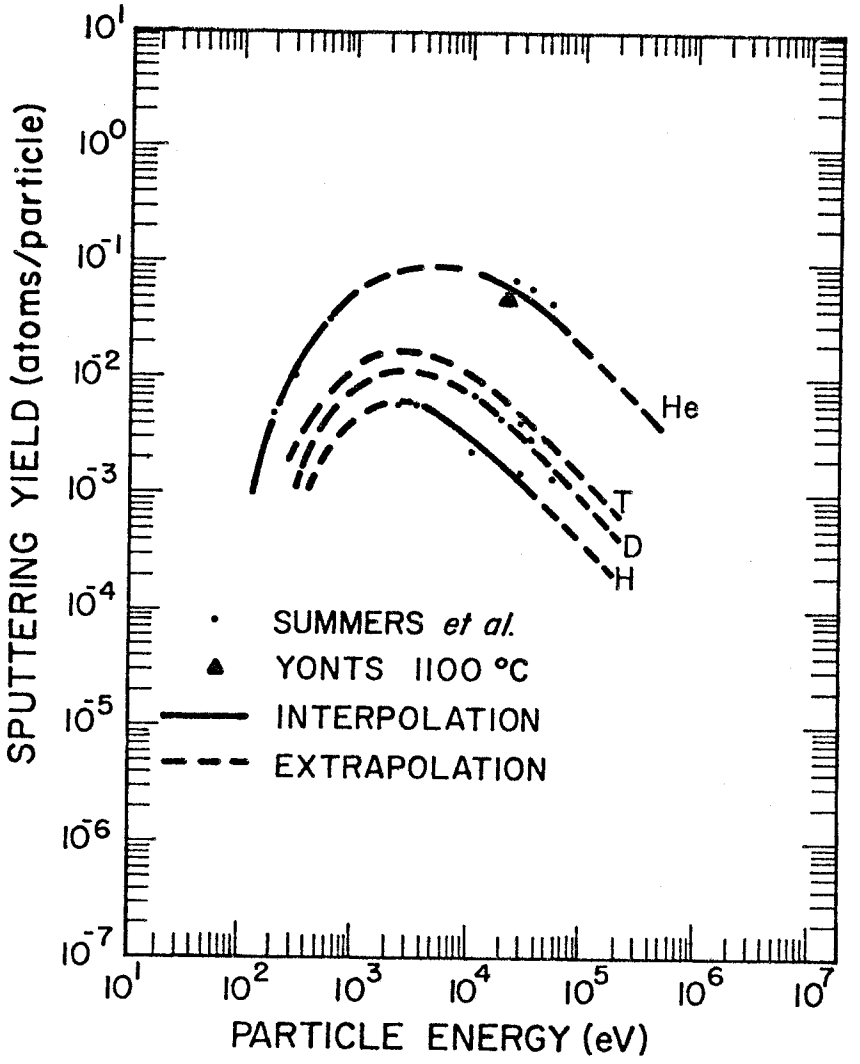

Figure VII-2

There isn't much information on the ion sputtering of vanadium and tungsten, but Behrish[54] reports that the sputtering yield of vanadium might be about a factor of 2-3 higher than for Nb, and W might be a factor of 2-3 lower than Nb. Relative magnitudes of the sputtering yields of these metals and others from 400 eV helium ions can be seen on Figure VII-3.[55] As we see the relative magnitudes are about the same as reported by Behrish.

The ion sputtering of carbon deserves special attention in that it is reported to react chemically with atomic hydrogen and its isotopes at certain temperatures.[28,56-59,62-67] Therefore, in addition to physical sputtering which occurs with all materials and ions, there is a form of sputtering called chemical sputtering that takes place when carbon is bombarded by H^+, D^+ or T^+. The difficulty, however, is finding the experimental values of the sputtering coefficient for D^+, T^+ and He^{++} at appropriate energies characteristic of a tokamak fusion reactor. There have been a few recent studies[56-59] utilizing hydrogen isotopes to measure the sputtering behavior of carbon and some results from these studies are summarized in Figures VII-4[56,59] and VII-5.[58] The basic difference between these studies is that the data in Figure VII-4 comes from 2-20 keV H, D and T ions on carbon which was heated to 1400°C while that in Figure VII-5 comes from carbon bombarded with very low energy (0.2 eV) hydrogen while the samples were heated to approximately 1900°C. Some general observations about Figures VII-4 and 5 are:

(1) The sputtering coefficients rise from a value of 10^{-2} atom/atom at room temperature to a maximum of ~8 x 10^{-2} at 600°C. This peak has been found to be associated with methane formation.

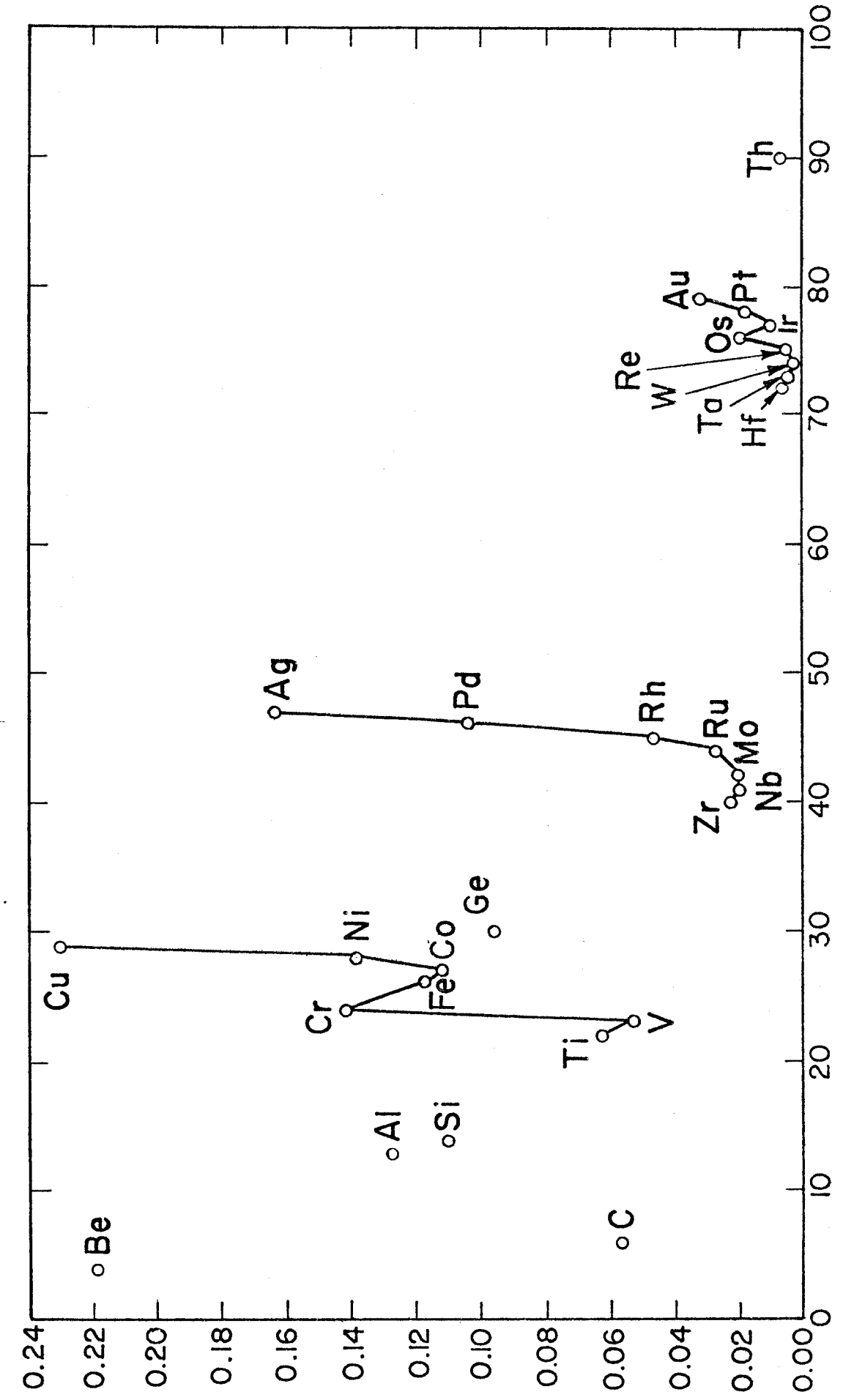
SPUTTERING YIELDS AT 400 eV HELIUM ION ENERGY
FOR 29 ELEMENTS VS. THE ELEMENT'S ATOMIC NUMBER
(ROSENBERG AND WEHNER)
YIELD (ATOMS / ION)
0.24
0.22
0.20
0.18
0.16
0.14
0.12
0.10
0.08
0.06
0.04
0.02
0.00
0
10
20
30
40
50
60
70
80
90
100
Z
Be
Cu
Ni
Cr
Fe
Co
Ge
Ti
V
Al
Si
C
Ag
Pd
Rh
Ru
Mo
Nb
Zr
Re
W
Ta
Hf
Os
Ir
Pt
Au
Th

Figure VII-3

Figure VII-4

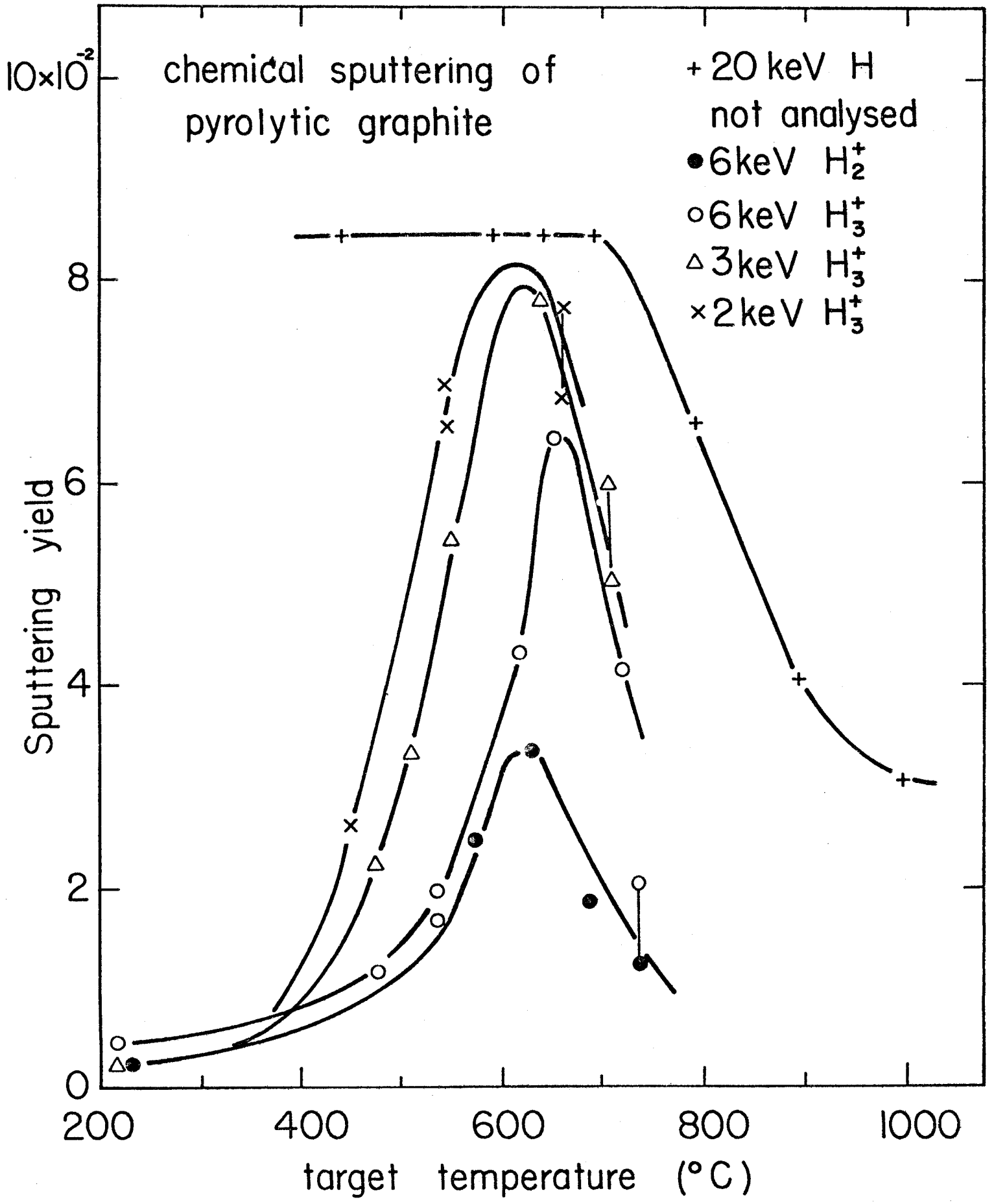
chemical sputtering of
pyrolytic graphite
+ 20 keV H
not analysed
● 6keV H_2^+
○ 6keV H_3^+
△ 3keV H_3^+
× 2keV H_3^+
10×10⁻²
8
6
4
2
0
Sputtering yield
200
400
600
800
1000
target temperature (°C)

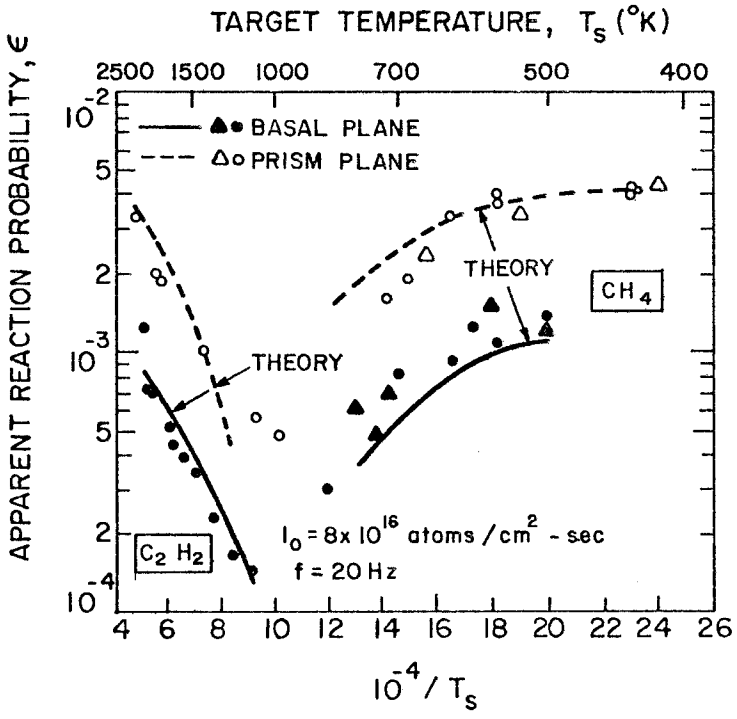

Figure VII-5

Effect of Temperature and Crystal Orientation on the Reaction Probability of Carbon (58)

(2) As the temperature is increased above 600°C, the sputtering values start to return to their low initial values. This is accompanied by a reduced methane formation.

(3) The sputtering coefficient from tritium is reduced as its energy is increased from 2 to 6 keV. However, 6 keV tritium is more effective in producing methane than is the same energy deuterium.

(4) The low energy hydrogen bombardment depicted in Figure VII-5 shows smaller absolute levels of methane formation than for higher energy hydrogen. Furthermore, the low energy sputtering is quite sensitive to crystal orientation.

(5) Above 1000°C, the formation of acetylene becomes important although the absolute values are still low ($<<10^{-2}$ atom/atom).

(6) There appears to be a region between 800 and 1200°C where little gasification occurs.

The peak in the sputtering yield vs. temperature curve around 600°C was also observed by other investigators.[57,62,63] G. J. Thomas, et al.[28] also report high methane formation around 650°C when they bombarded pyrolitic graphite with 150-300 keV H+ but they also report the formation of propane and its derivatives in the 800-1200°C range which has not been found by others.

R. Ekern, S. K. Das and M. Kaminsky of Argonne National Laboratory[65] irradiated rayon based WCA graphite cloth at room temperature, 400°C and 800°C with deuterons and ^{4}He+ ions at 100 and 250 keV energy. They observed considerable flaking of individual fibers at room temperature irradiations but at 400°C and 800°C irradiation surface damage was greatly reduced. In fact, in high temperature irradiations with ^{4}He+ they did not observe any flaking or other surface damage.

S. K. Erents, et al.[66] at Culham Laboratory in the United Kingdom also studied the methane formation during the interaction of energetic protons and deuterons with carbon. They found a behavior similar to that of the Garching group[56] with a maximum in methane production at about 575°C and a reduction in methane production and an increase in hydrogen release above 575°C. The maximum hydrogen release occurred at 925°C.

Physical sputtering of graphite by helium ions is thought to be practically independent of temperature.[67] Two independent measurements give the sputtering ratio as 0.06 for 0.4 keV He ions[68] and 0.07 for 0.5 keV He ions.[69]

The sputtering yield results for carbon on carbon are even more scarce than hydrogen and helium bombardment results. One value quoted in the literature is 0.4 for 45 keV C on C.[70] Assuming that this value is correct, the self sputtering yield of carbon under tokamak operating conditions (1-20 keV C on C) may be expected to be around 0.5-0.6.

The incident 14.1 MeV and lower energy back scattered neutrons will also cause atoms to be sputtered from the front surface of ISSEC. Unfortunately, there have been no 14 MeV neutron studies on Mo, W or carbon. Most studies have been carried out on Nb[71-75] and very little on V.[75] However, fission neutron sputtering results of Garber, et al.[76] show the neutron sputtering rates of Mo, Nb, V, and W within a factor of 2 of each other. The current 14 MeV neutron sputtering values on Nb range from approximately 10^{-4} to 10^{-3} on the high side[71] to 10^{-5} - 10^{-4} on the low side.[72-74] Lacking any specific data and using Nb as a model for Mo, V, W and carbon, it appears to be reasonable to choose a value of 10^{-4} atom/neutron for the 14 MeV neutron sputtering of all five ISSEC materials considered in this study.

In order to find the flux of particles leaving the ISSEC surface as a result of sputtering, we need to know the current of charged particles incident on the surface from the plasma, the energy of these incident particles and the sputtering coefficient at that energy. Using the values calculated for UWMAK-III[24] for the charged particle fluxes incident on the ISSEC, and the sputtering coefficients given in this section, we can calculate the flux of particles leaving the ISSEC surface by making use of the formula

$$\phi = \sum_i S_i(E)\ \phi_i(E)$$

where $S_i(E)$ is the sputtering ratio (atoms per particle) for the i'th particle with energy E incident on the ISSEC.

$\phi_i(E)$ is current of i'th particles at energy E on the ISSEC surface.

Table VII-5 gives the energy and the current of charged particles and neutrons incident on the ISSEC surface per 1 MW/m^2 neutronic wall loading under UWMAK-III[24] conditions (6% plasma burnup and 99.9% efficient divertor). Also listed in Table VII-5 are the sputtering coefficients for the various incident particle-target combinations at the incident particle energy shown. Table VII-6 gives the flux of sputtered atoms from various ISSEC surfaces due to D^+, T^+, He^{++} ions and 14.1 MeV neutrons. Comparing the values for the total flux of sputtered atoms from the surfaces of the five ISSEC materials from Table VII-6 with those given in Table VII-4 for vaporization, we see that the rate of vaporization is about the same as the rate of sputtering at about 1550°C for carbon, 1600°C for Mo, 1650°C for Nb, 1050°C for V and 2100°C for W. When the surface temperature of each material is below the value given above, the sputtering rate is higher than the vaporization rate, otherwise the vaporization rate is higher.

Table VII-5

Summary of Particles Striking the ISSEC Surface for UWMAK-III[24] Conditions

Particle	Mean Energy-keV	(1) Current-$cm^2 s^{-1}$	Physical Sputtering Coefficient Atoms/Particle				
			C	Mo	Nb	V	W
D^+	3	5.8×10^{12}	0.01	0.008	0.01	0.02	0.005
T^+	3	5.8×10^{12}	0.01	0.02	0.02	0.04	0.01
He^{++}	3	6.8×10^{11}	0.1	0.06	0.09	0.18	0.05
He^{++}	100	6.8×10^{10}	0.05	0.007	0.02	0.04	0.01
n	14.1×10^3	4.43×10^{13}	10^{-4}	10^{-4}	10^{-4}	10^{-4}	10^{-4}

(1) Adjusted to 1 MW/m^2 average neutronic wall loading.

Table VII-6

Flux of Sputtered Atoms From Various ISSEC Surfaces

Particle	Mean Energy-keV	Atoms/cm^2 sec				
		C	Mo	Nb	V	W
D^+	3	5.8×10^{10}	4.6×10^{10}	5.8×10^{10}	1.2×10^{11}	2.9×10^{10}
T^+	3	5.8×10^{10}	1.2×10^{11}	1.2×10^{11}	2.3×10^{11}	5.8×10^{10}
He^{++}	3	6.8×10^{10}	4.1×10^{10}	6.1×10^{10}	1.2×10^{11}	3.4×10^{10}
He^{++}	100	3.4×10^{9}	4.8×10^{8}	1.4×10^{9}	2.7×10^{9}	6.8×10^{8}
n	14.1×10^{3}	4.4×10^{9}	4.4×10^{9}	4.4×10^{9}	4.4×10^{9}	4.4×10^{9}
Total	-	1.9×10^{11}	2.1×10^{11}	2.5×10^{11}	4.8×10^{11}	1.3×10^{11}

VII-C-2. Blistering

Blisters have been observed in Mo,[77-81] Nb,[82-84] V[85-87] and W[77] with He^+ irradiations. In some instances they have also been observed with D^+ and H^+ irradiations on Mo.[78,79,81] In general, the blister skin thickness is about the same as the depth at which range probability distribution of incident particles peaks. The minimum fluence for blisters to form and exfoliate decreases with increasing temperature, increases with increasing ion energy and decreases with increasing particle current.

To the authors' knowledge, there has been no experimental data reported to show blisters forming in graphite with helium ion bombardment.[57,64,65,88,89]

It is not certain at this time whether blisters in metals keep reforming after every exfoliation or that they will stop forming after the first few exfoliations. Some recent results by Roth, et al.[90] show that if the ions have a spread in energies or if they strike the wall with varying angles of incidence, after the first few exfoliations, the surface becomes so porous that the bombarding particles diffuse out as fast as they are injected. If this happens to be true at high fluences, or if it turns out that no blisters form in carbon, metal surfaces could be carbon coated to avoid serious problems with blisters.

VII-D. Thermal Shock Resistance

Resistance to thermal shock is a measure of the ability of a material to resist crack formation and fracture when subjected to sudden heating or cooling. No standard tests exist which will accurately evaluate the property since shape is an important factor. A figure of merit number is obtained with the combination of parameters k, thermal conductivity, S, tensile strength, α, coefficient of thermal expansion, and E, modulus of elasticity as $\frac{kS}{\alpha E}$. The higher this number, the better the ability of the material to resist thermal shock.

Table VII-7 gives $\frac{kS}{\alpha E}$ values for the five ISSEC materials investigated at two temperatures. We see from the table that W has the best resistance to thermal shock followed by carbon, niobium, molybdenum and vanadium in decreasing order at 1600°C. At 1200°C niobium is next to W, carbon is third, and then molybdenum and vanadium.

There are two important things to mention in Table VII-7. One is that carbon, a non-metal, has as good as or better thermal shock resistance than metals at high temperatures. The other is that vanadium, because of its very low strength at high temperatures, is at the bottom of thermal shock resistance scale.

Table VII-7

Relative Figure of Merit for Thermal Shock Resistance of Potential ISSEC Materials*

Material	Temperature 1200°C	1600°C
C	51.	40.
Mo	47.	15.
Nb	70.	39.
V	0.35	0.35
W	200.	100.

* $\frac{kS}{\alpha E}$ Watts/cm - high numbers are desired

VIII. Discussion

A comparison of the five ISSEC materials considered in this study is made in table VIII-1 on the basis of how much they reduce the displacement and gas production rates in the 316 SS first wall, and how they change the total blanket (including ISSEC) radioactivity and the energy multiplication when they are used at maximum allowable thicknesses, respectively, for pure radiation and radiation plus conduction cooling schemes. We also list the fabricated materials costs of the five ISSECs if they were to be used in a UWMAK-type reactor with a 13 m major and 5 m minor radius and the thickness shown. Factors that limit the maximim thickness of each ISSEC material are shown in parenthesis by the thickness values. The maximim ISSEC temperatures are also shown.

It is interesting to note that all 5 materials reduce the displacement damage by ~1/2 (to within 25%) and the helium production is reduced by a factor of 2 to 6. The only ISSEC material to result in an overall reduction in blanket radioactivity at shutdown is carbon while all of the metallic ISSECs increase the activity. After 1 year of decay the total radioactivity of the ISSEC and blanket is reduced for all the materials except W. On the other hand, the long term activity (at 1000 years after shutdown) is increased for Mo, Nb, and V ISSECs while it is reduced by 23% with W and almost 50% with C. The carbon and V ISSECs reduce the energy production per fusion while the Nb and W slightly increase it and Mo results in a 15-17% energy production increase. Finally, the relative cost of the metal ISSECs to produce the above results is a factor of 30-55 higher than the cost of a carbon ISSEC. The advantages and disadvantages of each ISSEC material as compared to others considered in this study are summarized in Table VIII-2.

Examination of Tables VIII-1 and VIII-2 show that because of its various disadvantage such as high vapor pressure, low melting point, reduction in nuclear heating in the blanket, high cost, etc., V would

Table VIII-1

Comparison of the Five ISSEC Materials Considered in This Study

(a)

Radiation Cooling Only

Material	Maximum Thickness(cm)	Maximum Temp. (°C)	Reduction Factors in 316SS First Wall[1]		Total Blanket Radioactivity[1]			Increase in Energy Production[4]	Relative Fabricated Cost
			dpa	Appm He	Shutdown	1 Yr.	1000 Yr.		
C	9.5(V.P.)	2000	0.49	0.34	0.46	0.37	0.60	0.96	1[2]
Mo	7.5(V.P.)	1950	0.4	0.16	3.78	0.23	267	1.15	55
Nb	8.5(B.R.)	2050	0.36	0.15	3.83	0.34	9.87	1.04	48
V	4.5(V.P.)	1300	0.59	0.41	1.19	0.52	1.07	0.90	36
W	6(B.R.)	1900	0.37	0.19	5.11	1.66	0.77	1.05	53

(b)

Radiation Plus Conduction Cooling

C	13(B.R.)	1900	0.4	0.24	0.33	0.22	0.48	0.96	1[3]
Mo	10(B.R.)	1350	0.30	0.10	4.72	0.15	365	1.17	54
Nb	8.5(B.R.)	1300	0.36	0.15	3.83	0.34	9.87	1.04	35
V	8(V.P.)	1300	0.43	0.23	1.95	0.35	1.01	0.88	53
W	6(B.R.)	1150	0.37	0.19	5.11	1.66	0.77	1.05	39

V.P. = Vapor Pressure
B.R. = Breeding Ratio
(1) Values normalized to 1.0 in blanket with no ISSEC
(2) Normalized cost 3.94×10^6 $
(3) Normalized cost 5.4×10^6 $
(4) Using standard blanket as 1.0

probably not make a good ISSEC material. Comparing Mo and Nb one can see that Mo in every respect is as good or better than Nb. Therefore, Mo would be considered to be a better ISSEC material than both V and Nb. A comparison between Mo and W is difficult in that W has the most desirable advantages from the point of view of reducing radiation damage in the first structural wall, low vapor pressure, high melting point, and low long term radioactivity, but it is much harder to fabricate and it is also hard to breed tritium. In fact, as we see in Table VIII-1, a breeding ratio limited 6 cm thick W ISSEC is less effective than 10 cm thick Mo ISSEC (also limited by breeding ratio) in reducing the dpa and helium production rates in the first wall. Based on these considerations we feel that at least at the present time Mo would be the best of the four metals studied for use as an ISSEC material.

A definitive choice between a graphite ISSEC and a Mo ISSEC is also not clear. From radioactivity, afterheat, cost, and fabricability standpoint, graphite is clearly superior to Mo, but Mo reduces the radiation damage in the first structural wall more (by 20% in dpa and ~100% in He production) and increases the energy multiplication in the blanket (by as much as 15-17%). If indeed the question of C_2H_2 formation between hydrogen ions and C at high temperatures is resolved, the choice might become clearer, but at this time neither C nor Mo has a clear superiority over the other.

Table VIII-2

Comparison of Various ISSEC Materials Considered in this Study

	Carbon	Molybdenum	Niobium	Vanadium	Tungsten
Major Advantages:	. Low radioactivity	. Effective in reducing radiation damage to first wall	. Low vapor pressure	. High (n,2n) cross section	. Most effective in reducing the dpa and gas production rates in the first wall
	. Low afterheat	. Increases nuclear heating in blanket	. Increases nuclear heating in blanket	. Low long term radioactivity	. Low vapor pressure
	. Low cost	. High (n,2n) cross section	. High thermal conductivity		. High thermal conductivity
	. Easily fabricated	. High thermal conductivity	. Low vapor pressure		. High thermal shock resistance
	. Good vacuum properties	. High melting point			. High melting point
	. Low vapor pressure	. Low vapor pressure			. Low long term radioactivity
	. Low blistering rate				. Increases nuclear heating in blanket
	. High temperature strength				
	. Good thermal shock resistance				
Major Disadvantages:	. Less effective in reducing dpa and gas production rates in the first structural wall	. High short and long term radioactivity	. Embrittled by small amounts of C, O, N	. High vapor pressure	. Hard to fabricate
	. Reduces nuclear heating in the blanket	. Hard to fabricate	. High cost and U.S. resource problem	. Availability and high cost	. Availability
	. Chemical sputtering CH_4 at < 800°C C_2H_2 at > 1200°C (?)	. High cost	. High long term radioactivity	. Blistering	. High cost
		. Blistering	. Blistering	. Low thermal shock resistance	. Hard to breed tritium
				. Low melting point	. High radioactivity at shutdown
				. Reduces nuclear heating in blanket	. Blistering

IX. Conclusions

A few general conclusions can be gathered from these studies about both graphite and metal ISSEC cases.

•ISSECs reduce the displacement damage in the first structural wall. Reduction factors vary between 2-5 for a 10 cm thick ISSEC, between 5-50 for a 25 cm thick spectral shifter.

•The gas production rates in the first structural wall are also reduced by ISSECs. Helium production rates are reduced by factors of 3.2 - 12 with a 10 cm thick ISSEC and by factors of 12 to 275 with a 25 cm thick ISSEC. The reductions in hydrogen production rates are 2.5 to 12.7 and 8 to 235, respectively with 10 cm and 25 cm shield thickness.

•The short and intermediate term radioactivity, Biological Hazard Potential (BHP) and afterheat of the 316 SS first wall are reduced by all ISSECs, and the long term activities are actually increased by a 10 cm or thicker carbon ISSEC.

•All five ISSECs reduce the breeding ratio in the model blanket used in this study. Reduction factors vary between 1.25 and 2.1 for a 10 cm thick ISSEC and between 2.1 and 13.6 for a 25 cm thick ISSEC.

•Mo, Nb, and W ISSECs increase the total energy available per fusion in the model blanket of this study while C and V ISSECs decrease it.

•The radioactivity of the total blanket (including the ISSEC) a short time after shutdown is higher than the unprotected case for W, Mo and Nb ISSECs but it is lower with C and V ISSECs. At 1 - 10 years after shutdown the blanket has about the same radioactivity with and without an ISSEC. But a long time after shutdown (longer than 100 years) a Mo ISSEC system has the most radioactivity followed by the Nb ISSEC system. Carbon, W, and V ISSEC protected designs have about the same radioactivity as unprotected blankets.

•Maximum displacement rates in the ISSECs themselves per 1 MW/m^2 neutron wall loading per year vary between 8.4 for Nb and 12.5 dpa/yr for V. Maximum helium production rates vary between 3.7 for W and 2300 appm/yr for C.

•The radioactivity at shutdown of all metal ISSECs is about the same order of magnitude (1 - 10 Ci/W), and is higher than that of C ISSEC by a factor of about 10^4. At long times after shutdown (longer than 100 years) radioactivity in C, W and V ISSEC has decayed away while in Mo it is ~ 0.001 times its value at shutdown and in Nb about 10^{-4} times its shutdown value.

•Most ISSECs cooled only by thermal radiation are limited by their vapor pressure and the maximum allowable thicknesses are 9.5 cm for C, 7.5 cm for Mo, and 4.5 cm for V for a 1 MW/m^2 neutronic and 4 W/cm^2 surface heat loading. Niobium and tungsten are limited to 9 and 12.5 cm by vapor pressure and 8.5 and 6 cm by breeding ratio considerations, respectively.

•A conduction plus radiation cooled ISSEC can have greater thickness up to 15 cm or higher depending on the specific design.

•Molybdenum appears to be the best overall choice for a metal ISSEC (compared to W, Nb, V).

•A definitive choice between a carbon and molybdenum ISSEC cannot be made at this time as both materials have strong positive features but in different areas.

ACKNOWLEDGEMENT

This research was supported by a grant from the Energy Research and Development Administration, Division of Magnetic Fusion Energy.

References

1. G. L. Kulcinski, R. G. Brown, R. G. Lott, and P. A. Sanger, Nucl. Tech., 22, 20, 1974.

2. A Fusion Power Plant, R. G. Mills, Ed., MATT-1050, April 1974.

3. W. Danner, Max-Planck Institute fur Plasmaphysik Report #IPR 4/130, February 1975.

4. B. Badger, et al., "UWMAK-I, A Wisconsin Toroidal Fusion Reactor Design," Fusion Technology Program, University of Wisconsin, UWFDM-68, Vol. 1 and 2.

5. B. Badger, et al., "UWMAK-II, A Conceptual Tokamak Power Reactor Design," Fusion Technology Program, University of Wisconsin, UWFDM-112, October 1975.

6. G. L. Kulcinski, Y. R. Young, "The Influence of First Wall Lifetime on the Cost of Electricity in UWMAK Type Fusion Reactors," Proc. Int. Confer. on Rad. Eff. and Tritium Tech., Gatlinburg, Tennessee, October 1-3, 1975. Also Report UWFDM-140, Nuclear Engr. Dept., Univ. of Wis., Madison, Wisconsin, October 1975.

7. R. W. Conn. G. L. Kulcinski, H. Avci, and M. El-Maghrabi, Nucl. Tech. 26, 125, 1975.

8. G. L. Kulcinski, R. W. Conn, H. I. Avci, D. K. Sze, "Protection of CTR Metallic First Walls by Neutron Spectral Shifting," Report UWFDM-127, Nuclear Engr. Dept., University of Wisconsin, June 1975. Also Trans. Am. Nucl. Soc. 21, 50 (1975).

9. H. I. Avci and G. L. Kulcinski, "The Response of ISSEC Protected First Walls to DT and DD Plasma Neutrons," Proc. Int. Confer. on Rad. Eff. and Tritium Tech. for Fusion Reactors at Gatlinburg, Tennessee, October 1-3, 1975. Also Report UWFDM-135, Nucl. Engr. Dept., Univ. of Wis., Madison, Wisconsin, October 1975.

10. D. K. Sze, R. W. Conn, "Heat Transfer and Neutronics of ISSEC and Partial ISSEC Blanket Designs," Nuclear Engr. Dept., Univ. of Wisconsin Report UWFDM-128, June 1975. Also Trans. Am. Nucl. Soc. 21, 34 (1975).

11. W. W. Engle, Jr., "A Users Manual for ANISN," K-1693, Oak Ridge Gaseous Diffusion Plant.

12. D. J. Dudziak, "Fusion Reactor Nuclear Analysis-Methods and Applications," 8th Symp. on Fusion Technology, Noordijkerhout, The Netherlands, June 1974.

13. D. M. Plaster, R. T. Santoro, and W. E. Ford III, "Coupled 100 Group Neutron and 21 Group Gamma Ray Cross Sections for EPR Calculations," ORNL-TM-4872, April 1975.

14. N. M. Greene, et al., "AMPX: A Modular Code System for Generating Coupled Multi-group Neutron-Gamma Libraries From ENDF/B," ORNL-TM-3706, Oak Ridge National Lab.

15. M. Abdou, C. W. Maynard, and R. Q. Wright, "MACK: A Program to Calculate Neutron Energy Release Parameters (fluence to Kermer Factors) and Multi-group Neutron Reaction Cross Sections From Nuclear Data in ENDF Format," ORNL-TM-3994.

16. J. R. Knight and F. R. Mynatt, "MUG: A Program for Generating Multi-group Photon Cross Sections," CTC-17 (January 1970).

17. D. G. Doran, Nucl. Sci. Engr. 52, 398, 1973. See also Nucl. Sci. Engr. 49, 130, 1972.

18. G. L. Kulcinski, D. G. Doran, and M. A. Abdou, "Comparison of Displacement and Gas Production Rates in Current Fission and Future Fusion Reactors," ASTM STP 570, 1975, pp. 329-351.

19. W. C. Morgan, J. Nucl. Mat., 51, 209 (1974).

20. T. Y. Sung and W. F. Vogelsang, "DKR: A Radioactivity Calculation Code for Fusion Reactors," Report UWFDM-170, Nuclear Engr. Dept., Univ. of Wisconsin, Madison, Wisconsin, September 1976.

21. T. Y. Sung and W. F. Vogelsang, "Decay Chain Data Library for Radioactivity Calculations," Report UWFDM-171, Nucl. Engr. Dept., Univ. of Wisconsin, September 1976.

22. W. A. Beckman, "HEAT: Heat Transfer Computer Program in Fortran V Language," EES Report No. 37, Mechanical Engr. Dept., University of Wisconsin, Madison, Wisconsin (July 1972).

23. G. E. Myers, "FEM2D - A Finite Element Program for Solving Two-dimensional Conduction Problems," Mechanical Engr. Dept., University of Wisconsin-Madison, November 1976.

24. B. Badger, et al., "UWMAK-III, A Noncircular Tokamak Power Reactor Design," Report UWFDM-150, Fusion Technology Program, Nuclear Engr. Dept., Univ. of Wisconsin, Madison (July 1976).

25. T. A. Gabriel, J. D. Amburgey, N. M. Greene, "Radiation Damage Calculations: Primary Recoil Spectra, Displacement Rates, and Gas-Production Rates," Report ORNL/TM-5160, Oak Ridge National Lab. (March 1976). Also private communication with T. A. Gabriel, Neutron Physics Division, ORNL, Oak Ridge, Tennessee.

26. D. G. Doran and N. J. Graves, "Displacement Cross Sections and PKA Spectra: Tables and Applications," Report HEDL-TME 76-70, Hanford Engineering Development Laboratory, Richland, Washington (December 1976).

27. W. F. Vogelsang and E. Ramer, "The Gamma-Ray Dose Rate After Shutdown From a Tokamak Fusion Reactor," Trans. Am. Nucl. Soc., 23, 628 (1976).

28. G. J. Thomas, W. Bauer, P. L. Mattern and B. Granoff, "He and H Implantation of Vitrous Silica and Graphite," Report SAND 75-8718, Sandia Lab., Albuquerque, N.M. Also Proc. Am. Chem. Soc. Mtg., Chicago, Illinois, August 21-22, 1975.

29. J. B. Holt, et al., "Helium Generation and Diffusion in Graphite," Lawrence Livermore Lab., Livermore, California, April 1976.

30. J. Scott, Oak Ridge National Lab., private communication.

31. G. B. Engle and W. P. Eatherly, High Temperatures and High Pressures, 7, 319, 1969.

32. J. H. Cox and J. W. Helm, Carbon, 7, 319, 1969.

33. W. J. Gray and W. C. Morgan, BNWL-B-288 and BNWL-B-289, June 1973.

34. W. N. Reynolds, et al., "Radiation Damage in Graphite at 1200°C," 2nd Conference on Indust. Carbon and Graphite, Soc. Chem. Ind., April 1965.

35. B. T. Kelly, et al., "Fast Neutron Induced Dimensional Changes in Graphites and Carbons," Ibid.

36. B. T. Kelly, "Dimensional Changes and Lattice Parameter Changes in Graphite Crystals Due to Interstitial Atoms and Vacancies," Ibid.

37. M. R. Everett, et al., "Graphite Materials Data for High Temperature Nuclear Reactors," 3rd Conf. on Ind. Carbon and Graphite, Soc. Chem. Ind., April 1970.

38. G. L. Tingey, W. C. Morgan and E. M. Woodroof, "Near-Isotropic Graphites for Helium Cooled Reactors - A Review," BNWL-B-478 (Feb. 1976).

39. J. W. Helm and J. M. Davidson, "Effect of Neutron Exposure on the Distortion of Reactor Graphite," Carbon 1, 435 (1964).

40. J. W. Helm, "Radiation Effects in Graphite at High Temperatures," Carbon 3, 493 (1966).

41. M. Van Den Berg, M. R. Iverett and A. Kingsbury, "12th Biennial Conf. on Carbon," Pittsburgh, Penn., 1975, p. 307.

42. W. C. Morgan, "A Note on the Dimensional Change Rates of Graphite Irradiated Above 900°C," BNWL, 1976 (private communication).

43. I. Sviatoslavsky, Nucl. Engr. Dept., Univ. of Wisconsin-Madison, private communication.

44. R. Benenati, P. Tichler and J. R. Powell, "Low Activity Aluminum Blanket," Report BNL 21159, Brookhaven National Lab., March 1976.

45. D. Steiner, et al., "ORNL Fusion Power Demonstration Study: Interim Report," ORNL/TM-5813, Oak Ridge National Lab., Oak Ridge, Tennessee.

46. J. Davis, McDonnel-Douglas Astronautics Co. - East (private communication).

47. G. S. Allison, "Assessment of Materials Needs for Fusion Reactors," Report BNWL-1933, Battelle Northwest Lab., Richland, Washington (July 1976).

48. J. N. Hartley, et al., "Materials Availability for Fusion Power Plant Construction," Report BNWL-2016 (Sept. 1976), Ibid.

49. "The Industrial Graphite Engineering Handbook," Union Cardbide Co., 1970.

50. C. L. Mantell, "Carbon and Graphite Handbook," Interscience, New York (1968).

51. G. A. Beitel, "The Use of Graphite in High and Ultra-high Vacuum - A Review," J. Vac. Science and Tech., Vol. 8, No. 5, p. 647 (1971).

52. G. P. Lang and V. L. Holmes, "Gas Content and Sticking Probabilities for Fibrious Forms of Graphite as Applied to Fusion Reactors," Nuclear Fusion, 16, 162 (1976).

53. R. Behrish, to be published, 1976 Erice Summer School on Tokamaks.

54. R. Behrish, Nuclear Fusion, 12, 695 (1972).

55. D. Rosenberg and G. K. Wehner, J. Appl. Phys., 33, 1842, 1962. See also G. K. Wehner, General Mills Report No. 2309, July 1962.

56. H. Vernickel, EURATOM Association, Garching b. München, West Germany (private communication).

57. B. Feinberg and R. S. Post, "Graphite Surface Erosion and Blistering," Report UWFDM-141, Nuclear Engineering Department, University of Wisconsin, Madison, August 1975.

58. M. Balooch and D. R. Olander, J. Chem. Phys. 63, No. 11, Dec. 1975.

59. I. P. Busharov, E. A. Gorbatov, V. M. Gusev, M. I. Geseva and Y. V. Martynenko, "Chemical Atomization of Graphite by H^+ Ions," The I. V. Kurchatov Order of Lenin Institute of Atomic Energy, Moscow, 1975.

60. M. I. Guseva, The I. V. Kurchatov Order of Lenin Institute of Atomic Energy (private communication).

61. B. Feinberg, Nuclear Engr. Dept., Univ. of Wisconsin, Madison, private communication.

62. S. Veprek and M. R. Hague, "On the Chemical Erosion of the First Wall in the Next Generation of Tokamak Devices for Controlled Fusion," Univ. of Zurich, Zurich, Switzerland.

63. B. J. Wood and A. Wise, J. Phys. Chem. 73, 1348 (1969).

64. J. Bohdansky et al., "Erosion of Different First Wall and Limiter Materials by Low Energy Hydrogen Ions," Fus. Tech., Proc. of 9th Symp., p. 541, Pergamon Press (1976).

65. R. Ekern, S. K. Das and M. Kaminsky, "Temperature Dependence of Surface Damage in Graphite Cloth Irradiated with Deuterons and Helium Ions," 2nd Inter. Confer. on Surface Effects in Contr. Fus. Devices, San Francisco, Cal., Feb. 1976.

66. S. K. Erents, C. M. Braganza and G. M. McCracken, "Methane Formation During the Interaction of Energetic Protons and Deuterons with Carbon," CLM-P451, February 1976.

67. J. Koth, et al., "Physical and Chemical Sputtering of Graphite and SiC by Hydrogen and Helium in the Energy Range of 300 to 600 eV," Phys. Rev., 1962.

68. N. Laegreid and G. K. Wehner, J. Applied Phys. 32, 365 (1961) and D. Rosenberg and G. K. Wehner, J. Appl. Phys. 33, 1842 (1962).

69. G. Carter and J. S. Colligen, Ion Bombardment of Solids (American Elseveier Publishing Co., New York: 1968), p. 323, p. 325.

70. O. Almen and G. Bruce, Nucl. Inst. and Methods 11, 279 (1961).

71. M. Kaminsky and S. K. Das, "14.1 MeV Neutron Sputtering of Polycrystalline and Monocrystalline Niobium with Different Microstructures," J. Nucl. Mat., 60, 111 (1976). Also in ANL CTR quarterly progress report, Nov. 1975.

72. O. K. Harling, et al., "Recent Neutron Sputtering Results and the Status of Neutron Sputtering," J. Nucl. Mat. 63, 422 (1976) (see bibliography in this reference for earlier work by this group).

73. R. Behrish, "Neutron Sputtering," 6th Inter. Conf. on "Atomic Collisions in Solids," Amsterdam, September 22-26, 1975.

74. L. H. Jenkins, et al., Appl. Phys. Letters, 26, 426, 1975.

75. M. Kaminsky and S. K. Das, "Sputtering of Vanadium and Niobium Under 14 MeV Neutron Impact," 2nd Inter. Conf. on Surface Eff. in Cont. Fus. Devices, San Francisco, Feb. 16-20, 1976.

76. R. J. Garber, G. P. Dolya, V. M. Kolyada, A. A. Molden, and A. I. Foderenko, JETP Lett., 7, 296 (1968).

77. S. K. Erents and G. M. McCracken, CLM-P-323, September 1972.

78. H. Verbeck and W. Eckstein, "Applications of Ion Beams to Metals," Ed. S. T. Picraux, E. P. Eernisse, and F. L. Vook, Plenum Publ. Corp., N.Y., p. 597, 1974.

79. G. M. McCracken and S. K. Erents, CLM-P-359, November 1973.

80. W. Bauer and G. A. Thomas, SLL-73-5266, June 1973.

81. R. W. Knoll, M.S. Thesis, University of Wisconsin, Madison, August 1974.

82. M. Kaminsky and S. K. Das, Radiation Effects, 18, 245, 1973.

83. R. Behrish, et al., Appl. Phys. Letters, 27, No. 4, p. 199 (1975).

84. J. Roth, R. Behrish, B. M. U. Scherzer, J. Nucl. Mat., 57, 365 (1975). Also page 573 in reference 78.

85. S. K. Das and M. Kaminsky, 5th Symp. on Engr. Prob. of Fusion Res., Princeton, November 1973.

86. S. K. Das and M. Kaminsky, "Defects and Defect Clusters in BCC Metals and Their Alloys," Nucl. Met., 18, 240, 1973.

87. M. Kaminsky and S. K. Das, Nucl. Tech., , 22, 373 (1974).

88. R. Wright, R. Varma and D. M. Gruen, "Raman Scattering and SEM Studies of Graphite, CVD Pyrolitic and Vitreous Carbon, etc.," 2nd Inter. Confer. on Surface Effects in Contr. Fus. Devices, San Francisco, Cal., Feb. 16-20, 1976.

89. L. H. Rovner and K. Y. Chen, "Surface Erosion of C and SiC by 0.5-3.5 MeV He^+," reference 88. Also Report GA-A13812, General Atomic Co., San Diego, California.

90. J. Roth, R. Behrish, and B. M. U. Scherzer, J. Nucl. Mat., 57, 365, 1975.

Appendix A

Neutron and Gamma Multigroup Energy Structures Used in This Study

TABLE A.1

Neutron 46 Multigroup Structure in eV

Group	Group Limits E(Top)	E(Low)	E(Mid-Point)
1	1.4918 (+7)	1.3499 (+7)	1.4208 (+7)
2	1.3499 (+7)	1.2214 (+7)	1.2856 (+7)
3	1.2214 (+7)	1.1052 (+7)	1.1633 (+7)
4	1.1052 (+7)	1.0000 (+7)	1.0526 (+7)
5	1.0000 (+7)	9.0484 (+6)	9.5242 (+6)
6	9.0484 (+6)	8.1873 (+6)	8.6178 (+6)
7	8.1873 (+6)	7.4082 (+6)	7.7977 (+6)
8	7.4082 (+6)	6.7032 (+6)	7.0557 (+6)
9	6.7032 (+6)	6.0653 (+6)	6.3843 (+6)
10	6.0653 (+6)	5.4881 (+6)	5.7767 (+6)
11	5.4881 (+6)	4.9659 (+6)	5.2270 (+6)
12	4.9659 (+6)	4.4933 (+6)	4.7296 (+6)
13	4.4933 (+6)	4.0657 (+6)	4.2795 (+6)
14	4.0657 (+6)	3.6788 (+6)	3.8722 (+6)
15	3.6788 (+6)	3.3287 (+6)	3.5038 (+6)
16	3.3287 (+6)	3.0119 (+6)	3.1703 (+6)
17	3.0119 (+6)	2.7253 (+6)	2.8686 (+6)
18	2.7253 (+6)	2.4660 (+6)	2.5956 (+6)
19	2.4660 (+6)	1.8268 (+6)	2.1464 (+6)
20	1.8268 (+6)	1.3534 (+6)	1.5901 (+6)
21	1.3534 (+6)	1.0026 (+6)	1.1700 (+6)
22	1.0026 (+6)	7.4274 (+5)	3.726 (+5)
23	7.4274 (+5)	5.5023 (+5)	6.4648 (+5)
24	5.5023 (+5)	4.0762 (+5)	4.7892 (+5)
25	4.0762 (+5)	3.0197 (+5)	3.5480 (+5)
26	3.0197 (+5)	2.2371 (+5)	2.6284 (+5)
27	2.2371 (+5)	1.6573 (+5)	1.9472 (+5)
28	1.6573 (+5)	1.2277 (+5)	1.4425 (+5)
29	1.2277 (+5)	6.7379 (+4)	9.508 (+4)
30	6.7379 (+4)	3.1828 (+4)	4.9604 (+4)

Table A.1 (cont.)

Group	Group Limits E(Top)	E(Low)	E(Mid-Point)
31	3.1828 (+4)	1.5034 (+4)	2.3431 (+4)
32	1.5034 (+4)	7.1017 (+3)	1.1068 (+4)
33	7.1017 (+3)	3.3546 (+3)	5.2281 (+3)
34	3.3546 (+3)	1.5846 (+3)	2.4696 (+3)
35	1.5846 (+3)	7.4852 (+2)	1.1666 (+3)
36	7.4852 (+2)	3.5358 (+2)	5.5105 (+2)
37	3.5358 (+2)	1.6702 (+2)	2.6030 (+2)
38	1.6702 (+2)	7.8893 (+1)	1.2296 (+2)
39	7.8893 (+1)	3.7267 (+1)	5.8080 (+1)
40	3.7267 (+1)	1.7603 (+1)	2.7435 (+1)
41	1.7603 (+1)	8.3152 (+0)	1.2959 (+1)
42	8.3153 (+0)	3.9279 (+0)	6.1216 (+0)
43	3.9279 (+0)	1.8554 (+0)	2.8917 (+0)
44	1.8554 (+0)	8.7643 (-1)	1.3659 (+0)
45	8.7643 (-1)	4.1399 (-1)	6.4521 (-1)
46	4.1399 (-1)	2.2000 (-2)	2.1800 (-1)

TABLE A.2

Gamma 21 Multigroup Structure in MeV

Group	Group Boundaries E(Top)	E(Low)	E(mid-Point)
1	1.2E01	1.4E01	1.30E01
2	1.0E01	1.2E01	1.10E01
3	8.0E00	1.0E01	9.00E00
4	7.5E00	8.0E00	7.75E00
5	7.0E00	7.5E00	7.25E00
6	6.5E00	7.0E00	6.75 E00
7	6.0E00	6.5E00	6.25E00
8	5.5E00	6.0E00	5.75E00
9	5.0E00	5.5E00	5.25E00
10	4.5E00	5.0E00	4.75E00
11	4.0E00	4.5E00	6.25E00
12	3.5E00	4.0E00	3.75E00
13	3.0E00	3.5E00	3.25E00
14	2.5E00	3.0E00	2.75E00
15	2.0E00	2.5E00	2.25E00
16	1.5E00	2.0E00	1.75E00
17	1.0E00	1.5E00	1.25E00
18	4.0E-01	1.0E00	7.00E-1
19	2.0E-01	4.0E-01	3.00E-1
20	1.0E-01	2.0E-01	1.50E-1
21	1.0E-02	1.0E-01	5.00E-2

Appendix B

A Note on Displacement Cross Sections

The displacement cross sections used for this study were calculated by D. G. Doran.[17] Recently these cross sections were recalculated using ENDF-IV data and properly including charge particle out [(n,p), (n,α), etc.] reactions by T. A. Gabriel, et al.[25] and D. G. Doran and N. J. Graves.[26]

As an example, to show the difference between the old and newer set of cross sections we plot in Figure B-1 for 316 SS the older cross sections of D. G. Doran[17] and the newer set of cross sections calculated by T. A. Gabriel, et al.[25] The two sets of cross sections from references 25 and 26 generally are in agreement within 10%.

Then newer cross sections would increase the effectiveness of the ISSEC in reducing the displacement damage in the first wall, because dpa rates in the unprotected first wall would go up more than in the protected wall where the average neutron energy is lower. This is shown in Table B-1 where factors of reduction in the displacement rates in 316 SS first wall are higher when the newer set of displacement cross sections are used.

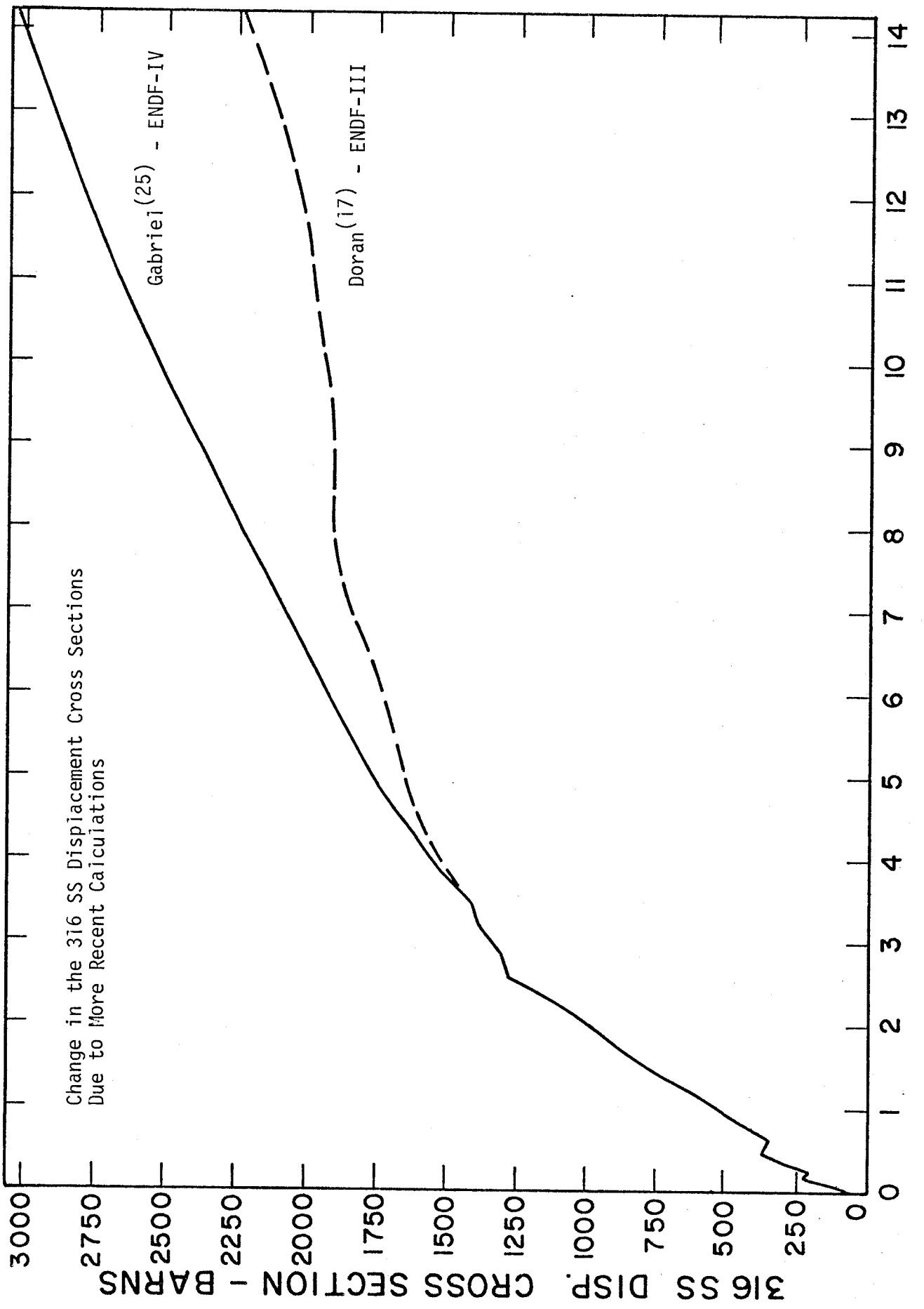
Change in the 316 SS Displacement Cross Sections
Due to More Recent Calculations
Gabriel[25] - ENDF-IV
Doran[17] - ENDF-III
316 SS DISP. CROSS SECTION - BARNS
NEUTRON ENERGY - MEV
0
250
500
750
1000
1250
1500
1750
2000
2250
2500
2750
3000
1
2
3
4
5
6
7
8
9
10
11
12
13
14

Figure B-1

Table B-1

Effect of More Recent Up-To-Date Displacement Cross Sections on the Reduction of Displacement Damage in 316 Stainless Steel First Wall by ISSEC

		Doran[17]-ENDF-III		Gabriel[25]-ENDF-IV	
	ISSEC Thickness	dpa/yr	Reduction Factor	dpa/yr	Reduction Factor
No ISSEC		10.13		12.54	
C ISSEC	5 cm	6.9	.68	8.2	.65
	10 cm	4.92	.49	5.64	.45
Mo ISSEC	5 cm	5.34	.53	5.95	.47
	10 cm	3.1	.31	3.30	.26
Nb ISSEC	5 cm	5.22	.52	5.85	.47
	10 cm	3.23	.32	3.44	.27
V ISSEC	5 cm	5.7	.56	6.51	.52
	10 cm	3.69	.36	4.01	.32
W ISSEC	5 cm	4.40	.43	4.93	.39
	10 cm	2.13	.21	2.29	.18